EMBODIED COGNITION ANALYTICS:

A FRAMEWORK OF EXPERIMENTAL PARADIGMS AND ANALYTICS TO STUDY AGENCY

By

JIHYE RYU

A dissertation submitted to the

School of Graduate Studies

Rutgers, The State University of New Jersey

In partial fulfillment of the requirements

For the degree of

Doctor of Philosophy

Graduate Program in Psychology

Written under the direction of

Elizabeth Torres

And approved by

_____

_____

_____

_____

New Brunswick, New Jersey

October, 2019

ABSTRACT OF THE DISSERTATION

Embodied cognition analytics:

a framework of experimental paradigms

and analytics to study agency

By JIHYE RYU

Dissertation Director:

Elizabeth Torres, PhD

Scientific findings abound with evidence that our behaviors are constrained by processes within our brain and body and by various external factors, leading us to wonder about the origin(s) of our behavior. In this thesis, I define agency as the capacity to change (at will) the immediate environment through one's behavior; and setting agency as an overarching reflection of many constraining factors, I introduce the embodied cognition analytics (ECA) framework. This framework is a tool to study varying degrees of agency with respect to the processes within the nervous systems.

In a series of three experiments, I demonstrate a set of experimental and analytical paradigms that allow characterizing the dynamic stochasticity and self-emerging cohesiveness of

disparate biophysical signals generated by the brain, the body, and the heart during natural, unconstrained actions. The final goal is to characterize the degree of agency, by examining the range of these dynamical changes, and comparing across populations of different agency. In the thesis, I limit the study of agency to the cognitive-motor domain, and compare the characterization across different populations, where the patient populations are assumed to have compromised cognitive/motor capacity, and the neurologically healthy population to have high cognitive-motor agency.

In the first study, I characterize the differing levels of motor control and cognitive load by adapting network analytics methods commonly used in the analyses of cortical signals (generated by the central nervous system; CNS) to the analyses of kinematics signal (generated by the peripheral nervous system; PNS), which were registered from motion sensors positioned across the upper body. In the second study, I extend the previous methods to capture the full CNS-PNS dynamical interactions, by co-registering and analyzing the biophysical signals generated by the CNS (of EEG data), PNS (of acceleration, magnetometer data), and ANS (of EKG data). I report on the changes in patterns of connectivity dynamically evolving across conditions (when the participant exerts control on his/her breathing pace) during naturalistic walking tasks, and compare them between healthy participants and patients with Autism Spectrum Disorder. In the last study, I examine the co-registered signals of the CNS (EEG data), PNS (magnetometer data), and ANS (EKG data), as in the second study, but have the participant perform a variety of tasks involving movements with different cognitive and memory processes. I later translate these tasks to the clinical realm by digitizing neurological diagnostic tests that assess cognition and memory in aging. Here, I present a set of analytics that we found to highlight the difference between Parkinson's patients and healthy participants, with the aim to understand the interactive nature of the neurobiological system from individuals with varying degrees of

cognitive-motor agency. These three experiments and analytics are not exhaustive, but would serve as proof-of-concept examples of the general framework to study agency.

Overall, the protocols and methods offered in this thesis provide a new unifying framework to characterize agency from the dynamical interaction of cognitive and motor processes registered by high resolution biophysical sensors. In this sense, the agency that I characterized is truly embodied, in that it is not a mere cognitive nor a motor capacity, but is a concerted and integrated capacity of both cognitive and motor behaviors. Furthermore, this framework enables an objective physical quantification of naturalistic cognitive activities in the laboratory and within clinical settings, thus providing new ways to connect basic and clinical sciences.

Acknowledgement

I would like to thank Dr. Elizabeth Torres, my committee members, Dr. Melchi Michel, Dr. Manish Singh, and Dr. Roseanne Dobkin, and all the members of the Sensory-Motor Integration Lab for their help with my thesis.

This work was funded in part by the Rutgers Data Science Informatics Institute, New Jersey Governor's Council for Medical Research and Treatment of Autism and the New Jersey Department of health. It was also supported by the Nancy Lurie Marks Family Foundation Career Development Award to E.B. Torres.

Table of Contents

List of Figure

List of Tables

1 Introduction

1.1 Origin of behavior

It is Friday afternoon, and you have a long weekend ahead. What would you do? You have the option to enjoy the beach nearby, or meet up with friends, or spend a peaceful time at home watching movies. With these options ahead of you, you eventually decide on a certain choice and take control of how you would spend your weekend. As such, we make countless decisions for countless actions, and this gives us the sense of control - the feeling that we ourselves are the origin and cause of our own behavior, and thus can control that behavior. But do we have such control?

1.2 Motivation of studying agency

The sense of control leads one to think there is free-will, which I define as the ability to act on one's accord unimpeded. Free-will has been an age-old topic of debate among philosophers and a curious pondering among laymen. Indeed, the existence of free-will is fundamental to our existence, as it provides a sense of empowerment to our everyday lives and confers moral responsibility to our actions.

However, in the recent century, there have been an accumulation of scientific studies undermining the existence of such free-will. In the 20th century, Galton (1875) opened a nature versus nurture debate, and argued how genetics are a large determinant of an individual's prospects. Many behaviorist psychologists (e.g.,(Pavlov, 1957; Skinner, 1947)) from the mid-20th century assumed that our behavior is a by-product of conditioning. Moreover, in a seminal study by Libet (1985), the cortical timing of motor planning was found to precede the timing of intention for a motor action, thereby alluding that intention may be a mere reconstructed notion. In the current scientific field, there abounds evidence in social psychology on how

social/external factors influence an individual's behavior (e.g., (Asch, 1955; Bandura, 1969; Janis, 2008) and in biological science including neuroscience on how the somatic state of the body influence the behavior (e.g.,(Adolphs, 2003; Green et al., 2008)). It does seem like there is little to no room for one's free-will.

Naturally, this leads us to limit this free-will to a more constrained notion - agency. Here, I define agency as the capacity to change one's immediate environment through one's behavior at will. Agency reflects the constraining factors that influence one's behavior (e.g, sensory stimulation, bodily degrees of freedom, somatic state, climate of one's location), by varying the degrees of capacity with which one can behave. Setting agency as the overall reflection of all these constraining factors, studying the mechanism of agency seems to be the next step in understanding the origins of our behavior.

1.3 Challenges to studying agency

Studying the mechanism of agency is not a simple problem. In the field of psychology, there have been studies on how the sense of agency impacts one's affect and behavior (e.g., Baumeister (2008)), how the sense of agency can be evoked in non-verbal children with autism spectrum disorders (Torres, Yanovich, & Metaxas, 2013) and how sense of agency can be quantified (Arzy & Schacter, 2019; Haggard & Clark, 2003). However, these do not address the main question on the mechanism of agency, which is the behavioral capacity to change one's immediate environment at will.

This question is challenging because the definition of agency is not clear to begin with. Agency is commonly defined as the "capacity to change one's immediate environment through one's behavior", but the scale of such behavior is subjective. This behavior may be small-scaled and specific, such as lifting a hand to a certain direction, or large-scaled and abstract, such as

changing the fate of a nation. Even if we focus on the small and specific scale of behaviors (e.g., Harris and Wolpert (1998)), we are still confronted with the problem of conceptualizing agency.

The common account of agency is a top-down perspective, where an organism computes the costs and benefits of performing a set of actions, decides on one action, and then performs that action according to that decision/goal (Haggard & Chambon, 2012; Miall & Wolpert, 1996). Here, the goal is determined based on the computation of risks and rewards that entail such action, and agency is the measure of how well the organism performed that action according to that goal.

Another perspective of agency is a bottom-up one, where behaviors do not originate from one source (assumed to be the brain), but instead is an emergent phenomenon of self-organization with control existing at multiple levels of the organism. From this perspective, it is affordance (defined as perceivable opportunities of the environment to perform action; (Gibson, 1978)) that guides an individual's behavior, where there is no need to appeal to top-down goals to explain behavior (e.g., (Bruineberg & Rietveld, 2014; Clark, 2008; Hoffmann & Pfeifer, 2018)). For example, when we see a knob on a door, we instinctively turn it (instead of pinching or poking it). In this perspective, our 'goals' are formed through the constant interactive sensory-motor processes within a horizontal-like structure (contrasting to a vertical-like structure, where the brain gathers sensory-motor information and makes decisions like a commander), and our 'goals' are not localized in the brain, but is rather distributed throughout the brain and body to control at different levels (e.g., position and orient the wrist to grasp the knob, maintain standing posture to keep close distance between the hand and knob, maintain breathing to stay alive). It seems that most goals described by the bottom-up perspective reflect the varying levels of control that exists within the nervous systems, which are internally evoked as we sense our self-generated activity and act upon accordingly. In contrast, the goals described in the top-

down perspective originate primarily from the external world and require some degree of awareness of that external world in relation to our internal one (Torres, 2011, 2018).

These two perspectives are not alternatives, but rather are complementary to one another, as continuous interactions occur between the goals and their ensuing behaviors from both perspectives. Indeed, in the developmental stages of an individual, the bottom-up perspective of agency is more informative to explain behavior, as an infant's motor actions are mostly spontaneous and reactive (Thelen, Kelso, & Fogel, 1987; Thelen & Smith, 1996). However, as maturation of neuromotor control settles in, the infant acquires cognitive control of self-generated actions and begins to discover cause and effect. It is within the healthy adulthood stage, that the top-down perspective of agency would be relatively more informative, as s/he makes more goal-directed actions with a better control of the body and the immediate surrounding. For an individual to achieve such agency would require a healthy maturation of the nervous systems to allow a proper foundation of self-organization that underlies the top-down control of one's behavior. As an example, for a neonate to achieve the cognitive capacity to predict and confirm their impending actions, it is required to attain systematic stochastic shifts in their motor variability that differentiates between goal-oriented motion and its consequential spontaneous motions (this is further elaborated in section 2.2.4) (Torres, 2018; Torres, Brincker, et al., 2013; Torres, Smith, Mistry, Brincker, & Whyatt, 2016).

Yet, most studies on agency fail to reflect the interactions and coordination between top-down and bottom-up control aspects of control. In fact, in the field of motor control, the bulk of the work focuses on planning and executing goal-directed actions that involve top-down control (Harris & Wolpert, 1998; van Beers, 2009; van Beers, Wolpert, & Haggard, 2002), but neglect to explain them in relation to the spontaneous self-organizing actions that unfold (i.e., bottom-up control) to support such goal-directed actions. On the other hand, studies that focus

on the coordination of rhythmic behaviors (e.g. using the non-linear complex dynamical systems approach) do not address top-down control, and instead favor interpretation of phenomena that primarily involves self-emerging synergies (e.g., Buchanan and Kelso (1999)). The need to integrate both approaches is evident in the nascent field of embodied cognition, where the mind and body interact and cooperate through the ebb and flow of shared control.

One aspect that serves as a challenge to both approaches is the self-generating, self-correcting nature of the neuromotor control that produces behaviors. This is because for the experimentalist focused on the top-down perspective, in order to control for extraneous factors, it is inevitable to externally impose a goal for the research participant to perform a set of actions. However, this approach neglects the processes of goals continuously changing and unfolding in the sequence of behaviors. In real life, these goals are not externally imposed (e.g., to press a target button), but emerge as the brain attends to shifting priorities which are in constant flux (Klein, 2008; Von Holst & Mittelstaedt, 1950). For the experimentalist with a bottom-up perspective, the self-generating nature of behaviors can be well observed, as the research participant is required to behave naturalistically with no specific goals imposed. However, in this case, the experimentalist has very little control over extraneous factors, and the internal/external goals are often unidentifiable. This results with the inability to disentangle the dynamical process of self-generating behaviors, and with little explanatory power.

Indeed, the problem of low external validity within an experiment that was designed with a top-down perspective has implications for characterizing the rewards which are the motivating factors behind agency, as they determine the goals that are evoked and evolved. Rewards are well recognized in the affective domain, as positive affect serves as a reward to influence behaviors through the dopamine pathways involved in cognitive and motor control (Aston-Jones & Cohen, 2005; Roy, Shohamy, & Wager, 2012). However, in the context of

studying agency, the notion of rewards would need to be widened to reflect an entire array of rewards that contribute to generating behaviors. Specifically, akin to supervised and unsupervised learning, there are rewards that are explicit such as those that provide positive affect (e.g., money, self-esteem) as in a supervised learning context, and there are rewards that are implicit such as the information you gather when you spontaneously behave as in an unsupervised learning context (Barlow, 1989). For instance, when we observe a toddler, parents reward the child with praises and smiles for certain behaviors (e.g., pronouncing a word correctly) thereby reinforcing them to repeat such behaviors; much like a supervised learning process. However, a toddler does not only behave based on such reinforcement, but spontaneously explore the environment and one's body in relation to the environment. This is not because the child has an explicit agenda to gather information to conquer the world and become omnipotent, but merely does so for the sake of learning which itself is a reward; much like an unsupervised learning process. As an adult, we are still learning with such implicit rewards, as we gaze into a distance and register countless perceptual information without an explicit intent to do so. As such, our behaviors are influenced by a wide range of rewards, which are dynamical and most often self-generated. However, imposing an artificial goal within a constrained environment (as in an experiment with a top-down perspective) fails to reflect such dynamicity and diversity of reward processing. On the other hand, the experiment with a bottom-up perspective will indeed reflect such dynamicity and thus contain high external validity, but due to little control of extraneous factors, this leads the experimenter with the problem of unidentifiable rewards and with little explanatory power. Without a doubt, both are important and complement each other.

Given the wide range of rewards, and their concomitant motor actions and behaviors, it is important to weigh the costs and benefits of external validity in designing experiments to

study agency. Because we are not concerned with a small aspect of an individual's cognitive system (e.g., visual perception of a line), but with agency that is indeed a global aspect of an individual's biophysical system, it is important to reflect both the top-down and bottom-up perspectives of agency in designing experiments, and to raise a certain level of external validity to study the self-generative and dynamical process of agency. With these criteria in mind, how can we study agency, and what is the appropriate framework to do this?

1.4 Embodied framework to study agency

Agency, according to Juarrero (2015), emerges from complex systems. Complex systems, which are ubiquitous in nature (e.g., brain, human, ecosystem, weather), are those that are influenced by many of its elements and by interactions among those many elements, and are self-organizing in nature. For example, the nervous system is a complex system, composed of neurons (elements) that interact with one another through synapses, and are self-organizing in that the synaptic patterns that may seem spontaneous eventually result in an organized behavior such as thoughts and actions. Life is also a complex system composed of organisms (element) that interact with one another through reproduction, competition, predation, and communication. These interactions may seem spontaneous, but these result in an organized behavior of evolution and survival at a larger scale.

Juarrero (2015) argues that for an individual to possess agency, one's behavior must be caused not only by external factors, but also by internal factors along with the relations and contexts in which behaviors emerge. As such, she reasoned that agency must involve a recursive informational flow between two different levels of organization – part (element) and whole (system). This viewpoint highlights the necessity to stage the paradigm in an embodied manner. That is, the paradigm needs to incorporate activities of the multiple layers within the nervous

systems embodied by an individual. Indeed, Torres (2011) proposed that the level of control ranges on a spectrum, and Torres (2016) argued that to attain volition (the acquired voluntary control of actions at will), one requires developing a proper balance of control across the multiple nervous systems, ranging from the autonomic, to the automatic, and to the voluntary control (Figure 1.1) .

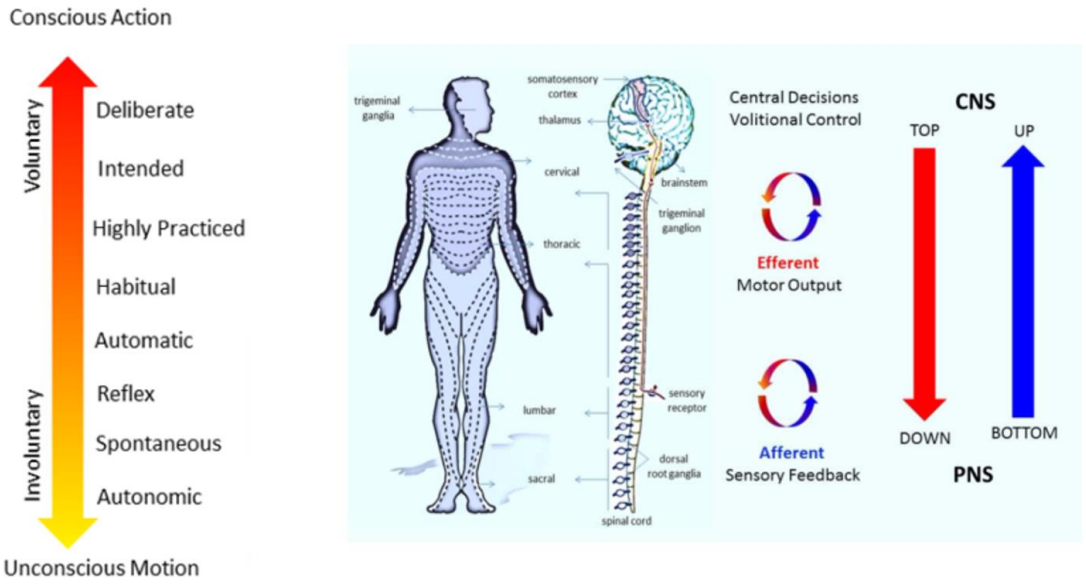

Figure 1.1. Conceptualization of Agency. (Left) The level of control ranges on a spectrum from those that are autonomic and involuntary (such as the heart-beat) to those that are automatic (such as walking) to those that are voluntary and deliberate (such as learning a new dance routine). Figure adapted from (Torres, 2011) **(Right)** In order to attain volition (i.e., the acquired voluntary control of actions at will), an individual needs to develop a proper balance of control that spans the different layers of the nervous system within one's body, which entails a healthy range of interaction between the efferent and afferent signals running top-down and bottom-up. Figure adapted from Torres (2011, 2016)).

Currently, there are several frameworks that reflect the systems biology aspects in understanding cognition. Notably, Freund et al. (2016) used the term 'embodied neurology' and offered an integrative framework in understanding neurological disorders. They claimed that by using a unified biophysical model of the human's nervous system structure and function, we could understand the interactions that occur on a multiple scale within the central and

peripheral nervous systems, and ultimately understand the nature of neural control and plasticity causing various mental disorders. Adams, Shipp, and Friston (2013) in the motor control field also argued for a systems biology perspective, as they considered both the efferent and afferent signals traveling within the multiple layers of the nervous system to be integral parts of the motor planning. In the cognitive science field, Torres, Isenhower, et al. (2016) have led the precision medicine approach in understanding neural disorders by examining data on a personalized basis (as opposed to an averaged group basis), referring to the uniqueness of each individual's nervous system. These frameworks can serve as building blocks in designing a framework to study agency and in understanding the interactive nature of the complex nervous systems.

1.5 Dissertation Overview - Embodied Cognition Analytics (ECA) framework

In this thesis, I introduce a set of studies that is based on a framework conducive to understanding agency – which I coin "Embodied Cognition Analytics".

In this framework, as a first step, I refine the definition of agency as "***the capacity to control one's behavior at will***" as this is the preceding step to control one's immediate environment (e.g., move an object, persuade a friend). In this thesis, I limit the study of agency to the cognitive-motor domain (for now) by comparing the characterization of agency between patients with compromised cognitive/motor control and healthy individuals. I attempt to characterize agency with respect to the processes within one's neurobiological systems, particularly of the cognitive and somato-sensory-motor activities that are involved in expressing one's agency. In this sense, the agency that I characterize is truly embodied, in that it is not a mere cognitive nor a motor capacity, but is an integrated capacity of both cognitive and motor behaviors, as I attempt to examine the biophysical signals generated by the CNS, PNS, and ANS,

and compare this across patients with different neurological disorders (which are accompanied by symptoms of both motor and cognitive difficulty). Indeed, a complete picture of agency would reflect all constraining factors, including external factors like the social environment, but for the purpose of this thesis, I limit it to the processes within one's internal neurobiological system.

In conceptualizing agency, the framework examines both goal-directed and spontaneous self-emerging behaviors that exhibit different coordination patterns of the full brain-body networks. To that end, we take the bottom-up perspective of agency, where behaviors are a byproduct of large interactive processes within a complex system (body), with goals distributed at numerous levels of control (e.g., low level set for autonomic control such as maintaining respiration, to high level set for cognitive control such as counting backwards). This entails examining naturalistic motor behaviors (e.g., spontaneous motions of automatically swinging arms during gait, or of spontaneously retracting motion as a consequence of touching a button) along with biophysical signals produced by different bodily functions (e.g., heart, kinematics, brain waves). Although this approach results with having much noise introduced by extraneous factors, the aim is to observe the forest through a holistic lens; with the hopes of making sense of the trees at a later stage. Indeed, although we are left with much noise using this approach, we are nevertheless able to take advantage of the signal variability emerging from some of these noise, as they do turn out to be the most informative signal (elaborated in section 2.2.4.1.1).

Using this framework, in the next three chapters, I introduce three experimental paradigms that allow examining the range of stochasticity and connectivity of biophysical signals, that are varied by physiological control (e.g., motor, respiratory) and cognitive processes. I aim to characterize the level of cognitive-motor agency by examining how the

biophysical systems dynamically change as a result of various factors, and by comparing them between healthy individuals and those with compromised cognitive/motor abilities. For instance, the biophysical signals that are extracted from these experimental paradigms are classified by intent level (e.g., deliberate motion vs. spontaneous motion) and by the nervous systems that the signals are generated from (e.g., brain signals from the CNS vs. heart signals from the ANS). In so doing, we can characterize the range within which the brain and body networks' patterns emerge across these varying conditions (whether that is by motor intent, or by the type of the nervous system). By comparing such range across populations with different cognitive/motor capability, the thesis attempts to understand the properties of cognitive-motor agency. Here, we assume high agency to be characterized as the patterns found among healthy individuals, and low agency as those exhibited by patients with compromised cognitive/motor control (**Figure 1.2**). Note, to be able to examine how they influence one's physiological system, it is inevitable to control for extraneous factors to some degree. For that reason, the research participants are, at times, imposed with external/artificial top-down goals or instructed to perform a set of constrained actions. This is not an ideal scenario of observing one's behavior naturally unfold, but it is a necessary compromise to facilitate interpretation of phenomena using statistical inference.

Also, note, I raise a distinction between cognitive/motor control and cognitive-motor agency. Both terms are related in that being capable of exerting high cognitive/motor control is correlated with higher levels of cognitive-motor agency. However, higher agency does not refer to the instance when top-down control is executed successfully, but rather is a global state when both top-down and bottom-up controls are implemented successfully. To examine this global state of behavioral capacity (i.e., agency), throughout the chapters, I will examine the range of stochasticity and dynamic connectivity of biophysical signals with respect to factors

such as motor intent and cognitive load. By quantifying and tracking the range of different movement classes that emerge from differing cognitive processes within participants, I aim to understand the dynamical processes within the human complex system that contribute to agency, and by comparing across different populations with different cognitive/motor capacity, I aim to characterize different levels of cognitive-motor agency.

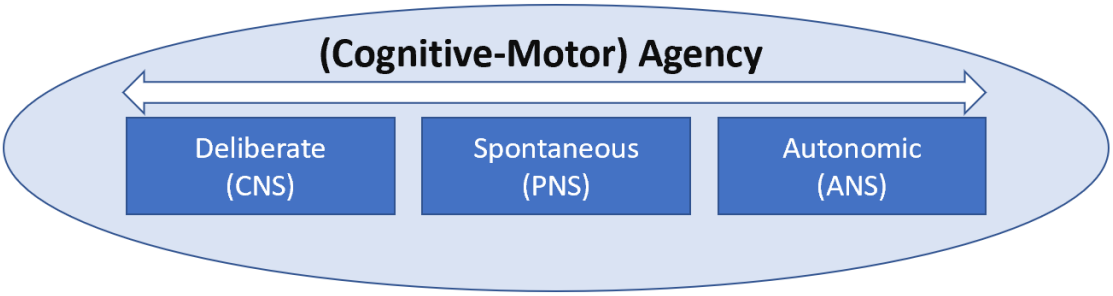

Dissertation approach to study agency

Def: Agency is the capacity to control one's physiological behavior at will, and is characterized by the wide range of dynamically changing connectivity patterns across different levels of control (from autonomic to deliberate) and across the full brain-body network

1. Conduct experiments that capture the deliberate/spontaneous/autonomic biophysical signals, which are categorized by exerted level of intent (e.g., deliberate motion vs. spontaneous motion) or by the nervous system from which the type of biophysical signal was generated (e.g., brain activity vs. heart activity)
2. Characterize deliberate/spontaneous/autonomic behaviors **within** individual
3. Compare such characterization **between** individuals from different populations , to characterize different levels of agency

Figure 1.2 General overview of the dissertation approach to build embodied cognition analysis (ECA)

In doing so, I present a variety of analytics that are useful to characterize the different levels of control exhibited by the research participants' biophysical signals obtained from these experiments. Because many of the data sets acquired from these experiments are datatypes that are not commonly analyzed in the field, we explored a variety of analytical methods

borrowed from fields outside of cognitive science (e.g., information theory, linear algebra, statistical mechanics and time series forecasting (Box, Jenkins, Reinsel, & Ljung, 2016)), with the aim of finding the best datatype and its analytics to characterize the behavior of our interest.

After reviewing these experimental paradigms and analytics, I discuss the application value of using the ECA framework. In particular, the study of agency under this framework is informative to the health science field, as it can become an objective and precise approach to preventing and assessing neurological disorders with compromised cognitive-motor agency (e.g., Autism spectrum disorder, Parkinson's disease). Here, I will review the studies described in the previous three chapters, highlighting the ways it can be used in the clinical domain.

2 Cognitive load and control represented as a network

2.1 Introduction

When you aim to lift your hand to perform simple tasks such as pointing, this act requires motor planning processes to coordinate the different parts of the body to perform that very task, along with other physiological processes to support that performance. For example, the ANS needs to maintain a healthy balance (e.g., healthy heart beats to keep the blood flowing through the brain and body) to have the capacity to perform a pointing action. Also, one needs to have a limited amount of cognitive load to perform the task, as an individual who is overloaded with other complicated cognitive task (e.g., learning to dance a complicated choreograph) would not have the capacity to attend to the task of pointing. All these seemingly unrelated aspects, such as cognitive load and heart activity, are factors that dynamically influence the process of a simple task such as pointing (Malcolm, Foxe, Butler, Molholm, & De Sanctis, 2018; Ryu & Torres, 2018). Conversely, such simple pointing tasks would also influence the processes of the

performing individual's physiological process (e.g., an extended series of pointing gestures would tax the individual and influence his/her heart and muscle activity) (Ryu & Torres, 2018).

Indeed, in an earlier study Ryu and Torres (2018), such dynamical interactions were characterized by the change in stochastic signatures of one's heart and kinematics activities due to additional levels of cognitive load. Also, from a series of work by Torres (2018), such interactions were observed by the change in stochastic signatures of kinematics variability within an individual exerting varying levels of motor control, and between individuals with different demographics (e.g., different ages, the presence of neurological disorders). These previous works highlight the interactive nature of physiological processes that span the different layers of the nervous systems (i.e., central and peripheral nervous system), and emphasize the informativeness of biophysical signals (e.g., heart, kinematics) in characterizing the varying degrees of cognitive processes and of motor control.

In the current study, we expand an earlier work by Ryu and Torres (2018), and examine the kinematics of different body parts in relation to network connectivity dynamically changing over the course of the experimental session. Here, we focus on the interactive nature of the physical body, where the spotlight is not only on the active hand that is performing the task (i.e., pointing), but on the entire upper body complex, to understand how the active and inactive parts of the body work together synergistically to produce a coordinated movement. We capture how these interactions change under different levels of motor control and cognitive load. By examining the range of network connectivity dynamics across the different levels of exerted control and cognitive load, this study is a first step to characterize a healthy individual's agency that emerges from a complex system.

To do this, we apply to a brain-body complex network connectivity framework that is commonly used to characterize complex systems (Barabasi & Oltvai, 2004). First we adapt the layout and analyses to the interconnected grid of sensors defining a dynamically changing network across the body; and then we extend it to the brain, heart, etc. This framework had been adopted by other labs to study the brain's non-linear dynamical patterns of activity, as the brain is treated as an interconnected complex network. Indeed, that body of work has illuminated our understanding of complex patterns within the brain activity, and have demonstrated the importance of examining the brain as a whole (Sporns, 2010). However, such methods had never been used in the analyses of peripheral activities from controlled actions, nor had been extended to include brain-body-heart interactions until very recently (e.g. Kalampratsidou and Torres (2018); Torres, Nguyen, et al. (2016b))

In this study, we apply this framework by extending it to the entire body. Here, the peripheral nerves innervating the body can be construed as extensions of the brain networks, and thus be modelled using the network connectivity approach, by building an adjacency matrix reflecting the dynamically evolving pairwise relations across the nodes of the network. In this case, we conceptualize the network nodes as body parts where motion sensors capture the kinematics signals, as shown in **Figure 2.1B**. Among the network models that can be used are linear models involving cross-correlation, and non-linear models involving cross-coherence and phase locking values, among others. The adjacency matrices can be constructed using a variety of metrics, including similarity metric distances (e.g. earth mover's distance) as well as synchronicity metrics (e.g. phase locking value, cross-coherence), to construct weighted directed or undirected graphs. For the purpose of this study, we examine the spatial and temporal domains of the kinematics signal, by using mutual information and cross-correlation metrics respectively in building an undirected adjacency matrix and its corresponding network. The

networks derived from such graphs can then be compared across different levels of cognitive load and motor control, to see how the body connectivity reflect different degrees of cognitive load and of motor control as it unfolds.

2.2 Methods

2.2.1 Participants

Nine undergraduate students (2 males and 7 females) between the ages 18 and 22 were recruited from the Rutgers human subject pool system. Two were left-handed and seven were right-handed, and all had normal or corrected-to-normal vision. All participants received credit for their participation, and provided informed consent, which was approved by the Rutgers University Institutional Review Board.

2.2.2 Motion Capture System

For all participants, motion capture system and a wireless heart rate monitor were used to record the motor and heart activities. For the purpose of this study, motor signals were only analyzed. Other analyses of both motor and heart signals can be found in Ryu and Torres (2018).

15 electromagnetic sensors at a sampling frequency of 240 Hz (Polhemus Liberty, Colchester, VT) were attached to the participant's upper body in the following locations: center of the forehead, thoracic vertebrate T7, right and left scapula, right and left upper arm, right and left forearm, non-dominant hand, and the dominant hand's index finger (**Figure 2.1**). These sensors were secured with sports bands to allow unrestricted movement during the recordings. Motor signals were recorded in real-time by Motion Monitor (Innovative Sports Training Inc., Chicago, IL) software, where the participant's body was constructed by a biomechanical model,

and movement data were preprocessed by an embedded filtering algorithm of the software, providing the location and kinematics of each sensor.

2.2.3 Experimental procedure

Participants sat at a desk facing an iPad tablet (Apple, Cupertino, CA), which was used to display stimuli during the experiment, and participants responded by touching the tablet screen. The tablet display on was controlled with an in-house developed MATLAB (Release 2015b, The MathWorks, Inc., Natick, Massachusetts) program and TeamViewer (Ver 14, TeamViewer Germany) application.

As shown in **Figure 2.1**, for each trial, the participant was presented with a circle on the tablet screen. This circle served as a prompt for the participant to touch the tablet screen within five seconds. Subsequent to the touch - after 100ms, 400ms, or 700ms - the participant heard a tone at 1000Hz for 100ms. Then, on the tablet screen, the participant was presented with a sliding scale (ranging from 0 to 1 second) to indicate how long he/she perceived the elapsed time between the touch and the tone. The response was to be made within five seconds upon the display of the sliding scale. The five seconds time-window was considered sufficient for the participant to provide a response, as it took approximately 1.5 s to touch the screen and retract the hand back to its original position. There were a total of three conditions – control, low cognitive load, high cognitive load - and each condition consisted of 60 trials. In the control condition, the participant simply performed each trial with no additional task; under the low cognitive load condition, the participant performed each trial while repeatedly counting forward 1 through 5; under the high cognitive load condition, they counted backwards from 400 subtracting by 3 while they performed each trial. Participants counted forward and backward at

their own comfortable pace, and they took breaks in between each condition. The experiment set up took about 30 minutes, and the recording took about 40 minutes.

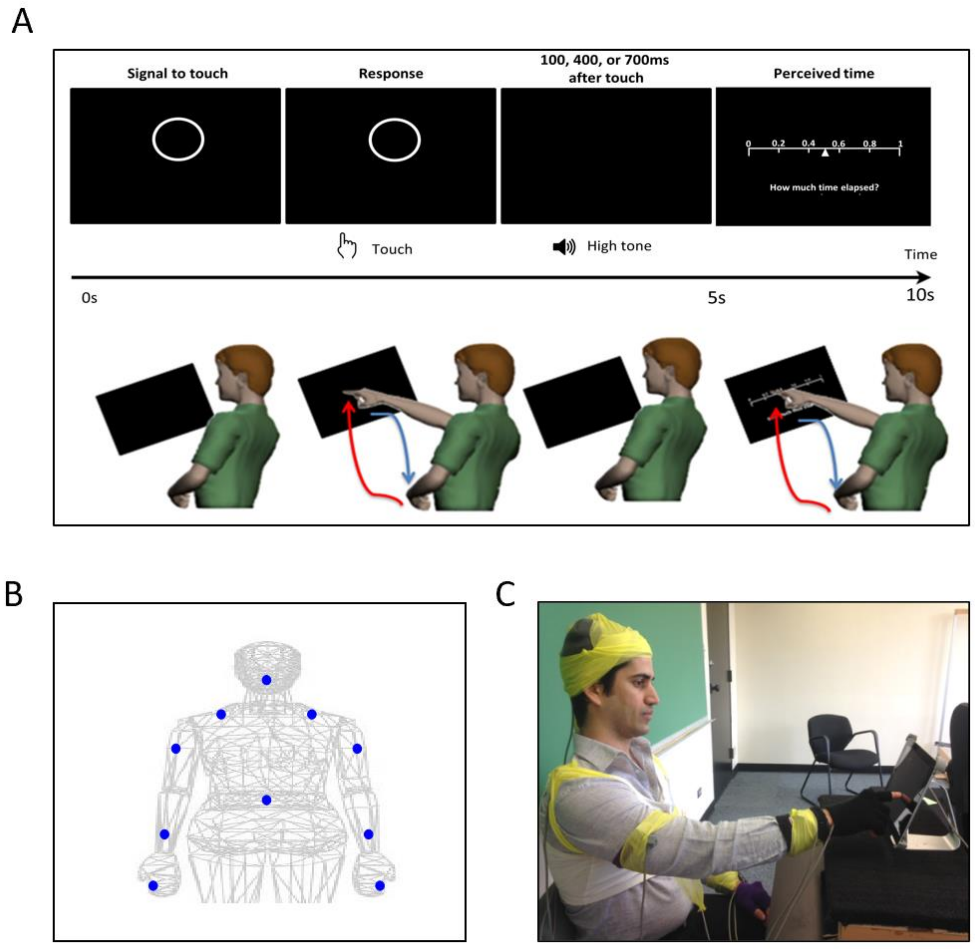

Figure 2.1. Experimental Procedure and Setup. (A) Experimental procedure. In a single trial, the participant was presented with a display screen as shown in the top panel. During the first 5 seconds, the participant was presented with a circle as a prompt to touch a circle on the screen. After the touch, the participant heard a tone. The duration between the touch and the tone was randomly set to be 100ms, 400ms, or 700ms. In the next 5 seconds, the participant was presented with a sliding scale, where he/she indicated how long they perceived the time to have elapsed between the touch and the tone, by touching the corresponding the number on the scale. For each trial, the participant made two pointing gesture - to touch the circle and to indicate their time estimation on the sliding scale. Such pointing gesture was composed of a goal-directed segment (red) and a spontaneous segment (blue) as shown in the bottom panel. **(B) Motion capture sensor positions.** The sensors were attached on the following body parts: center of the forehead, thoracic vertebrate T7, right and left scapula, right and left upper arm, right and left forearm, non-dominant hand, and the dominant hand's index finger. **(C) Snapshot**

of the experiment. During the experiment, the participant was seated in front of the tablet screen to perform the tasks, and the wired sensors were secured with athletic tape.

2.2.4 Data analysis

2.2.4.1 Standardized Micro-movement Spike (MMS) Amplitude Data

The current study applies a statistical platform for individualized behavioral analysis (SPIBA), which was created for personalized assessments as required in Precision Medicine (Hawgood, Hook-Barnard, O'Brien, & Yamamoto, 2015), by harnessing biophysical signals from the peripheral, autonomic, and central nervous systems to understand cognition and a variety of neural disorders. Within the SPIBA framework, we use a new datatype coined “micro-movements spikes (MMS)” of biophysical signals. Biophysical waveforms are generated by the nervous systems and are registered from different sensors (e.g., electrocardiogram, electroencephalography, motion-tracking magnetometer). These waveforms give rise to a time series of peaks (spikes) and valleys, but different modes of waveforms reside in different ranges, making it difficult to analyze them in tandem as they are not comparable apples-to-apples. Moreover, long term drifts in biophysical signals, which fail to be eliminated by certain signal processing methods, also make it difficult to compare a single mode of biophysical waveform at different time segments. In order to overcome this barrier, MMS waveforms can be utilized, which is a spike train derived from a time series of biophysical signals, where the spike amplitudes are standardized to [0,1] range, and non-spikes set to zero. The standardized spike amplitude values are computed by taking the regional minima and maxima values from the raw time series, thereby bringing different modes of signals to the same range and avoiding noise due to long term drifts. Using the MMS waveforms, we are able to reflect the fluctuations in the amplitude and timing of the biophysical signal, which are assumed to follow a continuous random process under the general rubric of Poisson Random Process, and are independently

and identically distributed, IID. In our approach we can relax the IID assumption by allowing sampling from the raw time series with overlapping windows and as such introducing co-dependencies of future events on prior events variations. However, in this thesis I will focus on the IID sampling whereby blocks are independently sampled, without overlapping.

In this study, we focused on the standardized spike amplitudes of the MMS data, obtained from the instantaneous angular accelerations from each body parts. There are many kinematic parameters that can be examined, but we focused on the angular acceleration for this study. Although motion sensors yield linear and angular positional data and their higher order derivatives - linear velocity, angular velocity, linear acceleration, angular acceleration – because the current analysis relies on the statistical power of the data set (i.e., number of normalized amplitudes), a larger number of data sets would be most desirable. For that reason, we chose to focus on the parameter - angular acceleration - which produced the largest number of spikes in the least amount of time. This way, we avoid fatiguing the participant just to gather more samples. Notice here that we can restrict the MMS to minute fluctuations beneath certain peak amplitudes, but in this thesis, we examine all peaks which could possibly contain instrumentation noise. Separating instrumentation noise from physiologically relevant signal has been the topic of other work in our lab (Wu, Jose, Nurnberger, & Torres, 2018). My work will focus on all existing peaks from the MMS train extracted from motion sensors' angular acceleration outputs.

To compute standardized spike amplitudes, we took each spike amplitude from the raw angular acceleration data, and divided by the sum of raw spike amplitude and average of the signals sampled within the two adjacent minima surrounding the spike (see

Eq 2.1). This is a common method to address possible allometric effects (Mosimann, 1970) that occurs due to individual anatomical differences (**Figure 2.3B**)

$$Standardized\ Spike\ Amplitude = \frac{Raw\ Spike\ Amplitude}{Raw\ Spike\ Amplitude + Average_{Min\ to\ Min}} \quad \text{Eq 2.1}$$

For analysis, we segmented the motion by deliberate (high control, involving higher awareness) and spontaneous (low control, involving lower awareness) segments, to observe the difference in connectivity when an individual exerts different levels of control. We segmented such motions by examining the continuous trajectory of the dominant hand index finger performing repeated pointing movements, and decomposed it into forward (deliberate; from the time when the hand is resting on the table to the time the finger arrives at the target) and backward (spontaneous; from the time the finger reaches the target to the time the hand retracts back to its resting position) segments. We can safely assume that the forward movement is a deliberate movement requiring more control, as the individual has a goal in mind to move the hand in a certain way, while the backward movement is a spontaneous one demanding less control, since the individual performs such action without any instruction (Nguyen, Papathomas, Ravaliya, & Torres, 2014; Torres, Heilman, & Poizner, 2011a; Torres, Raymer, Gonzalez Rothi, Heilman, & Poizner, 2010). The timing of the start and end of the two movement segments were determined by examining the linear velocity of the dominant hand finger, and identifying the time when the linear velocity reached instantaneous zero, as this would occur when the hand reached the target and when it returned back to its resting position (**Figure 2.3A**). The timing derived from the dominant hand's kinematics was used to extract the

corresponding deliberate and spontaneous segments of angular acceleration from other body parts. It is worth noting that, the spontaneous/backward motion segment is an immediate consequence of the deliberate segment. In the past, patients with lower cognitive-motor agency such as ASD have shown less distinction in stochasticity between deliberate and spontaneous motion segments (Torres, 2013), implying that they may not be able to differentiate and understand the cause (deliberate motion) and effect (spontaneous motion) of their motions as well as their healthy counterparts would be able to. As such, it is meaningful to compare between these two movements, as they would inform us about the extent to which healthy individuals have awareness and control of the many co-existing motion segments that their complex behaviors possess (Torres, 2011).

We also separated the data by the location of the body parts - dominant and non-dominant side. If the person was right-handed, the dominant side corresponded to the body parts: right scapula, right upper arm, right forearm, right hand; and the non-dominant side corresponded to the body parts: left scapula, left upper arm, left forearm, left hand; and for the left-handed person, vice versa. This allowed us to further differentiate movement by motions that are active and goal-oriented (i.e., dominant side) and motions that are passive and spontaneous (i.e., non-dominant side).

2.2.4.1.1 Noise-to-Signal Ratio

For each dominance side (i.e., dominant or non-dominant) of body parts, and for each deliberate and spontaneous segment, a set of standardized spike amplitudes were extracted and input to a Gamma process. During a typical participant's single pointing movement (either deliberate or spontaneous movement segment), a single body part's angular acceleration time series produce approximately 15 spikes, and aggregating these across the three conditions (control, low cognitive load, high cognitive load conditions) and trials (60 trials per condition)

yields approximately 2500 spike amplitude data. These data were plotted on a frequency histogram using Freedman-Diaconis binning rule (Freedman & Diaconis, 1981), and fitted to a Gamma probability distribution function using maximum likelihood estimation (MLE).

In the past, our lab explored the differences between multiplicative (e.g., lognormal family) and additive (e.g., exponential families) random processes of the kinematics MMS data across thousands of individuals from different population (e.g., athletes (Torres, 2011), patients with autism spectrum disorder (Torres & Donnellan, 2015), patients with Parkinson's disease (Torres, Cole, & Poizner, 2014), patients with schizophrenia (Nguyen, Majmudar, Papathomas, Silverstein, & Torres, 2016)) and during different motor performance (e.g., deliberate/spontaneous reaching (Torres, Heilman, & Poizner, 2011b; Torres et al., 2010) , natural walking (Torres, Nguyen, et al., 2016a) , involuntary head motions in resting position during fMRI experiments (Torres, Mistry, Caballero, & Whyatt, 2017) (E. B. Torres & Kristina Denisova, 2016)). Our experiences with these data showed that the continuous Gamma family of probability distribution functions (PDF) have the best fit to the kinematics data, according to MLE. For that reason, we chose to fit the standardized spike amplitude data to the Gamma PDF (see **Figure A 1** for PDF fitness).

The Gamma PDF is given by:

$$y = f(x|a,b) = \frac{1}{\Gamma(a)b^a} x^{a-1} e^{\frac{-x}{b}} \qquad \text{for x>0} \qquad \text{Eq 2.2}$$

where there are two parameters – shape parameter (a), and scale parameter (b) - and Γ as the Gamma function (Ross, 1996). Noticeably, the scale parameter is equivalent to the noise-to-signal ratio (NSR), since the fraction of the variance over the mean of this PDF results to be the scale parameter, as such:

$$b = \frac{\sigma_\Gamma}{\mu_\Gamma} = \frac{\cancel{\alpha} \cdot b^{\cancel{2}}}{\cancel{\alpha} \cdot \cancel{b}}$$

Eq 2.3

Along the scale parameter, distributions with high scale value (i.e., high NSR) tends towards an Exponential PDF, which is considered a memory-less distribution, where past events provide little value to predict future events; conversely, distributions with low scale value (i.e., low NSR) tends towards a Gaussian distribution, where past events predict future events with high certainty. This finding has been useful in interpreting the kinematics data, particularly among the patients with neurological disorders, who have shown to have high NSR than their healthy counterparts (Torres, Isenhower, et al., 2016).

For the purpose of this study, the NSR (i.e., the fitted scale parameter) was computed for each body part, and the values were compared between different dominance side of the body parts, and between different movement segment, in order to understand how much *noise* there is when different levels of control is exerted during one's motor movement.

2.2.4.1.2 Mutual Information (MI)

The frequency distribution of the standardized spike amplitudes of angular acceleration time series can also be analyzed with an approach based on information theory by Shannon (1948). According to the theory, with an obtained data set X = $< x_i >$, information is computed in bits as:

$$I(x_i) = log_2\left(\frac{1}{P_X(x_i)}\right)$$

Eq 2.4

which is the logarithm of the ratio of uncertainty before x_i was observed to the uncertainty after x_i was observed. For instance, if we have 2 unbiased coins, the probability of observing 2 heads (HH) is $P_X(x_i = HH) = \frac{1}{4}$. The ratio of uncertainty before HH occurred is 1, because

anything can happen at that point. Once HH occurred, the probability space of anything happening (i.e., uncertainty) is reduced to $\frac{1}{4}$. Essentially, the less likely the event is, the larger that event's information is. That is, if the event is predictable, we learn little from that event, and there is little uncertainty and information; if the event is unpredictable, we learn a lot and there is more uncertainty, and obtain much information from that event.

Information entropy is the weighted average of these information bits across the event space X (or source X), where $P_X(x_i)$ are weights for $I(x_i)$, and is computed as:

$$H(X) = E\big(I(X)\big) = -\sum_{x_i} P_X(x_i) log_2 P_X(x_i) \qquad \text{Eq 2.5}$$

Using the information entropy from two sources, mutual information (MI) can be computed. MI is the amount of uncertainty (information) reduced from obtaining the information from another source. Between sources X and Y, MI is the information entropy from X reduced by the information entropy of X if information of source Y is known. This can be computed as such:

$$I_{XY} = H(X) - H(X|Y) \qquad \text{Eq 2.6}$$

where the conditional entropy can be computed as:

$$\begin{aligned} H(X|Y) &= \sum_{y_j} P_Y(y_j) H\big(X\big|Y = y_j\big) \\ &= -\sum_{y_j} P_Y(y_j) \left\{ \sum_{x_i} \frac{P_{XY}(x_i, y_j)}{P_Y(y_j)} \; log_2 \frac{P_{XY}(x_i, y_j)}{P_Y(y_j)} \right\} \\ &= -\sum_{x_i, y_j} P_{XY}(x_i, y_j) log_2 \left(\frac{P_{XY}(x_i, y_j)}{P_Y(y_j)} \right) \\ &= -\sum_{x_i, y_j} P_{XY}(x_i, y_j) log_2 P_{XY}(x_i, y_j) + \sum_{x_i, y_j} P_{XY}(x_i, y_j) log_2 P_Y(y_j) \\ &= -\sum_{x_i, y_j} P_{XY}(x_i, y_j) log_2 P_{XY}(x_i, y_j) + \sum_{y_j} P_Y(y_j) log_2 P_Y(y_j) \end{aligned}$$

$$= H(X,Y) - H(Y) \qquad \text{Eq 2.7}$$

Hence,

$$I_{XY} = H(X) + H(Y) - H(X,Y) = \sum_{x_i,y_j} P_{XY}(x_i, y_j) log_2 \frac{P_{XY}(x_i,y_j)}{P_X(x_i)P_Y(y_j)} \qquad \text{Eq 2.8}$$

As such, MI values are roughly dependent on the following factors: entropy of X, entropy of Y, and overlap of X and Y. Within the context of comparing two distributions, if either X (or Y) had a larger spread, the uncertainty would be higher, and this would lead to a higher entropy value (i.e., H(X) or H(Y)). If X and Y had a larger overlap, such that the joint distribution has a smaller spread, the joint entropy of X and Y would be smaller (i.e., H(X,Y)). Given these, if the two sources are independent, MI equals 0. Assuming the dependence is constructed randomly (as explained in the following paragraph), if the variability of the single distribution(s) is higher, this leads to a higher MI value. In addition, if there is a large overlap in two distributions, this would also lead to a higher MI value. **(**Figure 2.2**)**.

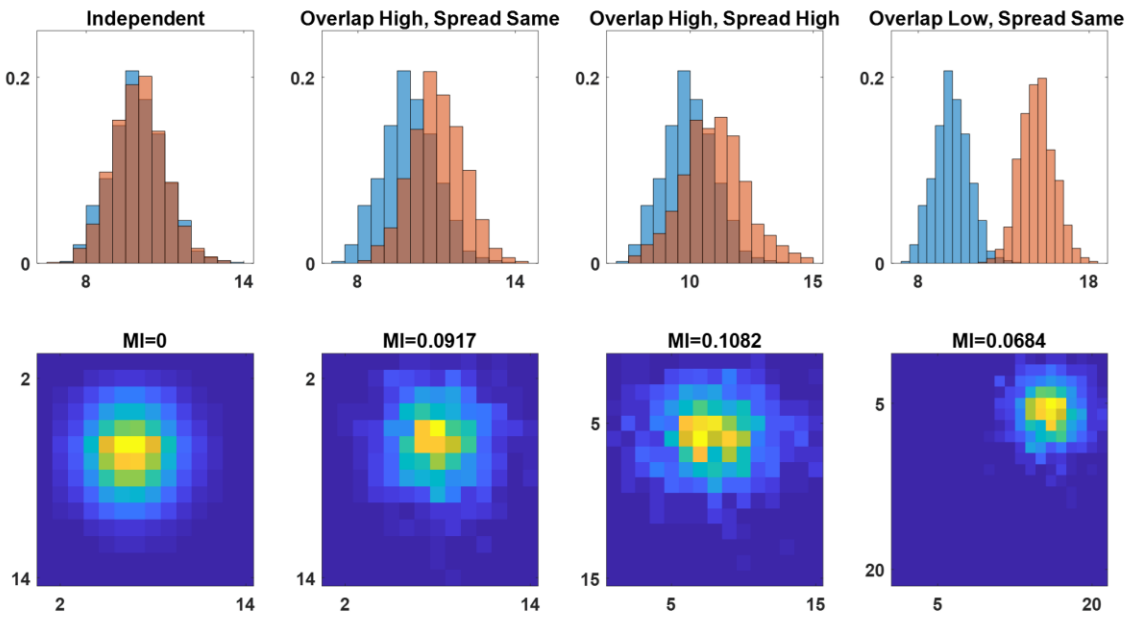

Figure 2.2. Mutual Information of two frequency distributions. (Top) Example of 2 frequency distributions, where the two are either independent, similar in range and spread, similar in

range but dissimilar in spread, and dissimilar in range but similar in spread (from left to right). **(Bottom)** Corresponding joint probability distribution of the corresponding above graphs, where the x-axis represents the blue histograms, and y-axis represents the orange histograms. In the context of this study, distributions that have larger spread will result with high MI, and those with larger overlap will result with high MI.

In the current study, MI was computed between histograms of two body part's standardized spike amplitudes of angular acceleration. Single probability distributions $P_X(x)$ for each body part were computed by constructing a histogram with 31 sampling bins set to range from 0.5 to 0.8, which encompasses the minimum and maximum fluctuations in amplitude values. This bin size is a close number to the sampling bin size if Freedman-Diaconis binning rule (Freedman & Diaconis, 1981) was applied. Note, we also tested with increments set at 0.015 with 21 bins (i.e., larger sampling bin), but this did not change the overall results. Joint probability distributions $P_{XY}(x, y)$ for a pair of different body parts could not be empirically determined, because the angular acceleration spikes from different body parts do not happen simultaneously. For that reason, the joint probability distribution was estimated by randomly sampling a pair from each body parts, X and Y, without replacement, and by constructing a joint histogram from these sampled pairs. Using the estimated joint probability distributions $P_{XY}(x, y)$, along with the empirical single probability distribution $P_X(x)$, we computed the mutual information I_{XY} , and repeated this computation 100 times. The median of the 100 estimated mutual information I_{XY} values was determined as the final value (Figure A 2).

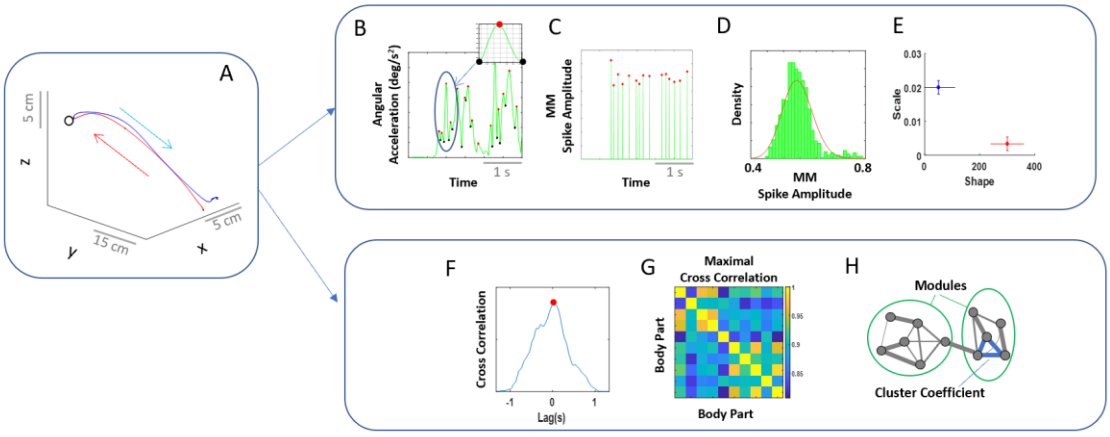

Figure 2.3 - Analytical and Visualization Methods. (A) Typical movement trajectory of the dominant hand performing a single pointing action towards a target. Each trajectory was separated by deliberate (red) and spontaneous segments (blue). **(B) Time series of angular acceleration of the dominant hand's index finger during a typical pointing task**. Peaks (spikes; maxima) and valleys (minima) are shown in red and black dots, respectively. The inset shows a zoomed-in picture of a single angular acceleration segment (i.e., two local minima and a single spike in between). This is a schematic of computing the standardized spike amplitude from a continuous time series of signal data, where the standardized spike amplitude is computed as dividing the spike value by the sum of the spike value and the average of the signal values between the two local minima as shown in **Eq 2.1**. **(C) MMS train for a typical pointing task.** All spike values from **(B)** were standardized between 0 and 1, while all non-spike values were set to 0. **(D) Frequency histogram of MMS Amplitudes fitted to a Gamma PDF.** All standardized spikes were gathered across trials and/or movement segments, and its histogram was used to compute the noise-to-signal ratio (NSR), and mutual information (MI) between different pairs of body parts per conditions and/or movement segments. **(E) Estimated Gamma parameters for each fitted histogram.** The histograms were fitted with a Gamma PDF using maximum likelihood estimation. For each fitted histogram, the Gamma parameters were plotted on a Gamma parameter plane (with shape parameter representing the x-axis and scale parameter representing the y-axis), with marker lines representing the 95% confidence interval. The fitted scale parameters (i.e., NSR) were later used for comparison between conditions and movement segments. **(F) Cross-correlation between different pairs of body parts.** For each trial, cross-correlation was computed for different pairs of body parts' angular acceleration time series**. (G) Matrix of maximal cross-correlation between different pairs of body parts.** From the cross-correlation results, maximal cross-correlation values were extracted from each trial. **(H) Network analysis of the weighted undirected matrix of cross-correlation.** Using the weighted undirected matrix of cross-correlations, networks were constructed, where the nodes corresponded to each body part, and the links corresponded to the maximal correlation values. From this network, modules and clusters were computed as a measure of segregation. Later, the medians of these measures were compared between conditions and/or movement segments.

2.2.4.2 Maximal Cross-Correlation data

In order to capture the temporal correlation across different parts of the body, we examined cross-correlations between the angular acceleration time series from all pairs of body part combinations. For each movement segment within a single trial, and for all three conditions, we computed the cross-correlations and between each pair of body sensors, and searched for the maximal correlation values (**Figure 2.3F**). This produced a matrix of maximal cross-correlation values across all pairs of body parts for each movement segment within a single trial.

Using these matrices, we were able to construct a peripheral bodily network, where the nodes corresponded to each body part, and the weight as the cross-correlations between each pair of nodes (Ryu & Torres, 2017; Torres, Nguyen, et al., 2016a; Whyatt & Torres, 2017). Using these networks, we computed the modularity and cluster coefficients, which are measures that characterize the local connectivity (i.e., functional segregation).

2.2.4.2.1 Cluster Coefficient (CC)

Network degrees between a set of nodes form triangles, and the fraction of triangle numbers formed around each node is known as the cluster coefficient. This measure essentially reflects the proportion of the node's neighbors (i.e., nodes that are one degree away from the node of interest) that are also neighbors of each other (Watts & Strogatz, 1998). Here, we computed the average *intensity* (geometric mean) of all triangles associated with each node, where the triangles reflect the degree strength, and is computed as shown below, using an algorithm by Onnela, Saramäki, Kertész, and Kaski (2005). For comparison, we computed this coefficient for each condition and movement segment, and took the median cluster coefficient as the summarizing value.

$$C_i = \sum_{i \in N} \frac{t_i}{k_i(k_i - 1)} \quad \text{Eq 2.9}$$

N: set of all nodes (composed of 10 body parts)
C_i: cluster coefficient for node $i \ \ (i \in N)$
t_i: geometric mean of triangles links formed around node $i \ \ (i \in N)$
k_i: number of degrees (links) formed around node $i \ \ (i \in N)$

2.2.4.2.2 Modularity Togetherness (MT)

Modularity is another measure of functional segregation, but unlike the cluster coefficient metric, this is done by subdividing the nodes into groups, which is configured to maximally connect within each group, and minimally connect between groups (Girvan & Newman, 2002), using an optimization algorithms by Leicht and Newman (2008). Through this subdivision, each node is grouped to a module; and this is done for each movement segment within a single trial for all three conditions.

One disadvantage of the modularity metric, when used to assess connectivity patterns in repetitive trials, is that node participation is not always guaranteed to be within the same module. For example, the network in trials 1-3 may consistently show 3 modules, with a certain number of nodes participating in each. The identity of the nodes in module 1 of trials 1-3 may differ from trial to trial. As such, we developed the notion of togetherness by examining consistent node participation in module from trial to trial. If the pair of nodes belonged to the same module, we called the pair being *together*. This approach gave us the advantage to track the node's participation in modules in a more systematic way, so we can rank self-emerging (kinematic) synergies within the body part nodes. Essentially, the modularity togetherness metric computes the proportion of the pair of nodes being *together* across the entire set of trials, as such:

$$Modulairty\ Togetherness_{i,j} = \frac{1}{Tr}\sum_{i,j\in N}\frac{\delta_{m_i,m_j}}{2} \quad \text{Eq 2.10}$$

m_i: module containing node i $(i \in N)$
δ_{m_i,m_j}: 1 if $m_i = m_j$, and 0 otherwise
Tr: total number of trials

2.3 Results

2.3.1 Standardized MMS Amplitude data (Spatial Domain)

As a first set of analysis, standardized spike amplitudes extracted from the angular acceleration data from each body part were aggregated across all trials, and arranged by different movement segments and different dominance side. The fitted histograms of these standardized spike amplitude data show an overall pattern, where a higher level of deliberate control (of moving the arm to complete the task) leads to higher noise-to-signal ratio (NSR) and higher mutual information (MI). Specifically, when an individual exerted motor control such as on the dominant side of the body and during a deliberate forward motion, NSR and MI was the highest. Conversely, when an individual did not deliberately intend to move the arm, as exhibited on the non-dominant side and during a spontaneous retracting motion, NSR and MI was the lowest. This relationship between NSR and MI can be appreciated in **Figure 2.4A, B**.

Examining this outcome for each participant, as shown **Figure 2.4C**, the median MI is higher on the dominant side than the non-dominant side for all participants, with statistical significance on 7 participants and one approaching statistical significance (**Table A 1**). Also, when comparing the median NSR between dominant and non-dominant side, all participants have higher values on the dominant side, with all but one showing statistical significance (**Table A 3**). When we examine the MI and NSR difference between dominant and non-dominant parts, separately for deliberate and spontaneous motion, we also find that participants exhibit a wider

difference for both MI and NSR during their deliberate motions, and show higher statistical significance (**Table A 1, Table A 3**).

Comparing between deliberate and spontaneous motions, as shown in **Figure 2.4D**, the median MI is higher during deliberate motions than spontaneous motions for all but one participant, and among those participants, 6 participants show statistical significance and one approach statistical significance (**Table A 2**). The median NSR is also higher during deliberate motions, and this is the case for all participants, with all but one showing statistical significance (**Table A 4**). When we examine the MI and NSR difference between deliberate and spontaneous motions, separately for the dominant and non-dominant side, we also find all but one participant exhibit a wider difference for both MI and NSR during their deliberate motions, and show higher statistical significance (**Table A 2, Table A 4**).

The distinctions that we observe from these findings, on how different levels of motor control (i.e., deliberate vs. spontaneous; dominant vs. nondominant) have separable stochastic and entropy characteristics allude to how the complex (brain/body) network of a healthy individual (with high cognitive-motor agency) transmits information so that the system as a whole can perceive the consequence of the action that is performed at each moment, and eventually construct a model of the consequential variations of impending actions. This type of predictive model compensates for the inherent transduction and transmission delays in sensory processing, sensory integration and sensory-motor transformations. Under the present methodology we can characterize such compensations by estimating the impending consequences in a precise statistical inferential and theoretical information ways.

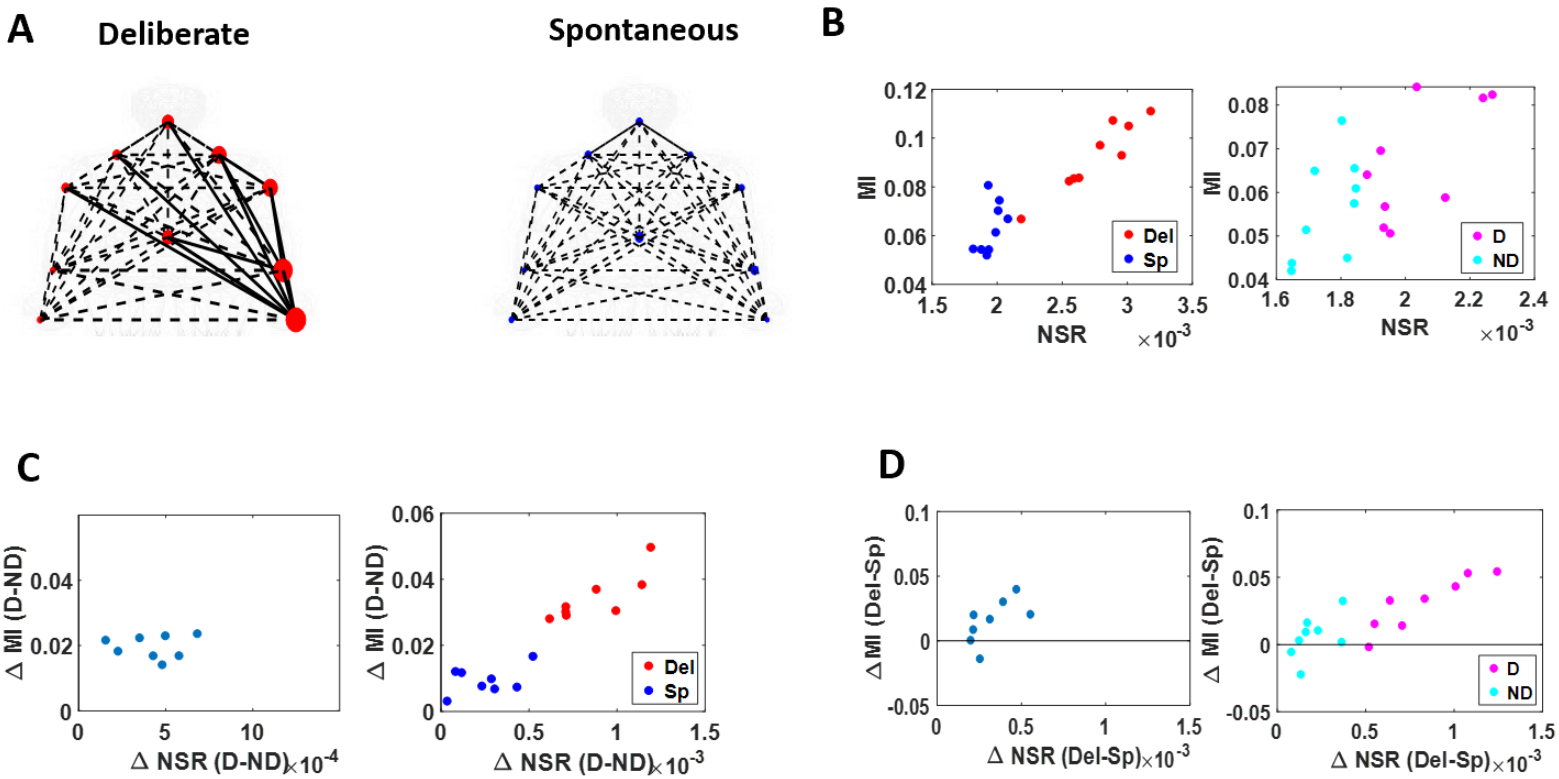

Figure 2.4. MI and NSR Comparison across different levels of motor control. (A) Mutual information (MI) and noise-to-signal ratio (NSR) of a right-handed representative participant. Mutual information (MI) was computed based on a set of histograms of angular acceleration standardized spikes across different pairs of body parts; and noise-to-signal ratio (NSR) was computed based on the fitted Gamma PDF of those histograms. MI is represented in line weight and NSR in node size, and both metrics are graphed in the same scale across different movement segment (i.e., deliberate and spontaneous segments). **(B) MI and NSR for different movement segment and dominance side.** Median of all MI and NSR values for each participant's different movement segments (left) and dominance side (right) are plotted. Generally, MI and NSR are higher during deliberate movement segment (Del; red) than during spontaneous segment (Sp; blue), and on the dominant side (D; pink) than the non-dominant side (ND; cyan). **(C) MI and NSR difference between dominant vs. non-dominant side**. Left panel shows the MI and NSR median

difference between the dominant and non-dominant side for each participant, denoted as a single marker. In general MI and NSR is higher on the dominant side for all participants. Right panel shows the MI and NSR median difference between the dominant and non-dominant side for deliberate motion (Del; red) and spontaneous motion (Sp; blue). When the difference between the dominant and non-dominant side is examined separately for each motion segment, the difference is wider during deliberate motion segments (Del; red) than during spontaneous motion segments (Sp; blue). **(D) MI and NSR difference between deliberate vs. spontaneous movement segment.** Left panel shows the MI and NSR median difference between the deliberate and spontaneous motion segment for each participant, denoted as a single marker. In general, NSR is higher during deliberate motions than spontaneous motions for all participants, and MI is higher during deliberate motions for most participants. Right panel shows the MI and NSR median difference between deliberate and spontaneous motion segment on the dominant side (D; pink) and non-dominant side (ND; cyan). When the difference between the two motion segments is examined separately for different dominance side, the dominant side (D; pink) shows a wider difference for both MI and NSR than the non-dominant side (ND; cyan).

2.3.2 Maximal Cross-Correlation data (Temporal Domain)

As a second set of analysis, for each trial, cross-correlation was performed across all pairs of body parts' angular acceleration time series, and the maximal correlation values were extracted to represent a matrix, where the maximal correlation denoted the connection strength. Borrowing methods from the network connectivity toolbox in MATLAB (Rubinov & Sporns, 2010), we designed matrices of pairwise cross-correlation as input, and two metrics of functional segregation were examined – cluster coefficient (CC) and modularity togetherness (MT). Overall, a higher level of cognitive load led to higher MT and CC; and a higher level of deliberate control led to higher CC (**Figure 2.5A,B**).

Comparing between high and low cognitive load conditions, the median MT is higher during high cognitive load than during low cognitive condition for 6 (out of 8) participants, and among those participants, 5 participants show statistical significance (**Table A 5**). The median CC is also higher during high cognitive load condition, and this is the case for all participants, showing statistical significance (**Table A 6**). When we examine the MT and CC difference between high and low cognitive load conditions, separately for deliberate and spontaneous motions, we find that the difference for both MT and CC are wider during spontaneous motions, with higher statistical significance. Note, the input matrices (maximal cross-correlation) for computing CC and MT for the entire pointing segment (**Figure 2.5C-left**), and for the separate deliberate and spontaneous segment (**Figure 2.5C- right**) are not additive in their relations. That is, the maximal cross-correlation for the entire pointing segment is not necessarily a value in between those values observed for the deliberate segment and the spontaneous segment. For that reason, the range of MT and CC values for the entire segment, would not necessarily fall between the range of values for the two separate movement segments.

For each participant, the median MT is higher during deliberate motions for 3 participants and higher during spontaneous motions for the other 5 participants, and all but two show no statistical significance (**Table A 7**). The median CC, on the other hand, is higher during deliberate motions for all participants, and all show statistical significance (**Table A 8**). When we examined the MT and CC difference between deliberate and spontaneous motions, separately for high and low cognitive load conditions, we find a difference in the MT pattern, such that under the low cognitive load condition participants generally show little difference between deliberate and spontaneous motions, and under the high cognitive load condition they generally show a lower MT during deliberate motions, with 5 people showing statistical significance. Also, the CC difference between the two motion segments is generally wider with higher statistical significance under the low cognitive load condition.

The distinctions that we observe from these findings, on how different levels of motor control (i.e., deliberate vs. spontaneous) and cognitive load (i.e., high vs. low) have separable network connectivity patterns, illustrates how the network topography transforms with the changes in one's cognitive processes. As we observe and characterize the changes in the patterns of healthy individuals (with high cognitive-motor agency), we gain knowledge on the types of network topography that embodies high agency. Also, given that these data are from healthy individuals, these can later be used to buildnormative criteria to measure the departure from typical levels of agency for other patient populations.

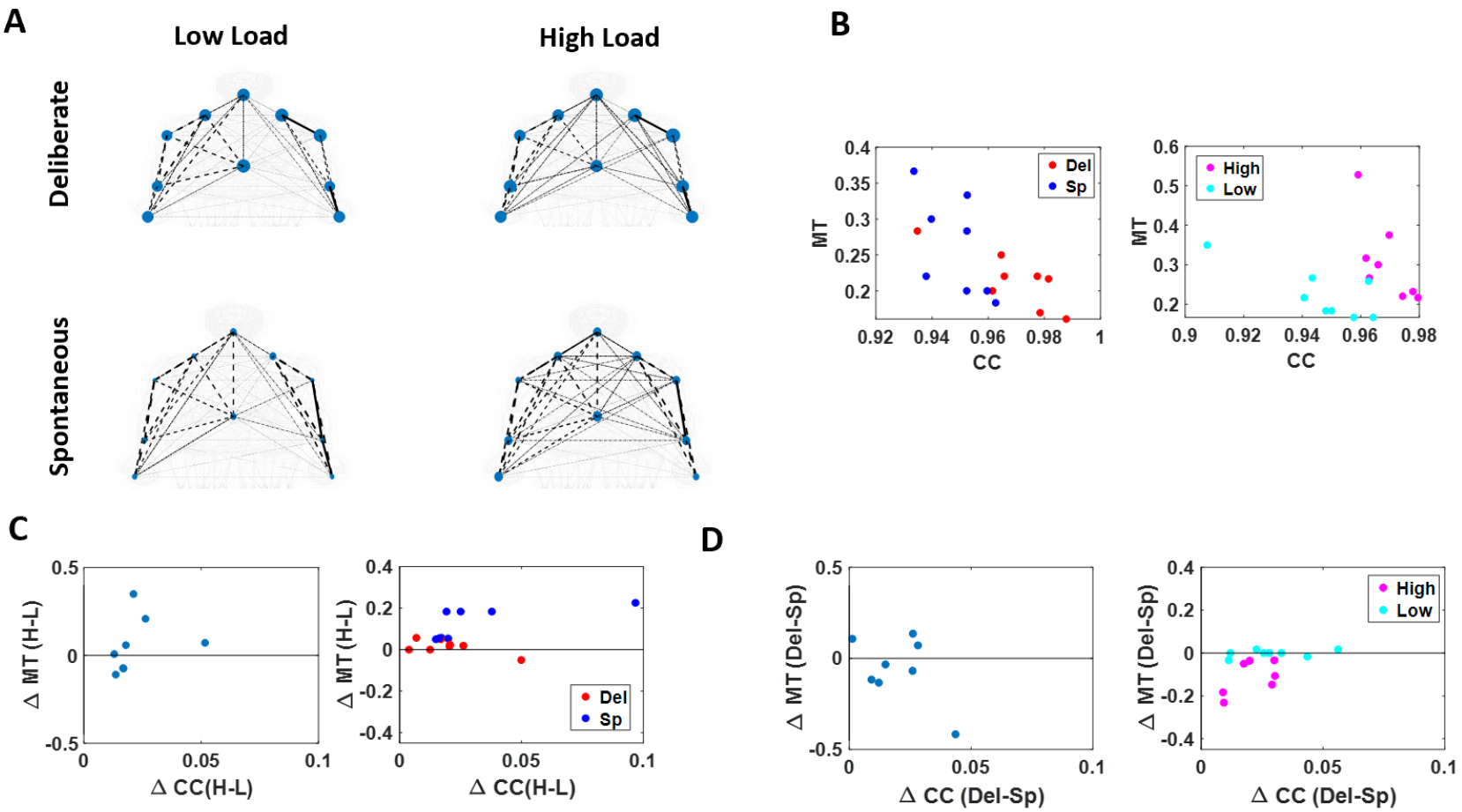

Figure 2.5. Modularity togetherness (MT) and cluster coefficient (CC) comparison across different levels of motor control and cognitive load (A) MT and median CC of a representative participant. MT and CC are visualized, where the MT is represented in the line weight and CC in the node size, during low cognitive load condition (left) and high cognitive load condition (right), and during deliberate movement segment (top) and spontaneous movement segment (bottom); both metrics are graphed in the same scale across different cognitive load condition and movement segment. **(B) MT and CC across different cognitive load conditions and movement segment.** Median of all MT and CC values for each

participant's different movement segment (left) and cognitive load conditions (right) were plotted. CC is higher for deliberate movement segment (red) than spontaneous movement segment (blue), and higher during high cognitive load (pink) than low cognitive load (cyan). **(C) MT and CC difference during high vs. low cognitive load condition.** Left panel shows the MT and CC median difference between high and low cognitive load conditions for each participant, denoted as a single marker. In general, CC is higher during high cognitive load condition. Right panel shows the MT and CC median difference between high and low cognitive load conditions during deliberate motions (red) and spontaneous motions (blue). Overall, the difference for both MT and CC is more pronounced during spontaneous motion than during deliberate motion. **(D) MT and CC difference between deliberate vs. spontaneous motion segment.** Left panel shows the median ΔMT and ΔCC between deliberate motions and spontaneous motions for each participant, denoted as a single marker. Aggregating across all three cognitive load conditions, ΔMT is found to have mixed result when comparing between the deliberate and spontaneous motion segment; on the other hand, the ΔCC has a higher value during deliberate motion than during spontaneous motion. Right panel shows the median ΔMT and ΔCC between deliberate and spontaneous motions during high cognitive load (pink) and low cognitive load condition (cyan).When comparing the difference between cognitive load conditions, MT is generally higher for spontaneous motion when under high cognitive load condition, and similar between movement segments under low cognitive load condition. The ΔCC between the movement segments shows to be slightly wider during low cognitive load condition than the high load condition.

2.4 Discussion

In this study, we focused on examining the interconnectivity of kinematic signals (i.e., signals as part of the somato-sensory-motor streams flowing between the peripheral and the central nervous system) across different parts of the body – both active (e.g., dominant arm; actively engaging in the task) and less active (e.g., non-dominant side; supportive of performing the task). By observing the changes in connectivity due to varying levels of cognitive load and motor control, we demonstrated the interactive nature of biophysical signals that flow across the brain and the body. By assessing the system of healthy individuals, particularly regarding the ranges and patterns of connectivity across their body, we are able to understand how the complex system of individuals with high agency communicate within the system. In this sense, we offer a first characterization of agency as defined in this thesis. Here, we borrowed concepts from stochasticity, information theory and network analysis, and adapted them to apply such analyses to the kinematic signals. We characterized such interactions and abstract concepts in an embodied manner. (**Figure 2.6**)

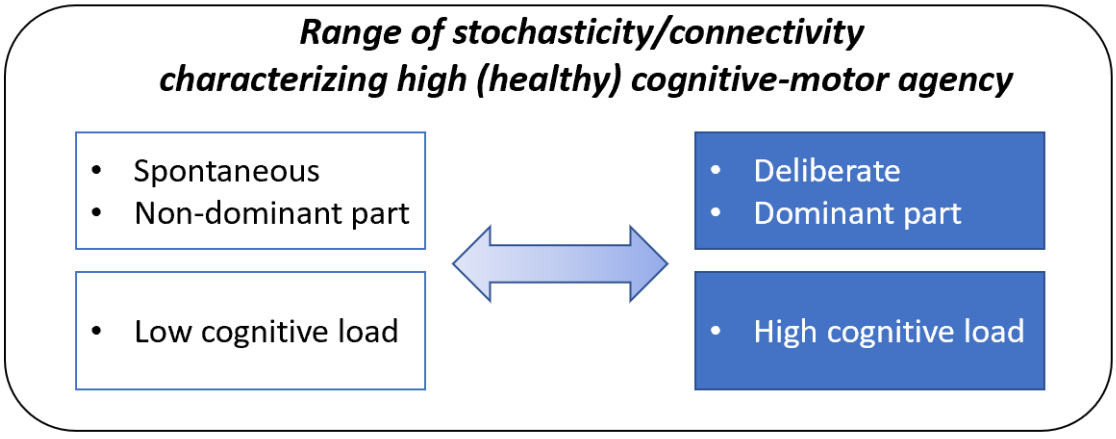

Figure 2.6. Schematic overview of the study

Overall, when we examine the spatial domain of the kinematics signal (i.e., standardized spike amplitude of angular acceleration), we find that **higher motor control (represented during deliberate motions and on the body's dominant side) is characterized by higher NSR and informational dependency (MI)**. Here, NSR can be a misnomer, as it seems to imply the presence of useless noise. However, in this context, NSR represents the variability of the biophysical signals, and large variability implies a signal ranging on a wide scale with flexibility. For that reason, when we conceptualize the spatial network of the kinematics signal, we can visualize the active and controlled parts of the body to be exchanging a wide range of information while keeping its range of stochasticity flexible as possible.

When we look at the temporal domain of the signals (i.e., cross-correlation of angular acceleration), and observe the functional segregation of the participant's kinematics network represented by CC, we find higher segregation under higher motor control (represented during deliberate motion segment) and higher cognitive load conditions. In this context, a node with high CC can be visualized as a well-connected hub within a network. As such, **when more cognitive processes are involved (as in experiencing higher cognitive load or exerting more control on motor action), we find a pattern where a set of body parts are organized in a more concentrated synergistic manner.**

MT is also a measure of functional segregation, representing small-world organizations (subgroups) within a network. Higher MT implies a concentrated group as a whole with less small-worlds (subgroups) within a network; conversely, lower MT implies a more distributed network with multiple subgroups. Under this measure, there were mixed results across participants when comparing across different motor segments and cognitive load conditions. However, when these comparisons were further subdivided, we find that during spontaneous motions, different levels of cognitive load are better characterized, such that the network is

more distributed under low cognitive load conditions. Also, during high cognitive load condition, different levels of motor control are better characterized, such that the network is more distributed during deliberate motor segments.

Aside from the properties of a healthy individual's (i.e., of high cognitive-motor agency) network connectivity mentioned above, it is worth to highlight several merits of this study. First, the study remarkably demonstrates how the peripheral signals can broadcast cognitive processes so clearly, thus suggesting the usage of motor activities as a proxy of the brain activities, when we examine through the lens of kinesthetic reafference (as the variability of kinesthetics becomes a content of information). Indeed, pointing motions have commonly been used in motor control studies, starting with experiments involving movements constrained to a plane and allowing only 2 joints to rotate and translate the hand to the target (Flash & Hogan, 1985; Uno, Kawato, & Suzuki, 1989), to experiments within a more naturalistic, unconstrained setting (Flanders, Daghestani, & Berthoz, 1999; Flanders, Pellegrini, & Geisler, 1996; Torres, 2011). The novelty of this study is in capturing the relationship between motor control and cognitive load across the body, as it captures the moment by moment changes in the internally generated activities of the nervous systems during simple pointing tasks, while participants process different types/levels of cognitive processes. This is a new embodied approach of studying cognitive phenomena, which is an improvement from the old methods of relying on an external observant. Furthermore, by segmenting motions as deliberate and spontaneous, the study provides a new way to see how the system inherent of healthy/high agency is able to perceive its cause (deliberate motion) and effect (spontaneous motion) effectively. Indeed, we visually perceive the difference between dominant and nondominant side of the arm, and the deliberate and spontaneous segments of actions. However, the data we analyzed are not visible to the naked eye, as they are minute fluctuations (MMS) of the kinematic signal. Hence, it is

illuminating to see how such miniscule type of biophysical signal is informative of the cognitive processes unfolding within the span of an experimental session. Such information of motor action is communicated to the brain by kinesthetic channels, and these re-entrant information (reafference) offers a new way to monitor the levels and quality of kinesthetic sensory feedback that the brain may be experiencing from moment to moment. Through the connectivity patterns of these kinematic signals, we were able to illustrate the communicative pattern that occurs within the system; particularly in the presence of high agency.

In conclusion, the study describes how different body parts and movement segments respond differently to changes in cognitive processes, revealing the different movement classes that self-organize and dynamically change under different contexts. We introduced an experimental paradigm and analytical methods that characterized such topographic organizations of the kinematics signals, and provided novel means to study how the body connectivity broadcasts different degrees of cognitive processes and of motor control. Furthermore, this approach to embodied cognition offers new avenues to bridge the currently disconnected fields of motor control and cognitive phenomena.

In this study, we examined the properties of a complex system characteristic of high agency. In the next study, we compare this with systems of lower agency (exhibiting compromised motor control), to understand how the connectivity patterns differ across varying levels of cognitive-motor agency.

3 Impact of entrained breathing on the nervous systems

3.1 Introduction

In the study from Chapter 2, we learned how complex systems of high agency (of healthy individuals) exhibit cognitive processes with varying degrees of cognitive demand as reflected by the topography of their kinematics networks. We uncovered the range of stochasticity and connectivity of biophysical signals within the peripheral nervous system (i.e., kinematics), clearly broadcasting different levels of motor control and awareness, and well-defined levels of cognitive load. In addition to the bodily kinematics, there are other biophysical signals that can be registered, and thus examined as integrative parts of the physical body, conceived as a complex non-linear dynamical system. Moreover, the act of control is not limited to the motor domain, as it includes other domains as well (e.g., respiratory control in the autonomic domain, and attention in the cognitive domain).

In the current study, we attempt to extend our analysis to the biophysical signals generated by the central nervous system (CNS), peripheral nervous system (PNS), and the autonomic nervous system (ANS), and explore a different kind of control – entrained breathing.

Breathing is an autonomic process that occurs beneath our awareness, as with other autonomic processes of the ANS (e.g. processes within blood vessels, stomach, bladder). However, breathing can be brought up to awareness and deliberately controlled by voluntarily pacing the time point of inhaling and exhaling (Herrero, Khuvis, Yeagle, Cerf, & Mehta, 2017; Sasaki & Maruyama, 2014). The time points can be cued through sounds that occur with discernable periodicity, such as that of a metronome. Such cues can spontaneously entrain one's biophysical rhythms, by having the person naturally behave while passively hearing a metronome beat; and the cues can also entrain the biorhythm through the person's deliberate effort, where the person would actively synchronize the breathing rate to the pace of the metronome. Indeed, if we had to attend to our breathing and consciously maintain a fixed pace all the time, it would be cognitively taxing. This leads us to question - what connectivity pattern

would be exhibited when effort is exerted to consciously entrain (pace) the breathing rate to a fixed beat, as opposed to when no conscious effort is exerted to such entrainment (when you are passively hearing a fixed beat) ?

This question motivated us to study this in the context of agency, since we can examine the direct impact of top-down conscious control (exerted by the CNS) on the different nervous system (ANS and PNS). In particular, we can examine the change in the connectivity due to a top-down control (when one deliberately paces the breathing rate) and a bottom-up/spontaneous control (when one passively hears the metronome beat while breathing naturally). In the end, by comparing the range of connectivity patterns between individuals with different levels of cognitive-motor agency - neurotypical population (NT) vs. patient population (with ASD), as the patterns evolve across conditions of different entrainments, we may be able to discern the difference in characteristics of complex systems exhibiting different levels of cognitive-motor agency. Furthermore, this characterization of agency in the context of healthy vs. compromised systems can provide a range of network connectivity patterns, that would inform us how much the system of those with neurological disorders departs from the normative healthy system.

To do this, we first observe an individual naturalistically walk for a fixed amount of time as a baseline; and add in a metronome sound in the background without instructing the person to do anything. This allows us to observe how naturally breathing, while passively hearing the metronome sound, may affect the temporal dynamics across bodily signals (metronome condition; spontaneous breathing). Lastly, upon instructing the person to breathe at the tempo of the metronome, we characterize deliberate entrainment of one's breathing rate to the metronome's beat. Then we ask how this voluntary state of breathing to a rhythm affects the bodily signals (paced breathing condition; deliberate breathing).

We note, however, that the implementation of such a study is a challenge, particularly because we aim to record the signals from multiple nervous systems in tandem. Since there are no research devices that allow us to simultaneously register multiple signals from different nervous systems (specifically, the cortical signals of the CNS, kinematics signals of the PNS, and heart signals of the ANS), it is a challenge to record these in tandem, and furthermore, to analyze them as a single datatype (as opposed to analyzing them separately). Some studies have made such an attempt to record multiple modes of signals in tandem (e.g., (Bulea, Kilicarslan, Ozdemir, Paloski, & Contreras-Vidal, 2013; Bulea, Kim, Damiano, Stanley, & Park, 2014; Butkevičiūtė et al., 2019; Cheron et al., 2016; Nordin, Hairston, & Ferris, 2019; Snyder, Kline, Huang, & Ferris, 2015)) but most do not offer the means to analyze these multimodal data as a single datatype. To complicate the matter, the cortical signals obtained by the electroencephalography (EEG) is inherently loaded with artefacts and extraneous noise, which is why the majority of EEG studies require the participants to stay sedentary with minimal movements and perform numerous repetitive trials to obtain an averaged dataset (e.g., (Luck, 2012)). However, EEG is the only non-invasive brain imaging device that is light enough to use during naturalistic actions with good time resolution. Indeed there have been few studies that attempted to record the cortical signals within a naturalistic task such as gait (e.g., (Gwin, Gramann, Makeig, & Ferris, 2011; Jung et al., 2000)) but they nevertheless constrain the motions to some extent, by e.g., walking on treadmills, and perform artificially repetitive tasks to obtain an average. These approaches where bodily motions are constrained, defy the overarching goal of our study, where we aim to observe the naturalistic behaviors dynamically unfolding.

In the following section, we describe the experimental and analytical methods that we employed to partially overcome these challenges. Notably, we integrate signals of different

modes into a single datatype, by incorporating the MMS train (see section 2.2.4.1) to represent multiple types of signals into a standard unitless representation of fluctuations in amplitude and timing. We then present the findings on how entraining one's breathing pace impacts the biophysical signals, and how they differ between individuals with different cognitive-motor agency (i.e., between healthy individuals and those with Autism Spectrum Disorder (ASD)).

3.2 Methods

3.2.1 Participants

A total of 13 participants partook in this study. Of those, 6 undergraduate students (2 males and 4 females) between the ages 18 and 20 were recruited from the Rutgers human subject pool system, and received credit for their participation. 3 patients with a medical diagnosis of Autism Disorder (2 males and 1 female) between the ages 13 and 18 were introduced to this study after participating in a related study within the Sensorimotor Integration lab, and received $25 in compensation for their participation (**Table A 9**). 4 researchers from the Sensorimotor Integration Lab (1male and 3 females; including the author) between the ages 22 and 35 also participated in this study as volunteers and received no compensation. All (but one) were right-handed, and all had normal or corrected-to-normal vision. All provided informed consent, which was approved by the Rutgers University Institutional Review Board.

3.2.2 Instrumentation and Data Preprocessing

Participants wore three different types of wireless sensors to capture the biophysiological signals from the central (CNS), peripheral (PNS), and autonomic nervous system (ANS), with electroencephalography (EEG), inertial measurement units (IMU) and electrocardiogram (EKG) respectively.

Cortical signals from the CNS were captured with a wireless EEG device (Enobio, Barcelona, Spain) at 500Hz sampling rate with 32 sensors positioned across the scalp, and the wireless device positioned on the back of the participant's head. These signals were recorded and preprocessed with 60Hz AC line noise removal using Neuroelectrics software (Enobio, Barcelona, Spain). Further preprocessing was done in Matlab (Release 2015b, The MathWorks, Inc., Natick, Massachusetts)-based toolbox EEGLab (Delorme & Makeig, 2004) and PrepPipeline (Bigdely-Shamlo, Mullen, Kothe, Su, & Robbins, 2015). Through the PrepPipeline toolbox, channels were referenced via a robust average reference procedure, where channels were iteratively referenced to the average signal, while bad channels, such as those showing extreme amplitudes (deviation z-score exceeds 5) or lacked correlation with any other channel (correlation less than 0.4) were excluded and interpolated in this process.

Motor signals from PNS were captured with Opal IMUs (APDM Inc., Portland, OR) at 128Hz sampling rate, and were acquired with Motion Studio software (APDM Inc., Portland, OR). 10 opal IMUs were attached to the participant with Velcro belts on the following body parts – left and right wrist, left and right upper arm, left and right foot, left and right ankle, posterior trunk and anterior chest (**Figure 3.1**). From each of the ten sensors, linear acceleration (m/s^2), and magnetometer (μT), and temperature (°C) was registered, and for the purpose of this study, linear acceleration and magnetometer were mainly examined.

The heart signals from the ANS were obtained using a wireless Nexus-10 device (Mind Media, The Netherlands) and Nexus 10 software Biotrace (Version 2015B; Mind Media, The Netherlands) at a sampling rate of 256Hz. Three electrodes were placed on the chest according to the standardized lead II method, and were attached with adhesive tape (**Figure 3.1**). In a typical EKG data, there are a set of QRS complexes, and in this study, inter-beat-interval (IBI) was examined by extracting the time points of the R-peaks, which are commonly known as the

heart beat. R-peaks were detected and extracted by band pass filtering the EKG signals at 5-20Hz using Butterworth IIR filter at 2nd order. The range of the band pass filter was selected based on the finding that a QRS complex is present in the frequency range of 5-30Hz (Kathirvel, Manikandan, Prasanna, & Soman, 2011).

Within the study, we attempted to temporally co-register the cortical and motor signals to record and analyze in tandem. To do so, we used an open-source package Lab Stream Layer (LSL) where the signals were streaming in LSL on the same computer, and were timestamped with mouse clicks on the display screen of that computer. Because the motor and cortical signals were registered at different sampling rates, EEG signals were down-sampled to 128Hz, so that the two signals could be analyzed as a single datatype.

Note, it is common to reject time segments and a variety of motor artefacts within the EEG data; however, for the purpose of this study, we are mainly focused on understanding the continuous dynamical process that flows internally within an individual's brain and body, so eliminating a certain time segment would undermine that purpose. Also, because the participant is continuously moving, it is inevitable to find large amount of motor artefacts in the cortical signals. If we removed these artefacts, there would be very little signals left. Needless to say, the large amount of data obtained from this study makes it infeasible to visually inspect and hand-pick to remove those artefacts. It is possible to apply bandpass filtering to remove the influence of gross motor movement, but this would result in losing the delta band waves (<4Hz) within the cortical signals. For that reason, we decided to forgo such signal preprocessing, and assume that the cortical signals are inevitably and inherently mixed with motor signals (particularly reflecting the head and facial muscle movements) with varying degrees across time and spatial positions of the electrodes.

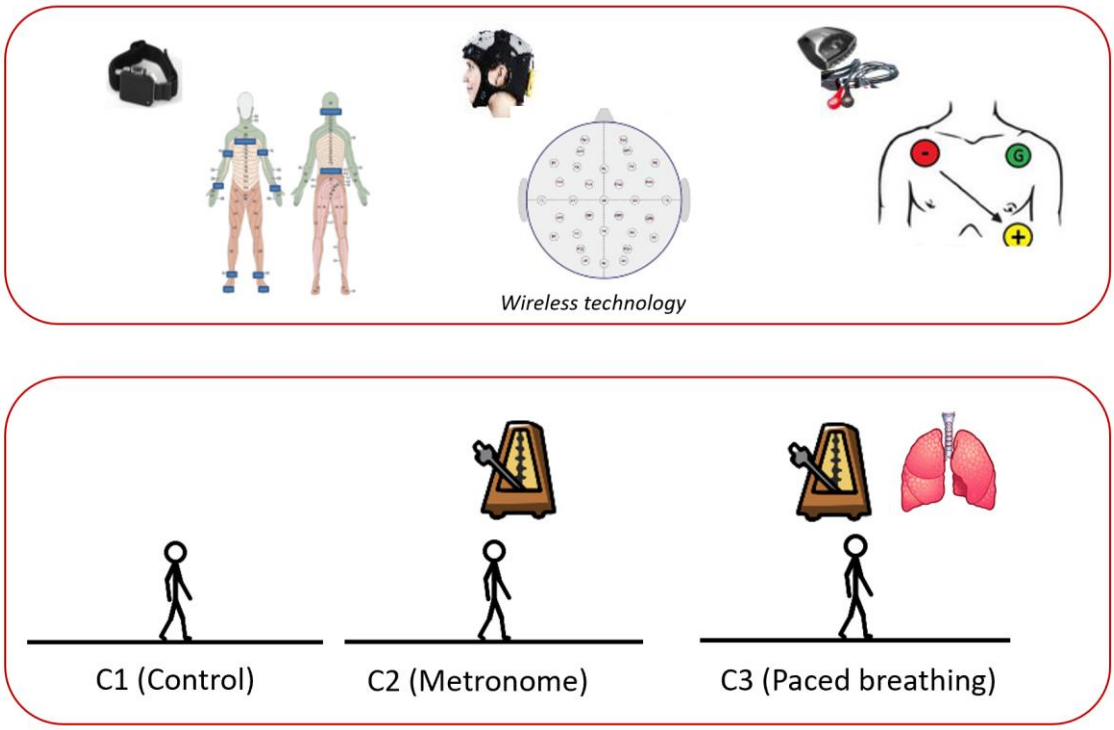

Figure 3.1. Experimental Paradigm (Top) Three modes of devices were used to register the biophysical signals – IMU accelerometer to capture motor signals, EEG to capture cortical signals, and EKG to capture heart signals. **(Bottom)** There were three conditions within the experiment. Under the control condition (C1), the participant naturally walked around the room; under the metronome condition (C2), the participant naturally walked around the room with the metronome sound playing in the background; under the paced breathing condition (C3), the participant walked naturally, while pacing the breathing rate to the metronome playing in the background.

3.2.3 Experimental procedure

The participant wore three different types of sensors - electroencephalography (EEG), inertial measurement units (IMU) and electrocardiogram (EKG). Once these sensors were calibrated, the participant was instructed to walk at their own pace for 10 minutes under three different conditions in a closed room. In the control condition (C1), the participant walked naturally for 10 minutes; in the second condition (C2), the participant walked naturally for 10 minutes while the metronome was beating in the background at 12 beats per minute. The metronome was set to play from a computer, and the volume was approximately 45 dBA. The

participant was notified of such metronome beats prior to starting condition C2, and was asked to consider it like background music and that he/she need not need change anything in the manner of their walking. In the third condition (C3), the participated walked for another 10 minutes as in condition C2, but paced the breathing rate to follow the metronome beat. Note, this breathing rate is slow and is known to provide therapeutic/calming effect to most individuals (Vaschillo, Vaschillo, & Lehrer, 2006). The setup of the experiment took about 30 minutes, and the walking tasks took about 40 minutes reflecting the optional breaks participants took between conditions.

This experimental paradigm was designed to examine the dynamical interactions occurring across the CNS, PNS, and ANS during naturalistic behaviors. The walking task was chosen as it requires the entire body to move in concert, thus providing abundant motor information, while allowing some restrictions (to walk in a confined space for a certain time) within a naturalistic setting. The paced breathing task in condition C3 was chosen to characterize the CNS activities when control is exerted on the autonomic processes that typically occurs automatically (i.e., breathing), and to characterize the change in ANS activities as a result of such control, all the while capturing the PNS activities that interact between the two systems (CNS, ANS). Here, the metronome condition (C2) was included as an intermediate step between conditions C1 and C3, allowing us to examine the spontaneous effect on the nervous systems when a constant beat is heard in the background.

3.2.4 Data analysis

Among the 13 participants' data, 5 participants data (comprised of 3 healthy controls and 2 patients with ASD) were fully synchronized between the three devices EKG, EEG, and IMU. For the remaining 8 participants, either the EEG or the IMU sensor failed to synchronize to EKG,

due to varying lengths of latency, or had software crashes in the middle of streaming. For that reason, the entire 3 modes of data (EKG, EEG, IMU) were analyzed as a single datatype for 5 people, and EKG data were analyzed as a single datatype for all 13 participants. For one ASD patient whose data was fully synchronized between the three modes of devices, the EKG signal crashed midstream during condition C1 and C2. For that reason, data for these two conditions were truncated and analyzed for the first few minutes when the signals were streaming successfully.

3.2.4.1 Stochasticity of Heart Signal (IBI)

IBI data extracted from the EKG signals were plotted as a histogram, and the stochastic characteristics were compared across conditions and across participants. In particular, because the histogram of IBI's showed to a good fit to the Gamma PDF (Ryu & Torres, 2018), the scale parameter of the Gamma PDF (i.e., NSR; see section 2.2.4.1.1 Noise-to-Signal Ratio) was compared across conditions and participants. In addition, to compare the stochastic change across conditions, mutual information (MI) of the IBI histograms between conditions were quantified (see section 2.2.4.1.2 Mutual Information (MI)) to understand the change in IBI stochasticity when different tasks were performed by the participant.

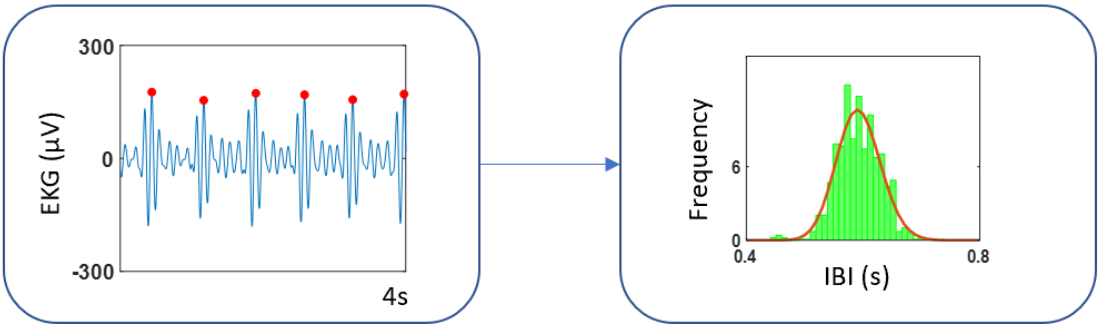

Figure 3.2. Analyzing the stochasticity of heart signal (IBI) (Left) EKG waveform sample. Within the EKG waveform are QRS peaks, where the R-peaks are denoted by the red nots. The time

between the red dots are inter-beat intervals (IBI). **(Right)** Histogram of IBI is fitted to a Gamma PDF to characterize the stochasticity of one's heart signals.

3.2.4.2 Cross-Correlation between EEG sensors

As a second set of analytics, for each 32 EEG sensor data, the sensor time series were normalized to a value between 0 and 1, by subtracting the minimum value of that sensor, and dividing it by the range of that sensor data as such:

$$\text{Normalized data} = (\text{Raw data} - \text{Min}_{\text{Raw data}}) / (\text{Max}_{\text{Raw data}} - \text{Min}_{\text{Raw data}}) \quad \text{Eq 3.1}$$

Then, these normalized EEG sensor data were segmented by the time segment of each IBI (i.e., time between two consecutive R-peaks). For each IBI segment, cross-correlation between all normalized 32 EEG sensors were computed, yielding a matrix of maximal cross-correlation values. Then, median of each matrices (i.e., cross-correlation values between all pairs of EEG sensors) were computed and plotted on a parameter space, where the x-axis represents the sequential order of IBI segment, and y-axis is the median cross-correlation value between all pairs of EEG sensors during that IBI segment. This depiction provides a dynamical characterization of the change in relations among the EEG signals. Note, we explored the change in cross-correlations between fixed time segment (instead of IBI segments), and with motor signals such as linear acceleration and magnetometer data (instead of EEG signals), but found the EEG signals per IBI segment to be most informative in portraying the dynamical changes across conditions and participants. (**Figure 3.3**)

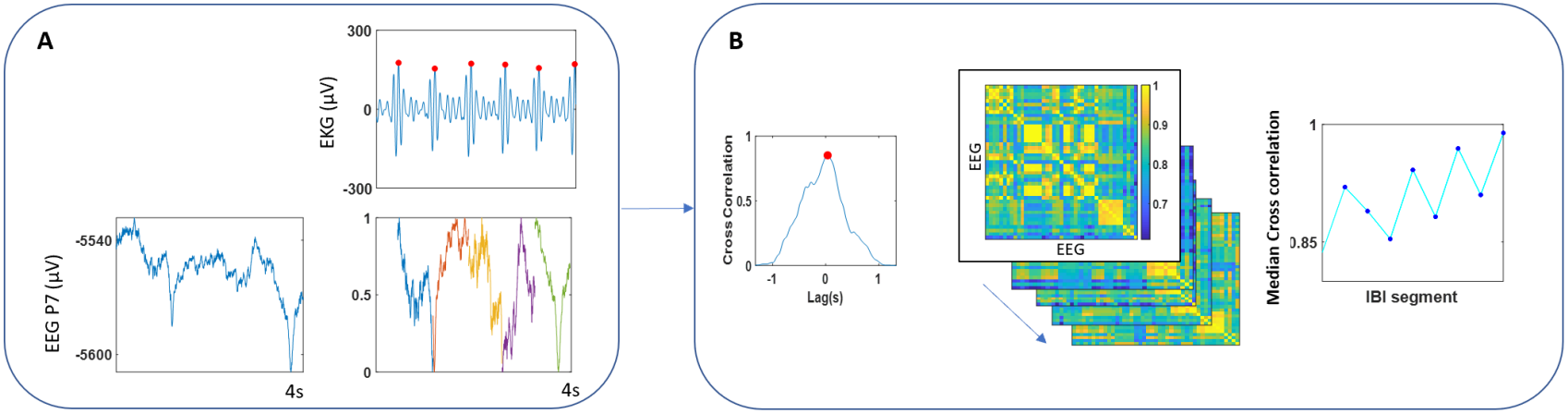

Figure 3.3. Analyzing the cross-correlations between EEG sensors. (A) For each EEG sensor waveform, the time points of R-peaks from the EKG timeseries were extracted, and accordingly, EEG sensor waveforms were segmented by each IBI segment. **(B)** For each IBI segment, cross-correlation was computed for all pairs of EEG sensor waveforms. To examine the dynamical change of the connectivity across time (i.e., IBI segment), the median cross-correlation value per IBI-segment was computed and plotted.

3.2.4.3 Mutual Information (MI) between EEG, Acceleration, and Magnetometer

From the time series obtained from the 32 channels of EEG signals, along with 10 body parts' linear acceleration and magnetometer data, the timing of spikes were extracted. From the 52 sets of time series (composed of 32 EEG data, 10 linear acceleration, and 10 magnetometer time series), inter-spike intervals (ISI) were computed in frame unit at 128Hz. Histograms of the ISI were constructed as single probability distributions $P_X(x)$, and with 21 sampling bins set to range from 2 to 128. This bin size is a close number to the sampling bin size if Freedman-Diaconis binning rule (Freedman & Diaconis, 1981) was applied. Note, because the sampling rate of these data are 128Hz, we discarded ISI values that exceed 128 (frame), as this corresponds to data with frequency less than 1Hz, which were deemed an outlier (z-score > 5). Also, because signals with frequency beyond 64Hz would be noisy (i.e., above the Nyquist rate), we also discarded ISI values less than 2 (frame). Joint probability distributions $P_{XY}(x, y)$ for a pair of the ISI histograms could not be empirically determined, as these data do not occur simultaneously. For that reason, the joint probability distribution was estimated by randomly sampling a pair from each histogram's ISI and constructing a joint histogram from these sampled pairs. Using the estimated joint probability distributions $P_{XY}(x, y)$, along with the empirical single probability distribution $P_X(x)$, the mutual information I_{XY} was computed, and this process was repeated 100 times. The median of the 100 estimated mutual information I_{XY} values was then determined as the final value. The final MI values were then compared across different pairs of sensor categories (e.g., pairs comprised of 2 EEG sensors; pairs comprised of 1 EEG sensor and 1 body part's acceleration; pairs comprised of 1 EEG sensor and 1 body part's magnetometer), and across the three conditions (**Figure 3.4**).

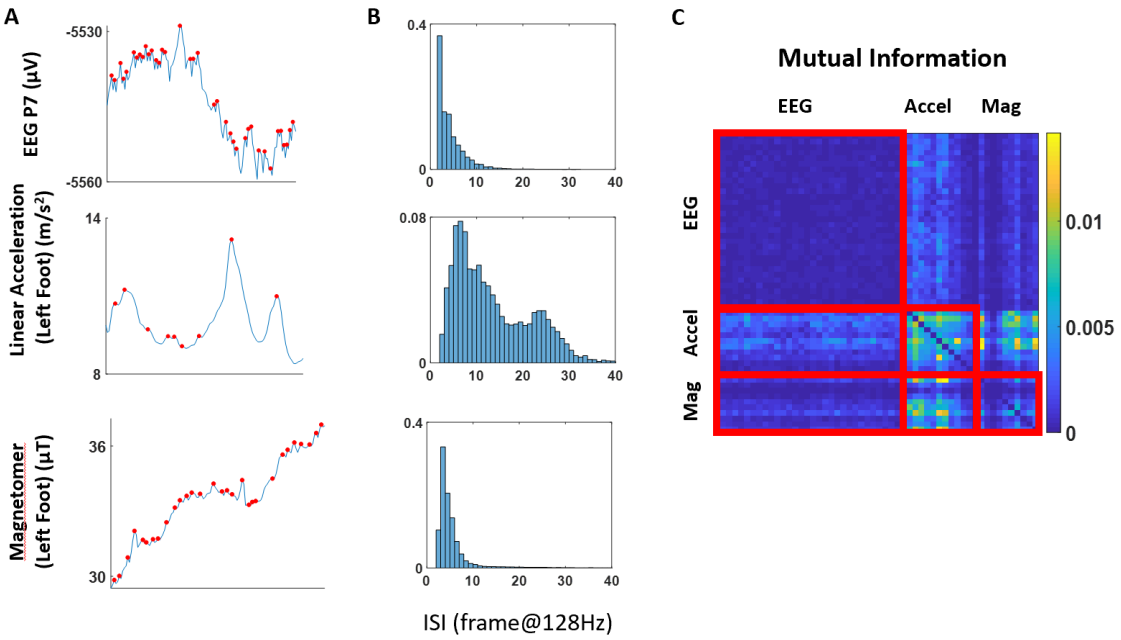

Figure 3.4. Analyzing mutual Information (MI) between EEG, Acceleration, and Magnetometer data (A) The timing of the spikes within signals obtained from EEG (top), accelerometer (middle), and magnetometer (bottom) data were extracted. **(B)** Histogram of time between spikes (ISI; inter-spike interval) were plotted for all sensor signals. **(C)** MI was computed from all pairs of ISI histograms. Because the distribution of the histograms vary across different modes of signals (as shown in **(B)**), the median MI of different signal categories were compared separately across the three conditions.

3.3 Results

3.3.1 Stochasticity of heart signals (IBI)

The IBIs were gathered and compared across the three conditions for all participants, and histograms were constructed to fit a Gamma PDF. The fitted Gamma parameters along with the 95% confidence intervals are shown in the **Figure 3.5A** for all participants. For most participants, stochastic parameters of their IBIs are separable across the three conditions, and for all participants, control (C1) and paced breathing (C3) conditions are separable by 95% confidence interval. In particular, when participants pace their breathing rate to 12 bpm (C3), the IBI stochasticity for all but one have a higher scale and lower shape parameters than when

they breathe at their own natural pace (C1); that is, the IBI PDF tend to have a wider and less kurtotic shape, exhibiting a larger variability in the IBI values (**Figure 3.5B**). Noticeably, one participant (P06) that does not show this pattern is a female patient with ASD, who instead shows a narrower range in IBI values when paced breathing (C3) is performed, as shown by its lower scale and higher shape parameter in its fitted Gamma PDF.

When the fitted Gamma parameters of IBI histograms are compared across all participants for C1 condition, ASD patients tend to have a higher scale (NSR) and lower shape parameters than NT as shown in **Figure 3.5C**. That is, their IBI PDFs tend to be wider in shape with larger variability in their IBI values. In order to understand how much stochastic changes are observed across the three conditions, mutual information was computed between the histograms of condition C1 and C2 (MI1), and between condition C1 and C3 (MI2). In this context, higher MI values imply that the IBI variability from later conditions (C2 or C3) are *dependent* to the past IBI variability (condition C1), as there is more information dependency to the past. The 3 ASD patients exhibit an overall higher MI than their counterpart NT participants, illustrating a stronger dependence of IBI stochasticity across tasks. Moreover, participants who tend to have a larger MI in their IBI stochasticity between condition C1 to C2, also tended to have a larger MI between conditions C1 to C3; and vice versa (**Figure 3.5D**).

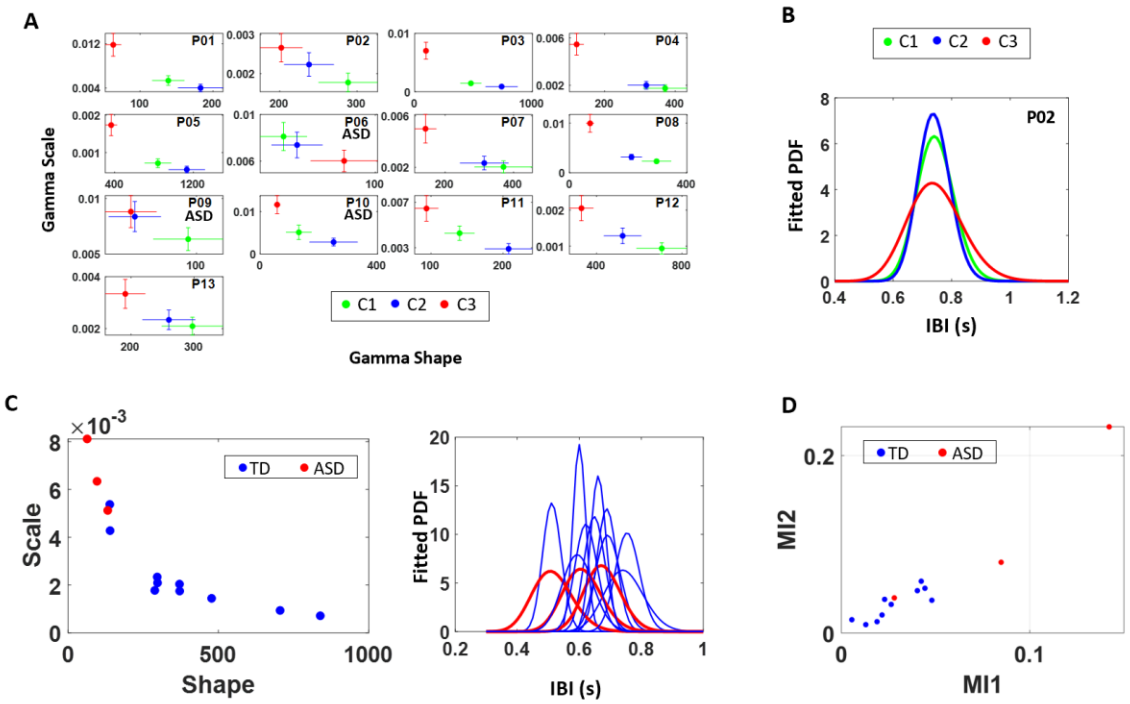

Figure 3.5. Stochasticity of heart signals (IBI) (A) Fitted Gamma parameters plotted on the Gamma parameter plane for each participant (subplot) for each condition (marker color). Most participants show a high scale and low shape parameter value during the C3 (paced breathing) condition with the exception of one ASD participant (P06). **(B)** Fitted PDF of a typical healthy participant's IBI distribution. The Gamma PDF of a high scale and low shape parameter is characterized by a wide and flat shape (red) than a PDF with low scale and high shape parameters (green). **(C)** Comparison of stochasticity between ASD patients and healthy individuals during condition C1. Noticeably, ASD patients (red) showed a high scale and lower shape parameter in their fitted IBI distribution, characterized by a more flat and wider PDF. **(D)** Change in stochasticity across conditions. The change was characterized by MI between IBI distributions from two conditions. X-axis (MI1) denotes MI between conditions C1 (control) vs. C2 (metronome), and y-axis (MI2) denotes MI between conditions C1 (control) and C3 (paced breathing). Overall, there is a larger change in the stochasticity between conditions for ASD patients (red) compared to the healthy participants (blue).

The stochastic changes across conditions exhibited in **Figure 3.5** imply that the different tasks performed in conditions C2 and C3 influence IBI. However, because these tasks were performed sequentially at different times, the changes may also be due to the natural variability inherent in the signals. In order to see whether the change in stochasticity is due to the inherent variability, regardless of the tasks performed in different conditions, the first and last 200 IBIs

within the same condition were extracted, fitted to the Gamma PDF, and plotted on the Gamma parameter space with 95% confidence intervals. As shown in **Figure 3.6**, we find that indeed the IBI stochasticity varies across time within the same condition, showing that the dynamical changes are due to both inherent variability of the signal and the different tasks performed. Moreover, given the little separation shown between conditions C1 and C2, as shown in the large overlap of the fitted Gamma parameters for these conditions, we can infer that the stochasticity change from condition C1 to C2 is influenced by the inherent variability of the heart signal, relatively more so than the changes from conditions C1 to C3 .

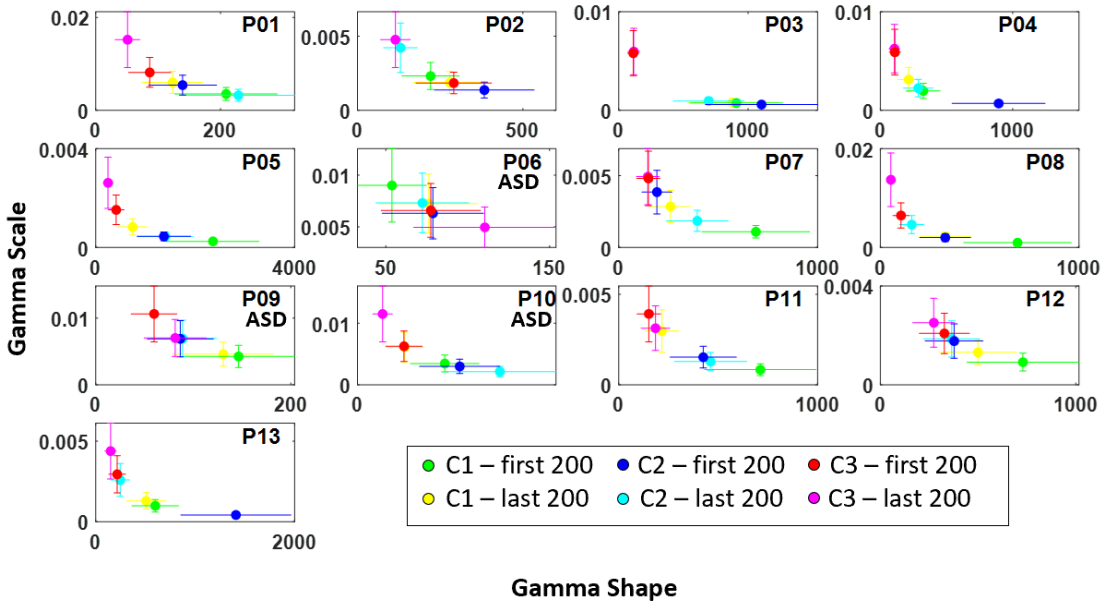

Figure 3.6. Fitted Gamma parameters plotted on the parameter plane For each participant (subplot), and for each three conditions, the first 200 IBI and the last 200 IBI within each condition were fitted to a Gamma PDF to see how the IBI stochasticity varies due to factors that are not relevant to the experimental variable (task required by each condition). As a general trend, the C3 condition tends to preserve its position on the parameter plane (red, magenta); however, the stochastic difference between C1 and C2 conditions are not clear.

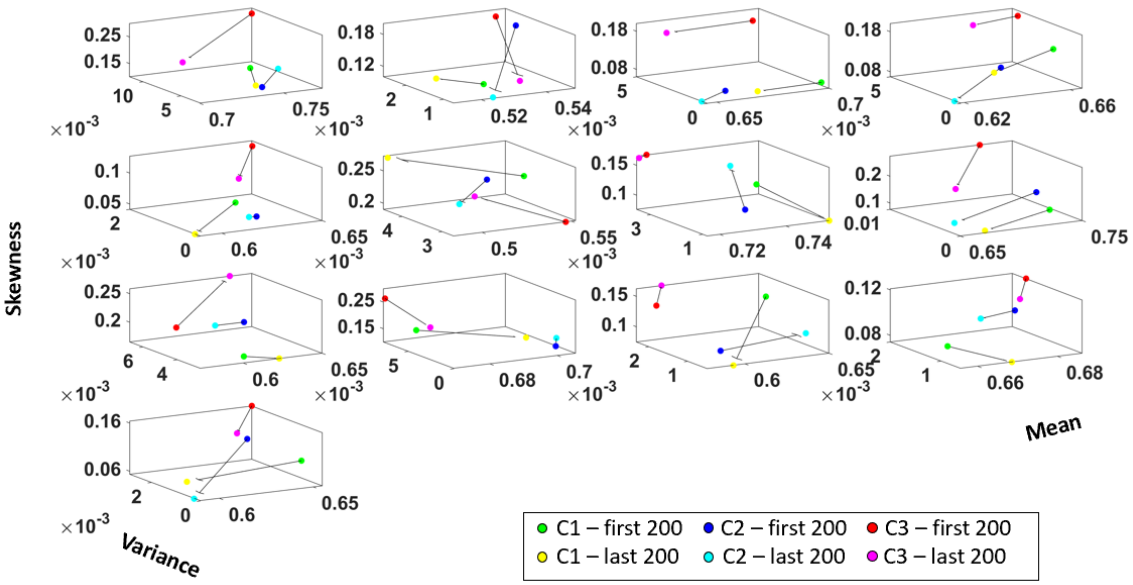

Figure 3.7. Fitted Gamma PDF moments For each participant (subplot; same order as in **Figure 3.6**), and for each three conditions, the first 200 IBI and the last 200 IBI within each condition were fitted to a Gamma PDF, and the first 3 moments (mean, variance, skewness) were plotted on the 3 axes of each subplot; and the black arrow indicates the temporal order within each 3 conditions. For most participants, datapoints from the condition C3 stands out with higher skewness value than the other two conditions.

3.3.2 Cross-Correlation between EEG sensors

Cross-correlation between all pairs of EEG sensors were computed for each sequential IBI segment for all 3 conditions, and the median of all pairs of sensors per IBI segment were extracted and plotted in **Figure 3.8A**. The magnitude change (absolute value of change) in the median cross-correlation between sequential IBI segments were computed and plotted as shown in **Figure 3.8B**. Such magnitude change from condition C1 to C3 was found to have statistical significance at 0.05 level, based on the Kolmogorov-Smirnov test for the three NT participants; however, this was not the case for the two ASD participants. Note, the Kolmogorov-Smirnov test was used, as this test is appropriate for data that do not follow a Gaussian distribution, and has a large sample size (n>1000) that may yield low statistical power.

In order to compare between the five participants, we assessed the magnitude change (absolute value of change) in the median cross-correlation between sequential IBI segments across participant pairs using the pairwise Kolmogorov-Smirnov test, from data obtained from condition C1, and find that the 2 ASD patients and one NT (NT1) do not show much statistical difference; while the other 2 NT participants show statistical difference from the rest of the participants (**Table A 11**).

To compare between the five participants, we also computed the median of the magnitude change in the median cross-correlations of all EEG sensor pairs for each three conditions, and the change in this magnitude was compared across conditions for each participant. As shown in **Figure 3.8C**, the direction of change in this median magnitude between conditions are different for each participant. However, we observe that the range in this magnitude values are noticeably different between NT and ASD participants, such that NT participants have a wider range of cross-correlation magnitude changes than ASD participants between conditions.

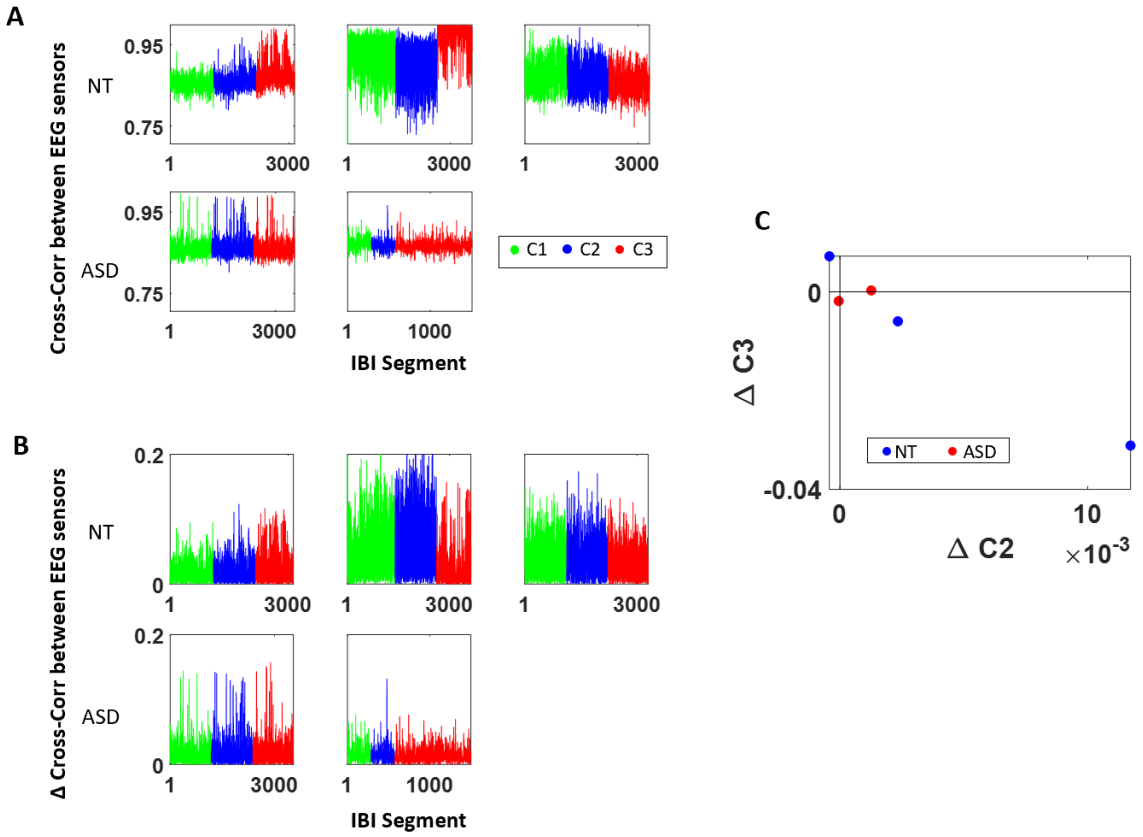

Figure 3.8. Trajectory of median cross-correlations between EEG sensors across IBI segments. **(A)** Median cross-correlation per IBI segment of all EEG sensor pairs during condition C1 (green), C2 (blue), and C3 (red) for 3 healthy participants (top) and 2 ASD patients (bottom). **(B)** Dynamical trajectory of median cross-correlation per IBI segment of all EEG sensor pair, where the y-axis is the absolute change in median cross-correlation from the previous IBI segment. ASD patients generally show a narrower range in change of the EEG connectivity. **(C) Difference in median absolute change of cross-correlations between conditions (Δ Cross-correlation between EEG sensors)**, where the x-axis (Δ C2) denotes change from condition C1 to condition C2, and y-axis (Δ C3) denotes change from condition C1 to condition C3. ASD patients show little change in the cross-correlations, in comparison to the healthy participants.

3.3.3 Mutual Information (MI) between EEG, Acceleration, and Magnetometer Data

Inter-spike intervals (ISI) were gathered for each sensor of three modes of data (EEG, linear acceleration, and magnetometer) resulting in 52 sets of ISI. Histograms were plotted based on these 52 sets of ISI, and MI between each pair of histograms were computed. Median of the MI's were then computed for different pairs of data modes, and plotted for each

individual in **Figure 3.9**. In this context, high value of MI implies there is more information to learn from one another (informational dependence). In **Figure 3.9**, MI during condition C1 is represented in the z-axis, and changes in MI value from condition C1 to C2, and from C1 to C3 are represented in x and y-axis respectively. Here, on the x- and y- axes, a large change in MI implies a large change in the information dependence across tasks.

Focusing on the difference between the 3 NT and 2 ASD participants, the overall MI is lower for ASD than NT for the pairs that involve the EEG sensors; specifically the following pairs: pair of 2 EEG sensors, 1 acceleration and 1 EEG sensor, 1 magnetometer and 1 EEG sensor. On the other hand, there are mixed results for the pairs: pair of 2 acceleration sensors, 1 magnetometer and 1 acceleration sensor. Also, ASD participants tend to have higher MI than NT for the 2 magnetometer sensor pairs. Overall, ASD participants show less information dependence in the EEG sensor signals; while showing more dependence in the magnetometer signals. Also, there is a slight trend, where overall small MI values tend have small change in the MI across conditions for all three modes of data. In fact, ASD participants tend to show smaller change in the MI for pairs that involve the EEG sensors. This is in line with the small magnitude change in cross-correlations among EEG sensors shown among ASD participants from section **3.3.2**.

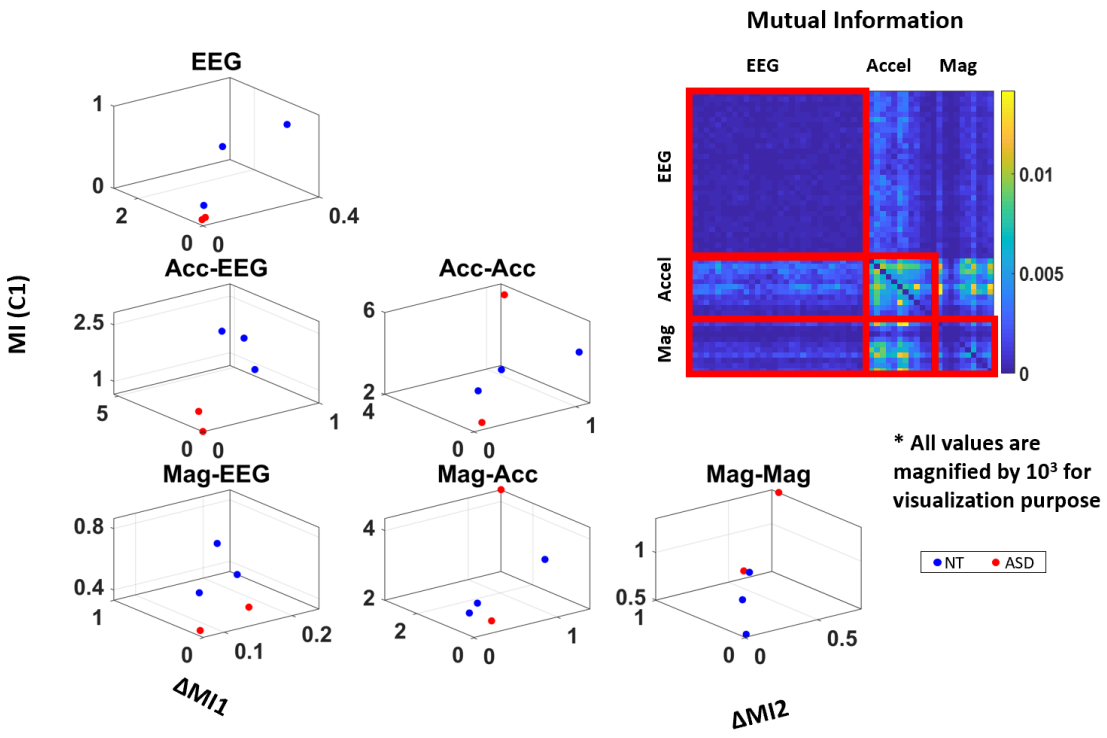

Figure 3.9. MI between EEG, Acceleration, and Magnetometer Data. Median MI across different sensor pair categories are plotted for ASD patients (red) and healthy participants (blue) during condition C1 on the z-axis. On the x-axis (ΔMI1), the absolute difference between median MI's during condition C2 and C1 are plotted; on the y-axis (ΔMI2), the absolute difference between median MI's during condition C3 and C1. Overall ASD patients show small MI values and small range of change for pairs that include the EEG sensor signals; on the other hand, ASD patients show large MI values and large range of change for pairs that include only magnetometer sensors.

3.4 Discussion

In this study, we analyzed the biophysical signals generated by the CNS (EEG data), PNS (acceleration, magnetometer data), and ANS (EKG data), in tandem, and compared them across the different conditions (conditions varied by spontaneous vs. deliberate entrainment), and between healthy participants and ASD patients.

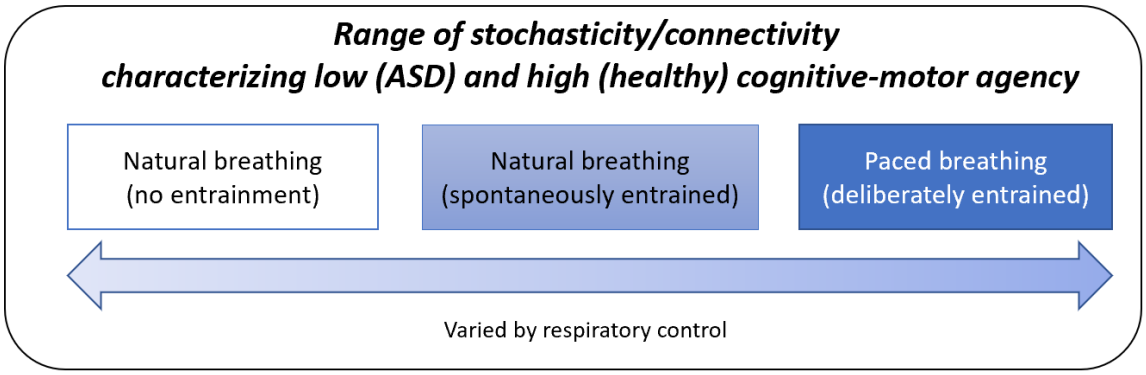

Figure 3.10. Schematic overview of the study

First, we analyzed the heart signals separately, and demonstrated the stochastic changes in heart-beat signals (i.e., IBI) becoming more variable in its range, when an individual exerts conscious control on one's breathing pace. We also found ASD patients to exhibit a more variable range in their IBI's (shown by the high NSR), and its stochastic changes due to paced breathing to be larger than the healthy participants. **This implies that the heart activity of ASD patients respond differently to respiratory control than their healthy counterparts.** Since we can safely assume that neurotypical controls have better cognitive-motor agency, and given the finding that their ranges of heart variability are more stable than those with ASD, we can then infer that more variable fluctuations in the autonomic system of the participants with ASD may define lower cognitive-motor agency.

Next, we analyzed the CNS, PNS, ANS data in tandem for 5 participants, composed of 3 healthy participants and 2 ASD patients, and found differences between the two demographics. Specifically, the dynamic change in cross-correlations between EEG sensor pairs was found to be narrower in range for ASD patients. Relatedly, the change in cross-correlations between such EEG sensor pairs were found to be small across the three conditions for ASD patients than their healthy counterparts. These findings allude to **the narrow range of connectivity in cortical signals among ASD patients**, regardless of whether deliberate effort was exerted or not.

However, we also note that the EEG signals were not exclusively composed of cortical signals, but were inevitably mixed with other signals (supposedly of head, muscle, and eye movement). Given that ASD patients exhibit unusual motor behaviors (e.g. the presence of ticks, late reflexes and involuntary head motions (Teitelbaum et al., 2004; E. B. Torres & K. Denisova, 2016)), it is possible that these unusual motions produced non-cortical signals that inevitably impacted the patterns of EEG signals. As we caveat that this EEG connectivity characteristics may represent both micro-muscle motions and cortical signals, the differences between controls and ASD may largely reflect the differences in motor behavior. This is important moving forward, as many of the cognitive issues in autism have not been interpreted in light of their motor phenomena. As such, the present framework opens a new door to re-interpret cognitive phenomena in autism.

Lastly, we studied the interactions between the CNS and PNS signals (from 3 modes of sensors EEG, acceleration, magnetometer) and their dynamical change across different conditions. Here, we computed the MI between different sensor pairs, and examined them by categories of sensor pairs. In general, **informational dependency of EEG sensor signals with other EEG sensor signals or kinematics signals (acceleration, magnetometer) were generally lower for ASD patients, and this dependency changed in a narrower range across the 3 conditions for these patients**. This is in line with the findings of cross-correlations varying by a narrow range for ASD patients. On the other hand, we found the magnetometer sensors to vary by a wider range for ASD patients than the healthy participants.

Overall, this study illustrates the interactive nature of biophysical signals along with the impact of conscious control (i.e., paced breathing) on such interactions, and highlights the different connectivity structures across different individuals with different levels of agency. In particular, by comparing the connectivity characteristics (shown by cross-correlation and MI metrics) between ASD patients (who exhibit a compromised degree of cognitive-motor agency)

and healthy participants (with higher cognitive-motor agency), we are able to observe how ASD symptoms of low cognitive-motor agency is manifested in the physiological connectivity. Noticeably, the narrow range of connectivity within the cortical signals (CNS), and wider/variable range of connectivity within the kinematics (PNS) and heart (ANS) activity seem to be characteristic of ASD's low cognitive-motor agency. Our results suggest that different connectivity patterns across the brain and body may serve to define different levels of cognitive-motor agency in ASD relative to NT controls.

However, this study had several limitations. Due to technical difficulty, we were able to synchronize the 3 modes of datasets for only 5 participants. For that reason, although we found some characteristic patterns of ASD patients that are distinguishable from their healthy counterparts, the small sample size does not yet allow for generalization. Another methodological difficulty in this study was the inevitable presence of motor/mechanical artefacts in the EEG signal (i.e., instrumental noise). It is well known that there are much non-brain related signals that are mixed in the EEG data, particularly if the participant is performing large motions such as gait, and signal preprocessing methods (as used in this study) provide limited relief. For that reason, although we found our analytics based on EEG data to be informative in revealing the biophysical connectivity, we caveat that this is not necessarily a product of mere cortical signals but rather a mixture with other factors (e.g., facial muscle movement, head movement, minute motions of EEG cap). Nevertheless, given the disparity in cognitive-motor agency and the profound differences in motor behavior, and their impact on EEG signals between ASD patients and NT participants, it may be possible to extend these methods to study on a larger sample in the future. Importantly, our results open new questions in autism research at the intersection of cognitive and motor control.

In the next chapter, I introduce an extended version of this pilot experiment with improved technical approaches to better probe into the brain and body connectivity across different population.

4 Paradigm to study embodied cognition

4.1 Introduction

In the previous two studies, I introduced experimental paradigms of pointing and walking, which was found to be informative of the interactive nature of the nervous systems, with regards to different levels of control/cognitive load. However, there were some limitations to these approaches. In the first study that involved pointing, we were restricted to examining just the kinematics connectivity (of PNS) without analyzing them in relation to the CNS/ANS processes. In the second study that involved walking, we were able to harness the biophysical signals from the brain and the heart along with the kinematics, and were able to combine the different modes of signals into a single datatype. However, due to technical difficulty, we were unable to gather sufficient number of participant data to analyze these signals and find generalized patterns in their connectivity.

In this study, we addressed these limitations by applying the same tasks (i.e., pointing and walking) in the experiment, but changing some features of the instrumental set up (described in section 4.2.2). We also added additional tasks of cognitive activities, selected from standardized cognitive tests (e.g., Montreal Cognitive Assessment) that require different cognitive capacities. In some of these tasks that involve drawing, we recorded the pen movement as well. While the participant performed a series of tasks that involved different levels of control and cognitive processes, we co-registered the EEG signal (CNS), magnetometer

signal (PNS), heart signal (ANS), and analyzed these signals in tandem to characterize the change in connectivity. Here, we present a set of analytics that examine the stochasticity and connectivity of signals (previously demonstrated in section **2.2.4**), and of positional geometry of body motions using concepts from linear algebra.

We recruited patients with Parkinson's disease (PD) along with one patient with ASD and another patient with essential tremor (ET). While we explored a variety of analytical methods that inform the interactive processes within the different layers of the nervous systems, we focused on finding a set of analytics that best characterize the behaviors of Parkinson's patients. Since these patients exhibit a range of compromised cognitive-motor agency, the analytics that we find from this study would allow us to see the structure and dynamics of the nervous systems, when a lower degree of cognitive-motor agency is involved.

We note that this work was published in the Journal of Visual Experimentation and is openly accessible in video form at https://www.jove.com/video/59827/dynamic-digital-biomarkers-motor-cognitive-function-parkinson-s

4.2 Methods

4.2.1 Participants

A total of 31 participants partook in this study. However, 9 participants' data had too much instrumental noise or could not be synchronized across different modes of devices. For that reason, a total of 22 participants' data were analyzed in this study. We note that although 9 participants' data were excluded in this study, they would be further analyzed as a set of unsynchronized datatypes in a subsequent study. Their data is not lost, but for the purposes of providing proof of concept in this thesis (that we can study several layers of functionality in the

nervous systems using non-invasive means), we will restrict the description of our methods and results to the subset of 22 participants.

Among these 22 participants, 11 individuals were healthy undergraduate students with ages ranging from 18 to 26 (10 female, 2 male), recruited from the Rutgers human subject pool system, and received credit for their participation. 7 participants diagnosed with Parkinson's disorder (PD) with age ranging from 64 to 77 (3 female, 4 male) were recruited from the Robert Woodrow Johnson Medical Center at Rutgers University, and received $50 for their participation. Their Movement Disorders Society Unified Parkinson's Disease Rating Scale (UPDRS) (Fahn & Elton, 1987) ranged from 16 to 44, and Hoehn and Yahr scale (Hoehn & Yahr, 1967) ranged from 2 to 4. 2 participants were healthy age-matched individuals with ages 65 and 68 (1 female, 1 male), and were either a family member of the patient participant or recruited from ClinicalTrials.gov. Lastly, 1 participant was diagnosed with Essential Tremor (age 39, male) and 1 participant was diagnosed with ASD (age 15, female). Both of these participants were high functioning individuals that did not show stark observable movement disorders. However, in our experience, it is at the micro-motion level (of the minute fluctuations in the biophysical signal time series that is undetectable by the naked eye) that these disorders manifest. These participants were recruited from ClinicalTrials.gov, and received $25 for their participation. Among the healthy young participants, one was left-handed, and among the Parkinson's patient participants, one was left-handed, and all had normal or corrected-to-normal vision. All participants provided informed consent, which was approved by the Rutgers University Institutional Review Board.

4.2.2 Instrumentation and Data Preprocessing

Participants wore two different types of wireless sensors to capture the biophysiological signals from the central (CNS), peripheral (PNS), and autonomic nervous system (ANS), with electroencephalography (EEG) and inertial measurement units (IMU).

Cortical signals from the CNS were captured with a wireless EEG device (Enobio; Barcelona, Spain) at 500Hz sampling rate with 31 sensors positioned across the scalp. The electrodes were spatially distributed as shown in **Figure 4.1A**, with the sensor Oz placed on the left abdominal. This sensor was used as a proxy of electrocardiogram (EKG) to capture the heart signals. The wireless device was positioned on the back of the participant's head, and the reference sensor was attached behind the left ear. Both EEG and EKG signals were recorded from the Neuroelectrics software (Enobio; Barcelona, Spain). Further preprocessing for the EEG signals were done in Matlab (Release 2015b, The MathWorks, Inc., Natick, Massachusetts)-based toolbox EEGLab (Delorme & Makeig, 2004) and PrepPipeline (Bigdely-Shamlo et al., 2015). Using the PrepPipeline toolbox, line noise at 60Hz was removed, and referenced via a robust average reference procedure, where channels were iteratively referenced to the average signal, while bad channels, such as those showing extreme amplitudes (deviation z-score exceeds 5) or lacked correlation with any other channel (correlation less than 0.4) were excluded and interpolated in this process. To eliminate the trend while preserving the cortical signals as much as possible, the EEG signals were further band-passed at 1-100Hz using Butterworth IIR filter at 1^{st} order (Niedermeyer, 2011). The EKG signals were band-passed at 5-30Hz using Butterworth IIR filter at 1^{st} order (Kathirvel et al., 2011; Tereshchenko & Josephson, 2015) to eliminate trend while preserving the heart signal's QRS complex as much as possible.

Note, in a previous study (**Chapter 3**), the EKG signals were analyzed by examining the R-peaks within the QRS complex. However, because the heart signal was recorded with the reference channel positioned in less-than-optimal space (behind the left ear), the R-peaks were

not detectable with signal processing method. This positioning was inevitable, because if we recorded the heart signal from a separate device and a separate software, with the reference channel positioned in the optimal location, there would be three different modes of signals recording through three different software's on the same computer. This runs the risk of computer crash due to limited computation power. Indeed, when we attempted to do this in the previous study (section **3.2.2**) , 13 participants data were recorded but only 5 participants' data were fully synchronized across the different modes of signals. In order to avoid this risk, we attempted to record the heart signal by using one of the EEG sensor on the abdominal and sharing the same the reference channel with other EEG sensors intended to record the cortical signals. This way, the computer would record from two devices (EEG and IMU) and two softwares, and thus avoid the risk of having frequent computer crashes. However, the downside was the rampant noise in the obtained EKG signal and the inability to extract R-peaks. For that reason, in this study, we analyzed the overall inter-spike interval (ISI) where the spikes were composed of all peaks from the QRS complex (i.e., P,Q,R,S,T peaks), instead of the inter-beat interval (composed of R-peaks only).

Motor signals from the PNS were captured with IMUs based on Xsens motion capture technology (Roetenberg, Luinge, & Slycke, 2009) sampled at 60Hz, and were acquired with Xsens MVN Studio software (Xsens; Netherlands). 17 sensors were attached to the participant with Velcro belts and additionally secured with athletic tape on the following body parts – head, sternum, posterior trunk, left and right shoulder, left and right upper arm, left and right wrist, left and write hand, left and right upper leg, left and right lower leg, left and right foot. These sensors allowed for creating the participant's avatar (**Figure 4.1B**), and registering each body part's position, kinematics (linear (m/s) and angular velocity (deg/s), linear (m/s^2) and angular acceleration (deg/s^2)), and magnetometer data (arbitrary unit; normalized from G). For the

purpose of this study, linear velocity, position, and magnetometer data were mainly examined. Linear velocity, the first derivative of position was chosen as it provided the least signal noise. When higher derivatives (e.g., acceleration) are computed, instrumentation noise is amplified, so it is safer to use the first order change, while we watch for any possible noise artifacts. The magnetometer data was chosen as it is relatable (and convertible) to the EEG signal which is in μV unit.

In addition, the voice of the participant and the experimenter was recorded with a microphone sampled at 48,000Hz. However, the audio data was not examined in this thesis, and will be further analyzed in subsequent study.

As with the previous study (described in section **3.2.2**), these biophysiological signals were temporally synchronized by using an open-source package Lab Stream Layer (LSL). All softwares along with LSL were run on the same computer, and events were timestamped with mouse clicks on the display screen of that computer (**Figure 4.1C**). Because the EEG (cortical and heart) and motor signals were registered at different sampling rates, the EEG signals were down-sampled to 60Hz, so that all modes of signal could be analyzed as a single datatype.

As with the previous study, the preprocessing of EEG signals did not include rejection of artefact components or certain time segments, as this would undermine the purpose of examining the dynamical process of biophysiological interactions across the different nervous systems (for rationale, see section **1.3**). However, for certain parts of the analysis, EEG signals were decomposed into components that were categorized as either cortical and non-cortical; this way, it was possible to differentiate the signals that were generated by cortical activities, and those that were generated from elsewhere. Details of this process is explained in section **4.2.4.4**.

Lastly, certain tasks required drawing with a digital pen (Wacom; Japan) on a white paper which was taped on top of a digitizing tablet (Wacom; Japan). The pen movement was recorded from the software MovAlyzer (Neuroscript; Tempe, AZ), which sampled the position of the pen tip motion at 133Hz. These pen motion data were not synchronized to the other instruments (EEG, IMU), and were later analyzed separately (**Figure 4.1D**).

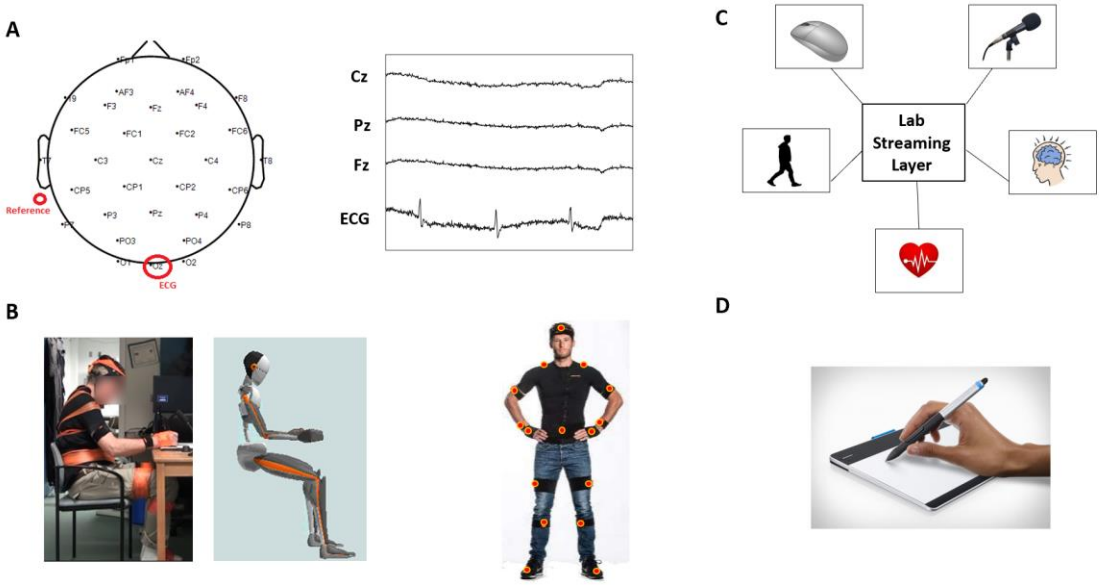

Figure 4.1. Instrumental Setup. (A) (Left) Location of EEG sensors, reference channel, and of the sensor (Oz) that recorded the heart activity; (Right) Sample EEG signals and EKG signal obtained from select EEG sensors. **(B)** (Left) Picture of the participant performing a drawing tasks along with his avatar registered in real-time. (Right) Positions of the IMU sensors. **(C)** Lab Streaming Layer synchronized the signals registered from multiple modes – mouse clicks, voice, kinematics, EKG, EEG. **(D)** During a series of drawing tasks, the participant's pen movement (position and velocity) on a digitizing tablet was registered.

4.2.3 Experimental Procedure

The setup of the instruments took about 30 to 45 minutes, which included donning the sensors and calibration of the systems. After the setup was complete, the participant performed the following tasks in the order described. Each of these tasks involve some movement (limited to the hand as in drawing, or the full body as in walking), and our goal is to probe into the

cognitive processes and their interactions with the body that unfolds during these tasks. Full description of the entire protocol can be found in Ryu, Vero, Dobkin, and Torres (2019).

4.2.3.1 Drawing task

The participant was seated at a chair with a table in front. On the table was a digitizing pen and tablet, with which he/she was instructed to use to complete a total of seven drawing tasks. These drawing tasks were subtasks from multiple standardized clinical diagnostic tests.

First, they were instructed to copy a Benson Complex Figure (Possin, Laluz, Alcantar, Miller, & Kramer, 2011), and to memorize the figure, as they would draw the same figure from memory at a later point during the experiment. This task is used to assess visuo-constructional and visual memory function (**Figure 4.2A**). Next, they were instructed to complete four trail making tasks, which is to connect circles composed of either numbers and/or alphabet letters in an ascending order. Specifically, the first trail making test was a sample test (Maze1) for the subsequent test (Maze2), where the sample test consisted of 8 numbers and the actual test consisted of 25 numbers. The third test was another practice test (Maze3) for the subsequent test (Maze4), where the sample test consisted of 4 numbers and 4 letters, and the actual test consisted of 13 numbers of 12 letters. These trail making tests are a component of the Army Individual Test Battery (1944), that assesses processing speed and executive function and visuomotor and perceptual-scanning skills. (**Figure 4.2B**). Next, they were asked to draw an analog clock with numbers 1 through 12, and to set the time to 10 past 11. This test is part of the Montreal Cognitive Assessment (Nasreddine et al., 2005) and assesses the participant's visuo-constructional skills (**Figure 4.2C**). As a last task in the drawing task segment, the participant was asked to draw the Benson Complex Figure (Possin et al., 2011) from memory.

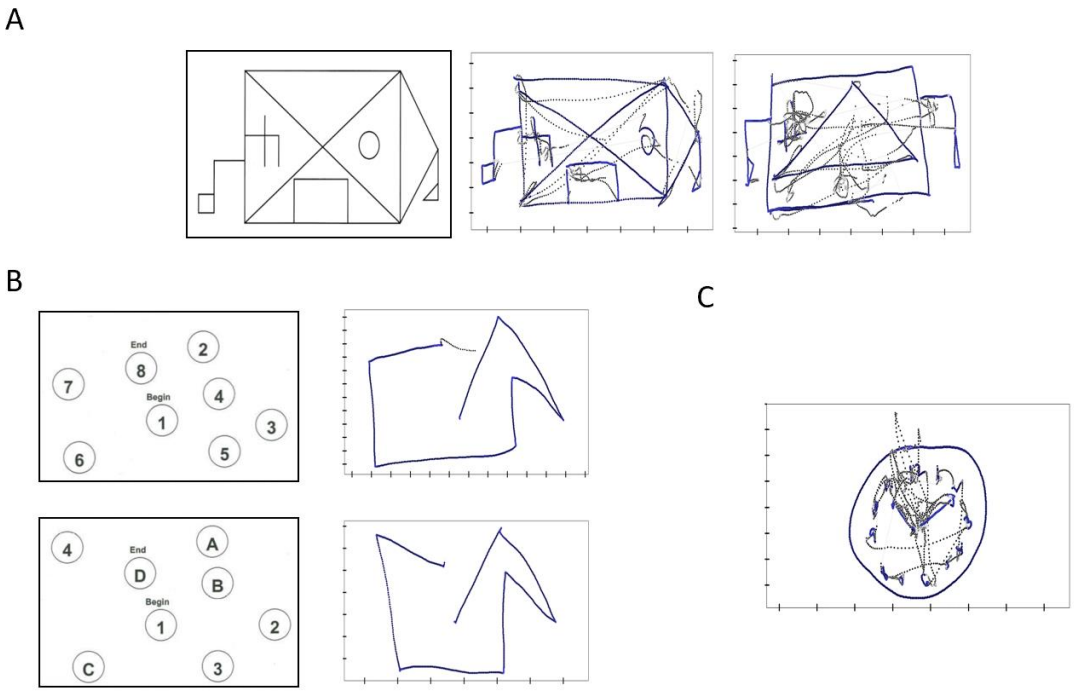

Figure 4.2. Drawing tasks (A) Benson complex figure. The participant copied the Benson complex figure shown (middle) and also drew the figure from memory at a later point (right). The blue lines represent the trajectory of pen motion when it was pressed on the tablet; the dotted lines represent the motion when the pen was lifted from the tablet. **(B) Trail making.** The participant connected the dots in sequential order for numbers (top) and for a combination of numbers and alphabets (bottom). **(C) Clock drawing.** The participant drew an analog clock with the time set to 11:10.

4.2.3.2 Memory Task - Number Span Test

Subsequent to the drawing tasks, the participant continued to sit at the same chair, and started the memory task. Here, the experimenter instructed the participant to repeat the numbers in the same order for the forward memory task, and in the reverse order for the backward memory task. For both tests, the experimenter read a sequence of numbers (Beekly et al., 2007) ranging from 3 to 9 digits for the forward task, and 2 to 8 digits for the backward task, in the order of small to large length of digits. The experimenter continued testing until the participant failed to correctly repeat two number strings of the same length. Here, the forward

task measures the capacity to briefly hold information, while the backward task also measures the ability to manipulate numbers as the participant is required to reverse the sequence.

4.2.3.3 Pointing task

The participant continued to sit at the same location, and started the pointing task, which consisted of three conditions. In condition P1 (control), the participant pointed at a target with the dominant hand repeatedly 40 times freely at one's own pace. For each pointing motion, the participant was instructed to start with the dominant hand in a resting position on the table, and to touch the target in front and retract the hand back to its resting position. In condition P2 (metronome), the participant performed the same task as in condition P1, but did so while the metronome was beating in the background at 35 beats per minute. The metronome was set to play from a computer, and the volume was approximately 45 dBA. The participant was instructed to freely point at the target without being mindful of the metronome beating in the background. In the last condition P3 (paced pointing), the experimenter continued to keep the metronome beating at 35 bpm. However, now, the participant was instructed to touch the target at the pace of the metronome beat, where the participant would either touch the target or start reaching for that target at each metronome beat. This experimental paradigm was designed to examine the connectivity of biophysical signals, while the dominant hand is either moving at one's natural pace (condition P1); or moving at one's natural pace while passively hearing a constant metronome beat (condition P2); or consciously/actively pacing one's movement to an external metronome beat (condition P3). This would allow understanding the dynamical flow of the underlying biophysical signals when one is either spontaneously entrained by the metronome beat, or when one is actively exerting control to entrain to the metronome beat by pacing the motions accordingly. Moreover, the pointing task allows to further distinguish motions when it is deliberate/goal-oriented (i.e., exert a relatively higher level of

motor control) and when it is spontaneous (i.e., lower level of motor control) by differentiating between forward and backward motions of the pointing trajectory (for details, see section **2.2.3**).

4.2.3.4 Walking task

For this task, the participant was taken to a different space, where there was ample room to walk around. Here, the participant was instructed to walk around the room for 15 minutes under three different conditions. In condition W1 (control), the participant naturally walked around the room at one's natural speed and in any direction for 5 minutes. In condition W2 (metronome), the participant naturally walked for another 5 minutes but with the metronome beating in the background at 12 bpm. In condition W3 (paced breathing), the participant walked for another 5 minutes while pacing the breathing rate to the metronome beat. These tasks were identical to those described in the previous study (see section **3.2.3**), but with shortened length.

4.2.4 Data Analysis

There are many parameters that we can extract from the biophysical signals generated by the person's nervous systems. Here, we focused on the EEG waveforms' inter-spike interval (representing CNS output); pen movement, body segments' position and linear velocity, and body segments' magnetometer data's inter-spike interval (representing PNS output); and the heart signals' inter-spike interval (representing ANS output). There are many ways of characterizing and analyzing these data, but for the purpose of this study, five analytics will be discussed that we found to best physiologically characterize and separate patterns of patients with Parkinson's disorder in relation to healthy participants and patients with other neurological

disorders, as this approach would allow us to find characteristics of varying levels of cognitive-motor agency.

4.2.4.1 Gamma PDF fit of pen movement during drawing tasks

The position trajectory of the pen tip was registered, and its linear velocity of the pen movement was computed. The time series of this linear velocity was then converted to a unitless micromovement data, where the spike amplitudes were standardized by using the equation :

$$Standardized\ Spike\ Amplitude = \frac{Raw\ Spike\ Amplitude}{Raw\ Spike\ Amplitude + Average_{Min\ to\ Min}} \quad \textbf{Eq 4.1}$$

In the case of standardized spikes of pen movements, we observed that most values were concentrated at 0.5, and its frequency histogram to exhibit a shifted exponential-like distribution shape, which did not allow a good fit with many of the family of distributions. Here, the smallest possible value of such standardized spikes is 0.5, as the largest possible "Average" component would equal the "Raw Spike Amplitude" in the equation. For that reason, the standardized spike amplitude values were shifted by subtracting 0.5 uniformly from all the amplitude values. As a result, the histogram of such shifted standardized spike showed the best fit to a Gamma PDF, in comparison to other family of distributions based on MLE (Details of distribution fit can be found in **Figure A 3**). In this study, in order to find patterns of different participant cohorts, for each participant, the fitted Gamma parameters were plotted on a Gamma parameter plane, and the fitted Gamma PDF moments (i.e., mean, variance, skewness) were also plotted on a 3-dimensional graph.

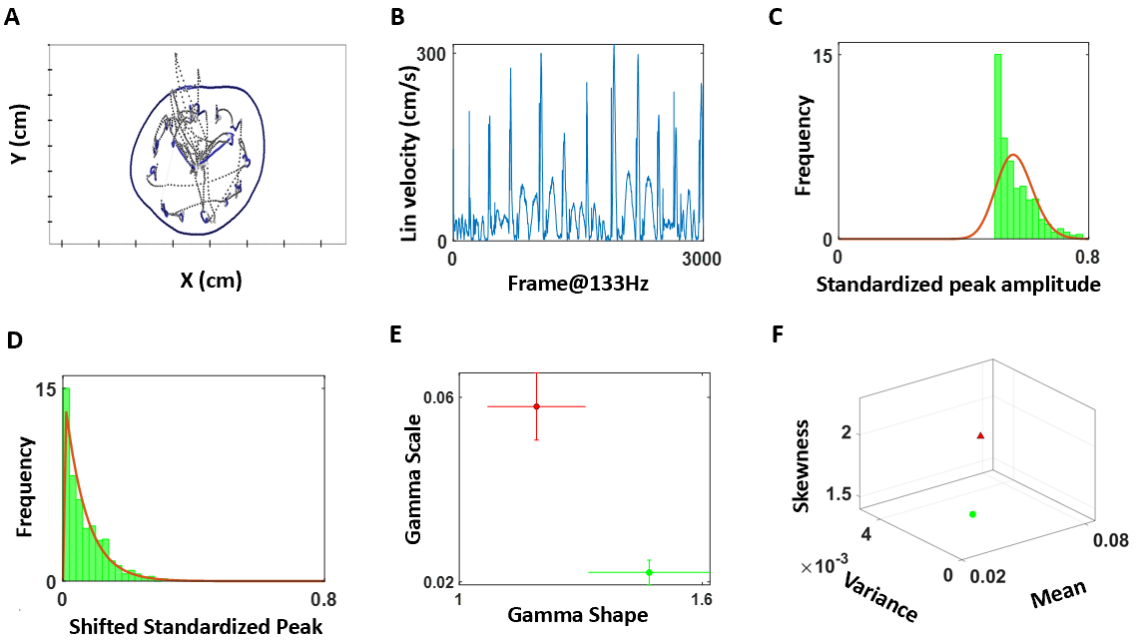

Figure 4.3. Analyzing the stochasticity of pen movement. Example from a clock drawing task **(A)** The position of pen motion was recorded at 133Hz. **(B)** Based on the position data, instantaneous linear velocity was computed and plotted as a waveform. **(C)** Peaks (spikes) and valleys within the linear velocity waveform were extracted to compute standardized spike amplitudes. Histogram of standardized spike amplitudes was plotted, and showed to have a bad fit to a Gamma PDF. **(D)** In order to allow a better fit to a Gamma PDF, the histogram from (C) was shifted by 0.5 to the left and then fitted a Gamma PDF. **(E)** The fitted Gamma parameters were plotted on a Gamma parameter plane with colors denoting different demographic cohort. **(F)** The first 3 moments of the fitted Gamma PDFs were computed and plotted on a 3-dimensional graph with colors denoting different demographic cohort.

4.2.4.2 Gamma PDF fit of center of mass (COM) during walking tasks

The position trajectory of the center of mass (COM) was computed based on accelerometry by the Xsens MVN software (Fuschillo, Bagalà, Chiari, & Cappello, 2012). With the position data, linear velocity of the COM was computed, and the time series of this linear velocity were then converted to a unitless micromovement data, where the spike amplitudes were standardized by using **Eq 4.1**

$$Standardized\ Spike\ Amplitude = \frac{Raw\ Spike\ Amplitude}{Raw\ Spike\ Amplitude + Average_{Min\ to\ Min}} \quad \textbf{Eq 4.1}.$$

As with the

standardized spikes of pen movements, the histograms of COM standardized spikes were concentrated around the minimum value 0.5, with an exponential-like distribution shape, and did not allow a good fit with many of the family of distributions. For that reason, the standardized spike amplitudes were uniformly reduced by 0.5, and fitted to the Gamma PDF. Such shifted standardized spike amplitudes also showed a good fit to the Gamma PDF in comparison to other family of distributions (as shown in **Figure A 3**). Similar to the pen data, the Gamma parameters and the Gamma moments were plotted for all participants, to find stochastic patterns of different participant cohorts.

In this study, the COM data was collected for all tasks during the study, but the three walking tasks showed to be the most informative in separating different participant cohorts. For that reason, we focused on analyzing the COM data obtained during those three walking conditions. Also, among the many kinematics data we obtained from the motion capture system (e.g., of left hand, torso, right foot), we chose to focus on the COM data as it is a reflection of the entire body parts' movement.

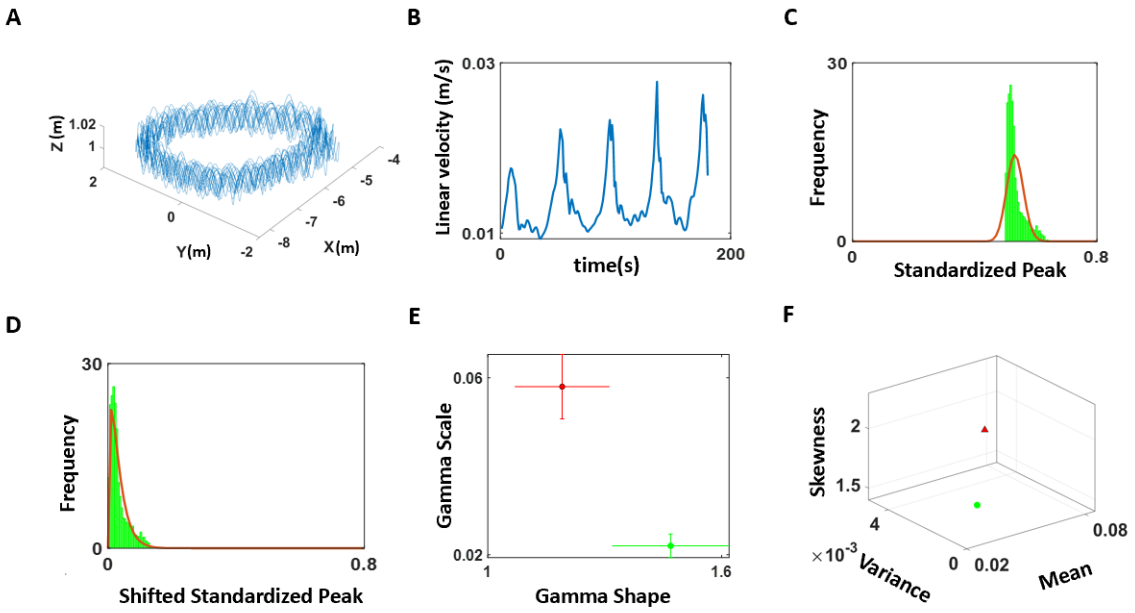

Figure 4.4. Analyzing the stochasticity of COM. Example from the walking task **(A)** The position of COM was recorded at 60Hz. **(B)** Instantaneous linear velocity was plotted as a waveform. **(C)** Peaks (spikes) and valleys within the linear velocity waveform were extracted to compute standardized spike amplitudes. Histogram of standardized spike amplitudes were plotted, and showed to have a bad fit to a Gamma PDF. **(D)** In order to allow a better fit to a Gamma PDF, the histogram from (C) was shifted by 0.5 to the left and then fitted a Gamma PDF. **(E)** The fitted Gamma parameters were plotted on a Gamma parameter plane with colors denoting different demographic cohort. **(F)** The first 3 moments of the fitted Gamma PDFs were computed and plotted on a 3-dimensional graph with colors denoting different demographic cohort.

4.2.4.3 Dynamical changes in body part distances from center of mass (COM)

As a third set of analytics, we used the positions of all body parts and COM, and computed the distances of each body parts in relation to the COM, and the trajectory of these distances were analyzed. In general, when an individual is performing a cyclical task, such as walking, the distance of the foot in relation to the COM would form a cycle, where the distance would be large when the foot is away from the torso (which is an approximate location of COM), and small when the foot is close to the torso.

Here, we focused on the moment-to-moment dynamical change of such distances across each sampled frame at 60Hz. Specifically, the distance was converted into 3 dimensional dataset, where the coordinates are the distance at time (t, t+1, t+2). Such datapoint reflects the instantaneous position at 3 sequential frames by its coordinate values, along with its velocity and acceleration by its displacement from the vector that spans in the direction (1,1,1). We observed the pattern of these 3-dimensional datapoints for each body parts (**Figure 4.5A**) during the three walking tasks, and we found that these could approximately fit a plane.

Regression onto a plane was done with these 3-dimensional datasets, by computing the distance from each point (x,y,z) to a plane ax + by + cz + d = 0, and finding the coefficients of the plane that minimizes the total distance as such:

D_i = Distance between point P(x_i, y_i, z_i) and plane ax + by + cz + d = 0

$$(squared)\ Total\ Distance\ (D)\ = \sum_{i}^{N} D_i^2$$

$$= \sum_{i}^{N} \frac{(ax_i\ + by_i + cz_i + d)^2}{(a^2 +\ b^2 +\ c^2\ )} \qquad \textbf{Eq 4.2}$$

First we set the plane equation to reduce one coefficient (d), by taking the derivative with respect to d:

$$\frac{dD}{d(d)} = \sum_{i}^{N} \frac{2\ (ax_i + by_i + cz_i + d)}{(a^2 +\ b^2 +\ c^2\ )} \qquad \textbf{Eq 4.3}$$

D is minimized when we set the numerator (above) to 0, thus providing the following equation:

$$d = \sum_{i}^{N} \frac{-(ax_i + by_i + cz_i)}{N}$$

$$= -(ax_o + by_0 + cz_o) \qquad \textbf{Eq 4.4}$$

where x_o, y_o, z_o are means of their respective data points. Using the d information above yields the following plane equation:

$$(a(x - x_0) + b(y - y_0) + c(z - z_0)) = 0 \qquad \textbf{Eq 4.5}$$

Using the obtained plane equation, we re-formulate the total distance, and minimize this distance as such:

$$argmin\ D^* = \sum_{i}^{N} \frac{(a(x_i - x_0)\ + b(y_i - y_0) + c(z_i - z_0))^2}{(a^2 +\ b^2 +\ c^2\ )}$$

$$= \frac{\|\ X\ A\ \|^2}{A^T A} = \frac{(XA)^T XA}{A^T A} = \frac{A^T X^T XA}{A^T A}$$

$$\text{where A} = \begin{bmatrix} a \\ b \\ c \end{bmatrix}, \text{X} = \begin{bmatrix} (x_1 - x_0) & (y_1 - y_0) & (z_1 - z_0) \\ \vdots & \vdots & \vdots \\ (x_N - x_0) & (y_N - y_0) & (z_N - z_0) \end{bmatrix} \quad \textbf{Eq 4.6}$$

Here, D^* is represented in a Rayleigh Quotient form, and can thus be minimized by the eigenvector corresponding to the smallest eigenvalue of $X^T X$. Eigenvectors and values were obtained by singular value decomposition (SVD) of $X^T X$. From the decomposed vectors, the two eigenvectors with larger eigenvalues were set as the axes of the plane, while the eigenvector corresponding to the smallest eigenvalue was set as the normal vector to that plane.

Then, 3D datapoints were projected onto the plane for each body parts as shown in **Figure 4.5B**. In general, body parts that were the most active in its movement (such as the foot during walking, or the dominant hand during pointing) had the most circle-like shape with a hole in the center when it was projected onto the plane. These active body parts also had larger residuals of the plane fitting.

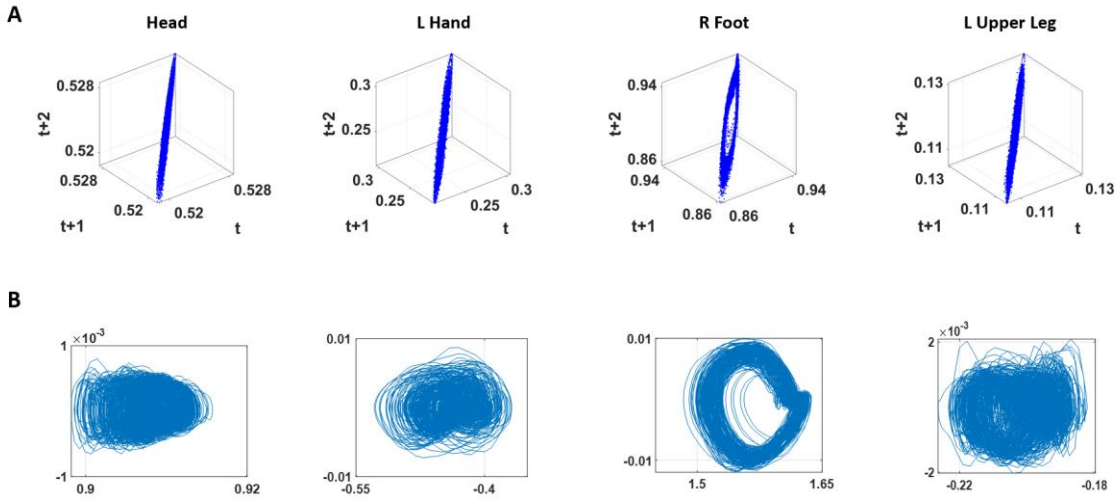

Figure 4.5. Trajectory of distances between a single body part and COM Example from the walking task. **(A)** Trajectory of distances between a certain body part and COM was represented in a 3-dimensional coordinate, by the distance at time t, t+1, t+2 as x, y, and z coordinate respectively. **(B)** The trajectory of these coordinates were regressed onto a 2-dimensional plane, and the projection of those 3-dimensional coordinates on this plane were plotted for each body

part. In general, we found a donut-like structure on the projections from the body part that was most actively moving.

Given the 2 axes vectors and normal vector of the fitted plane, we then examined the angle between the normal vector and the reference vector. Here, the reference vector refers to the vector that spans (1,1,1) coordinate. If datapoints lie on this reference vector, we can interpret that there was no movement of that body part, since the distance is the same at time (frame) t, t+1, and t+2. The eigenvector with the largest eigenvalue is generally close to this reference vector, as main datapoints hover around this reference vector, but deviates from it in relation to the magnitude of the body part movement. Hence, if the angle between the reference vector and the normal vector is exactly $\frac{\pi}{2}$, that implies that there were no movement; conversely, if the angle deviates much from $\frac{\pi}{2}$, then that implies that there were large movements (**Figure 4.6 C,D**). We analyzed this angle across the different tasks and compared it between different cohorts of participants (**Figure 4.6F**). Note, this parameter choice reflects the magnitude of body movement, and one may think this can simply be represented by the linear velocity instead. However, incorporating the position of each body part at 3 sequential frames (time t, t+1, t+2) allows us to reflect both the velocity and acceleration of the movement, which we found to be more useful in characterizing the patient cohorts against NT participants.

For the purpose of this study, we focused on the pointing and walking tasks, as it entailed repetitive motions that is necessary to observe the cyclical shape and to perform planar regression within these analytics.

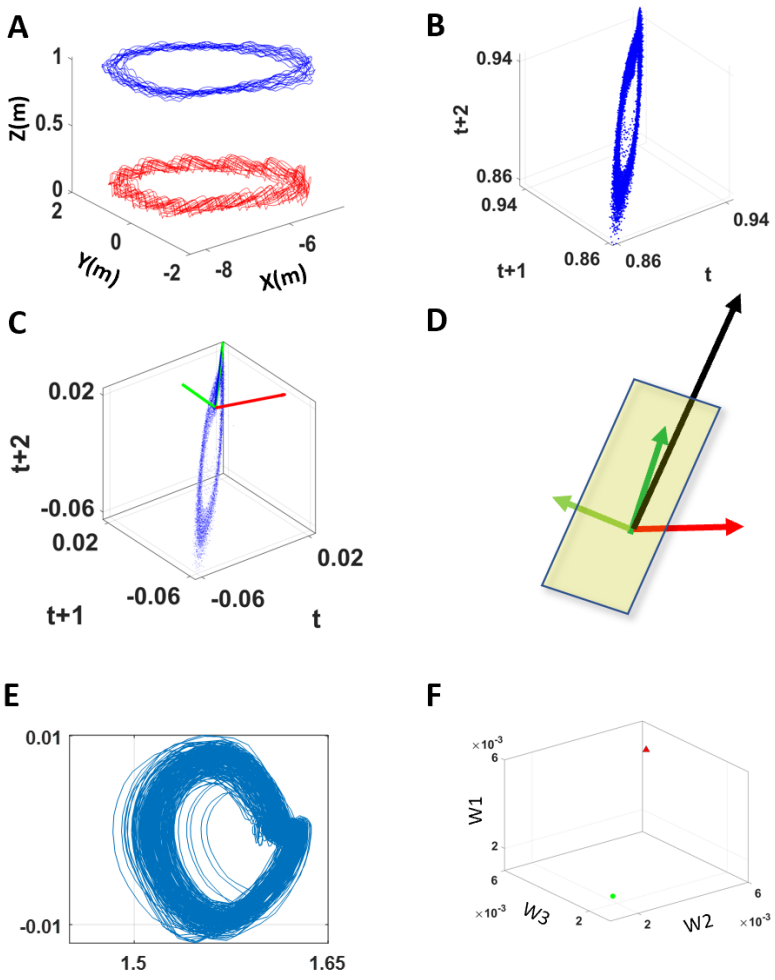

Figure 4.6. Analyzing the dynamical changes of body positions in relation to COM. (A) Trajectory of positions of the right foot (red) and COM (blue) during walking. The trajectory of the distance between the 2 positions was measured. **(B)** Trajectory of distances between the right foot and COM was represented in a 3-dimensional coordinate, by the distance at time t, t+1, t+2 as x, y, and z coordinate respectively. **(C)** The trajectory of the 3-dimensional coordinates was regressed onto a 2-dimensional plane, with the correspondent axes of the plane and the vector that is normal to that plane shown in green and red respectively. **(D)** The regressed plane is illustrated with unit vectors (axes) that reflects the most variation of the data marked in dark green, and the residual variation of the data marked in light green, and a vector that is normal to that plane marked in red. A normalized reference vector denoted in black is also shown to point towards (1,1,1) coordinate, which represents the instance when there is no change in the distance between time t, t+1, and t+2 (which most likely reflects no movement for 3 consecutive frames). **(E)** The projection of the 3-dimensional coordinates in (B) on the regressed plane were plotted, and the shape of such projection was examined. **(F)** The parameter of interest was the deviation of the angle between the normal vector (red) and reference vector (black) in (D) from $\frac{\pi}{2}$ (i.e., abs(angle -$\frac{\pi}{2}$)). In general, a large deviation value would imply large motions across 3 consecutive time frames. The angle deviations were computed for each walking tasks (W1, W2, W3) and plotted on the 3-dimensional graph, where each axis denoted the deviation value from the 3 walking tasks, and marker color represented different demographic cohort .

4.2.4.4 Mutual information of inter-spike interval (ISI) between EEG independent components, EKG, and magnetometer data

As a fourth set of analytics, we extracted the ISIs from three modes of data – EEG to reflect the CNS, magnetometer to reflect the PNS, and EKG to reflect the ANS. To represent the PNS, we chose to use the magnetometer data, as this would represent a more apples-to-apples comparison with the other two modes of data – EEG, EKG – since its unit is a function of voltage. The motion capture device used in this study yields magnetometer data in arbitrary unit (au), which is a normalized value of Gauss unit. For the purpose of this study, we are focused on the timing of the spikes, and not the amplitude, so the normalization of the values should not affect the result of this analytics.

The EEG data used in this study were not obtained directly from the 31 channels of EEG sensors, but instead were decomposed through independent component analysis (ICA) using the Infomax ICA algorithm (Delorme & Makeig, 2004; Makeig, Bell, Jung, & Sejnowski, 1996; Whitmer, Worrell, Stead, Lee, & Makeig, 2010) with at most 512 iterations. Such decomposition allows locating a set of sources from which the signal originated from. This decomposition was done per task (condition), and provided a set of time series of 15 to 31 components (depending on how many rank/null space was present across task/participant), which were a set of spatially static, and maximally independent component processes. Subsequently, source localization of each of these components was performed, using Dipole fitting method (Oostenveld & Oostendorp, 2002) that computed an equivalent current dipole modeling co-registered to fit the scalp topography of a Spherical Four-Shell (BESA) head model (**Figure 4.7**). The locations of the obtained sources of each independent component were then categorized into ‘in-brain’ and ‘out-brain’. Components that were categorized as ‘in-brain’ were those with sources located within 83 mm from the center of the BEM head model; and sources located beyond 83 mm from

the center of the head model were categorized as ‘out-brain’. Given that channel sensors were located uniformly 85 mm away from the center, 83 was a conservative choice that accounted for sources that were located on the scalp, which is supposedly due to head and facial muscle movements. The separation of components inside and outside the brain allowed us to distinguish signals that are generated within the brain and those generated from the muscle and other non-brain related artefacts. In general, there were approximately 0-5 components (out of 15-31 components) whose dipole locations were categorized to be ‘in-brain’, and the rest were considered ‘out-brain’. The fitness of each component dipole modeling is summarized by the residual variance, which is the unexplained fraction of the data variance. Although there is not a set standard on what is an acceptable threshold for this residual variance, a recent study by Gwin et al. (2011) which measured the EEG signals during treadmill walking eliminated components with residual variance that was more than 20%. In our study, the residual variance of a typical participant during walking task ranged from 5% to 45%. Given the small number of in-brain components per task/participant, excluding some components with large residual would lead to loss of data altogether. For that reason, we kept all components that were provided by the dipole fitting, while taking notice of the diverse range of model fitness.

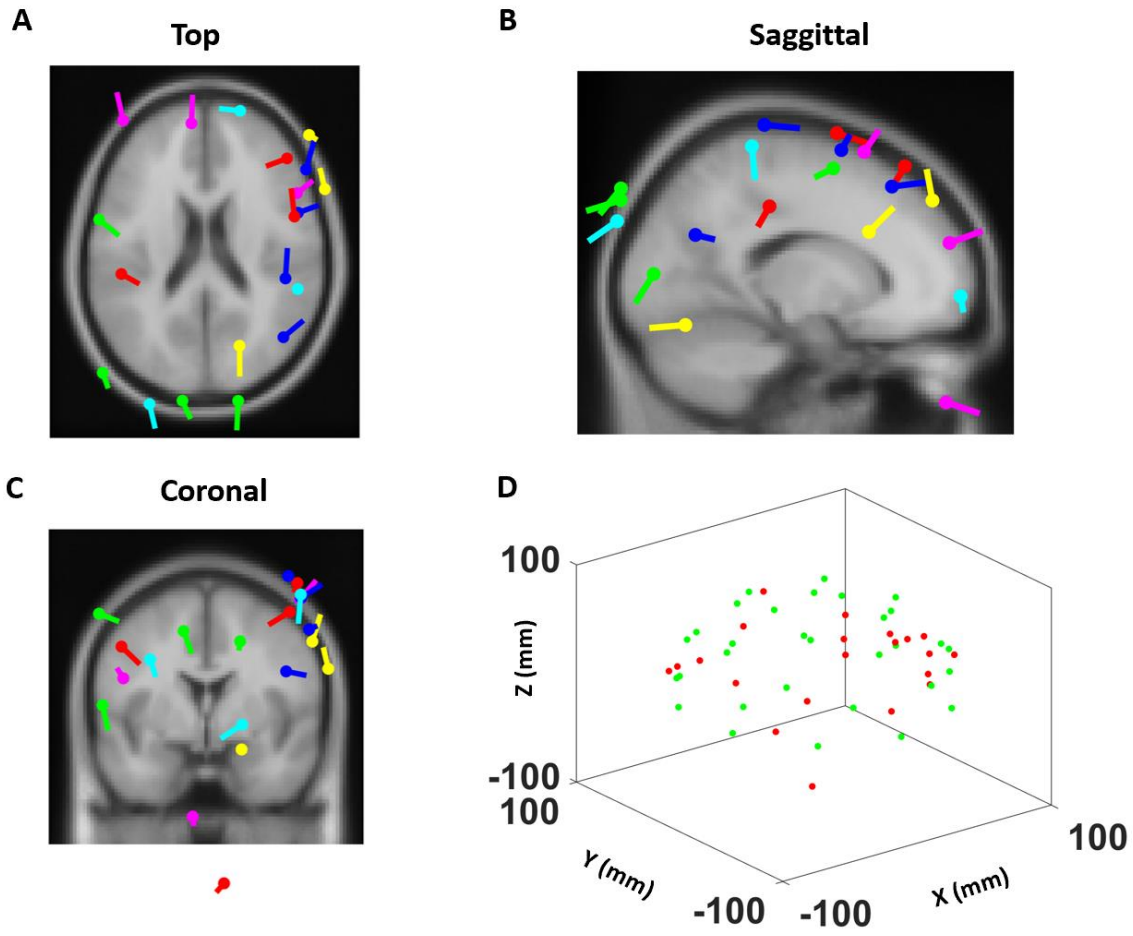

Figure 4.7. Source locations of independent component (IC) from a typical participant's EEG data. (A) IC source locations from the top viewpoint, **(B)** sagittal viewpoint, and **(C)** coronal viewpoint. Some are located along the boundaries of the scalp, implying them to be signals generated by non-cortical activities (e.g., facial muscle movement, EEG cap movement, head movement). **(D)** Location of these IC's denoted in red, and of physical channel sensors denoted in green.

After the ISIs of the EEG components, magnetometer, and EKG were gathered for each condition per participant, histograms of ISIs were created for all EEG sensors, all magnetometer sensors, and EKG sensor, yielding 33-49 histograms per condition (depending on how many independent components were derived from the EEG data) (Figure 4.8**B**). Based on these histograms, pairwise mutual information was computed to understand the ISI information dependence of signals across different tasks. These histograms were constructed as single

probability distributions $P_X(x)$ with bin width as 1 frame (1/60s), minimum bin value as the minimum ISI, and maximum bin value as the lower of 30 and the maximum ISI. Any ISI that exceeded 30 frames (0.5s) were not included in this analysis, as this would most likely be due to instrumental noise. Joint probability distributions $P_{XY}(x, y)$ for a pair of the ISI histograms could not be empirically determined, as the ISIs do not occur simultaneously. For that reason, the joint probability distribution was estimated by randomly sampling a pair from each histogram's ISI and constructing a joint histogram from these sampled pairs. Using the estimated joint probability distributions $P_{XY}(x, y)$, along with the empirical single probability distribution $P_X(x)$, the mutual information I_{XY} was computed, and this process was repeated 100 times (see section **2.2.4** for details). The median of the 100 estimated mutual information I_{XY} values was then determined as the final value. The final MI values were compared across different pairs of sensor categories (e.g., pairs comprised of 2 EEG sensors; pairs comprised of 1 EEG sensor and 1 body part's magnetometer; pairs comprised of 1 EKG sensor and 1 body part's magnetometer), and across the three conditions (Figure 4.8**C**).

MI values were compared across participants, by plotting the values of MI in the control condition (W1 or P1), and the absolute change in the median MI values during the metronome condition (W2 or P2) and paced condition (W2, P3) from the control condition (W1 or P1) as shown in Figure 4.8**D.** Different marker colors were used to denote different cohorts to observe any clustering patterns emerging from this plot.

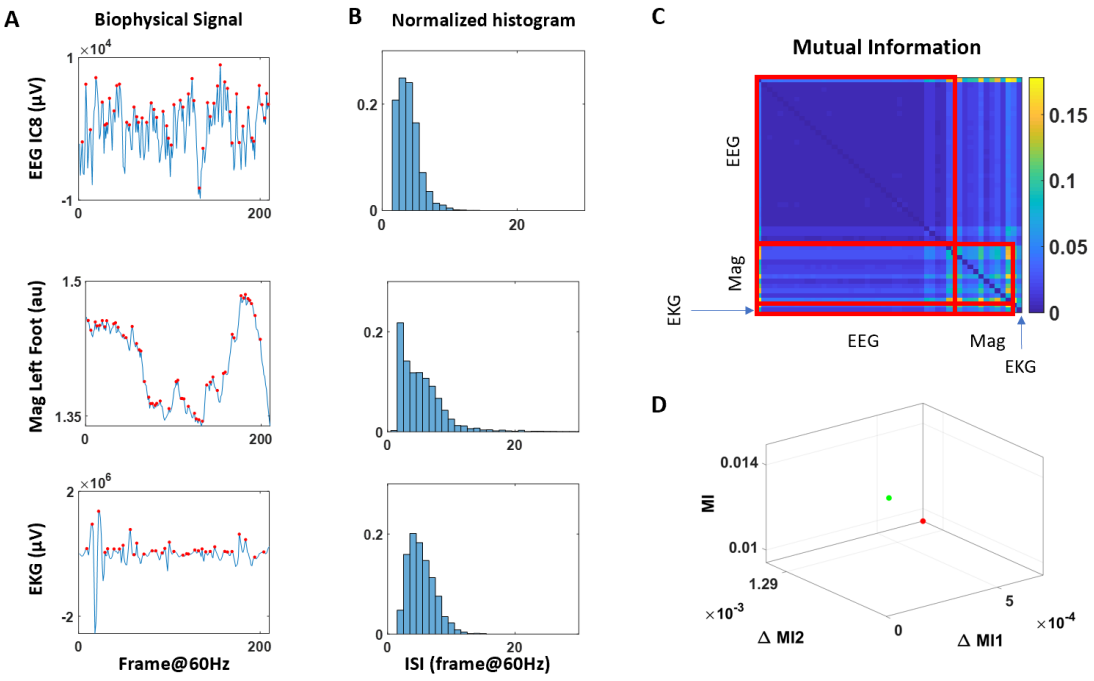

Figure 4.8. Analyzing MI of inter-spike intervals (ISI) between 3 modes of signals (A) Biophysical waveforms of the EEG independent component in μV (top), magnetometer in arbitrary unit (middle), and EKG in μV with spikes denoted in red. **(B)** Time between spikes (ISI) were computed for all sensors, and a frequency histogram was plotted. In order to make these histograms comparable across different modes of sensors, the frequency was normalized to values between 0 and 1. **(C)** Matrix of MI for all pairs of sensors (from 3 modes of signals – EEG, Magnetometer, EKG) was plotted for each participant/task. **(D)** For each category of sensor pairs, the median MI was computed for each condition. The median MI during the control condition (P1,W1) was represented on the z-axis (MI); the absolute change in the median MI to the metronome condition (P2, W2) from control condition (P1,W1) was represented on the x-axis (ΔMI1); the absolute change in the median MI to the paced condition (P3,W3) from control condition (P1,W1) was represented on the y-axis (ΔMI2); and different demographic cohorts was represented by marker color.

In addition, to understand the relations of EEG sensor signals with magnetometer/EKG signals, with respect to those generated from within the brain and outside the brain, the same analysis was done by separately examining the EEG component signals for those from the 'in-brain' category, and those in the 'out-brain' category.

While the above analytics examine the overall MI value across different participants, we also examined the variability of the MI values between different sensor pairs. Specifically, for

each participant, there are approximately 80,000 MI values per task condition, since there are approximately 40 sensor's ISI histograms per participant (ranging between 33 and 49). As such, a pairwise computation of MI on these ISI histograms would yield approximately 800 MI values (=40 x 40 / 2) , and 100 runs of MI computation yields approximately 80,000 MI values. Based on these MI values, we compiled a set of 3 dimensional coordinates, where for a certain pair of sensors at a certain iteration (out of 100 runs), the x – coordinate correspond to the absolute change in MI value between the metronome condition (P2 or W2) and the control condition (P1 or W1); the y-coordinate correspond to the absolute change in MI value between the paced condition (P3 or W3) and the control condition (P1 or W3); and the z-coordinate correspond to the MI value at control condition (P1 or W1).

Note, the number of total sensors is different for each condition, as the number of EEG IC are different across tasks. For that reason, when comparing the change across conditions for pairs that included the EEG IC, the choice of EEG component was random. For example, if there were a total of 10 EEG components in the control condition, 12 components in the metronome, and 14 components in the paced condition, we took the minimum number of components (i.e., 10) from the 3 conditions, and randomly chose 10 components among the 12 in the metronome, and 10 components among the 14 in the paced condition. As a result, the 3-dimensional coordinates pertaining to the EEG data do not exactly correspond to each other; that is, the x- and y- coordinate of the paired sensors that include the EEG IC do not exactly reflect the change in MI of the pairs represented in the z-coordinate. That is, if the z-coordinate was the MI between EEG component #1 and #2, the x-coordinate may be the difference in MI of EEG component #1 and #2 in the control condition and the MI of EEG component #10 and #11 in the metronome condition; while the y-coordinate may be the difference in MI of the EEG component #1 and #2 in the control condition and the MI of EEG component #10 and #14 in the

paced condition. We note that such arbitrary correspondence was inevitable, as there is rarely an exact spatial correspondence between different IC. Nevertheless, given the large amount of data used in these analytics, we argue that such difference would be minor in characterizing the patterns of different participant cohorts (**Figure 4.9A**).

Once these 3-dimensional coordinates were obtained, these datapoints were used to create a set of Delaunay triangulation surfaces. Given a set number of discrete points, Delaunay triangulation (Delaunay, 1934) creates a matrix of N x 3, where the 3 columns represent the datapoint indexes that would form the 3 vertices of each N triangle. These triangles are formed such that no other point is inside the circumcircle of the formed triangle (**Figure 4.9B**). Here, we took a list of these triangles and computed the surface area for each, and plotted a frequency histogram. In order to compare the frequency histograms across different participants, it is necessary to keep the total frequency to be the same across all participants. For that reason, the minimum number of triangle areas across all participants was computed (which was 59500); then, for all participants with a larger number of triangle areas, 59500 (i.e., minimum number of triangle areas) of the triangle areas were randomly sampled (**Figure 4.9C-left**) and reflected on the frequency histogram. Here, the triangle areas represent the spread of these datapoints, where a larger value would imply wider range of informational dependency of across conditions.

Because of the large number of triangles and skewed distribution of such histograms (as shown in **Figure 4.9C-left**), these were examined by applying logarithm to both axes of the histogram (**Figure 4.9C-right**). Given the linear shape of such power-law distribution, we then regressed this to a line, to examine the spread of such triangle areas. Essentially, the wide spread of triangle areas (represented by a flatter slope and lower intercept of the power-law distribution) would imply a wider range of information dependency between different sensors; conversely, a narrower spread of triangle areas (represented by steeper slope and higher

intercept of the power-law distribution) would imply a narrower range of information dependency between different sensors.

This way of representing the MI data is different from those shown in Figure 4.8, which essentially reflects the median triangle areas; that is, the median magnitude of change in information dependency across different conditions. Here in **Figure 4.9**, the shape of the power-law distribution of triangle areas reflects the *variability* of dependencies between different modes and location of sensors, where a flatter shape would imply a wide variability of dependency across different physiological signals.

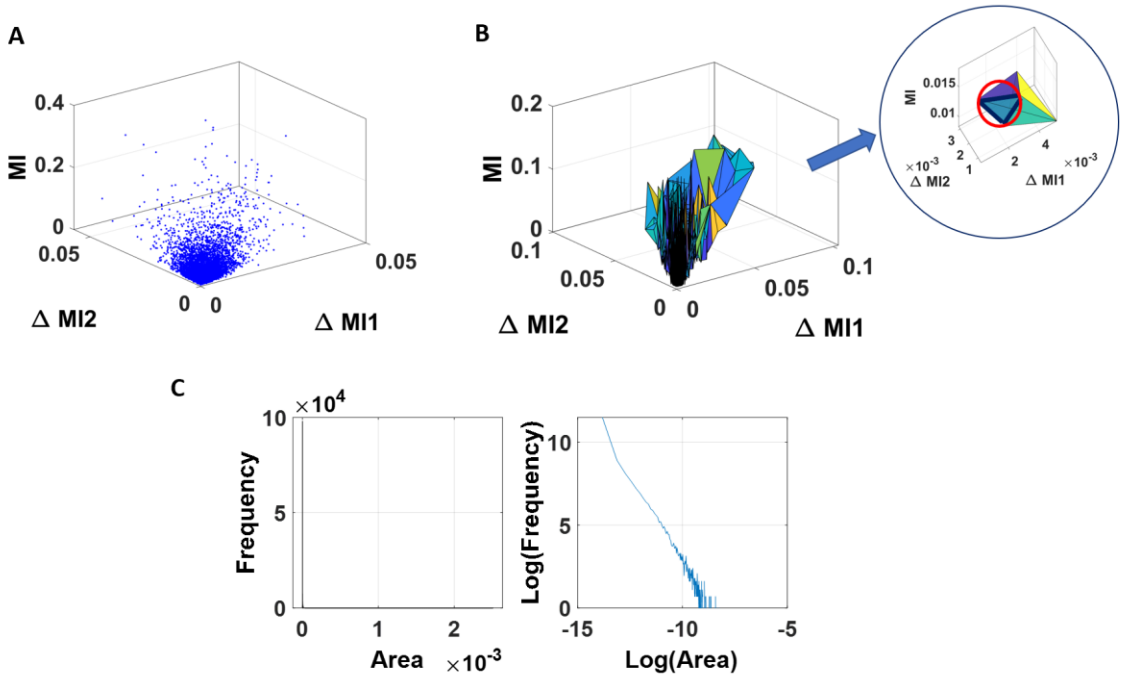

Figure 4.9. Analyzing dispersion of connectivity structure and dynamics characterized by MI. **(A)** For all sensor pairs, the corresponding MI values from the control condition (z-axis, MI) and its change to the other two conditions (x-axis, ΔMI1; y-axis, ΔMI2) were plotted. Note, for each sensor pair, there are 100 MI values, as they were repeatedly computed with random selections of ISI's. **(B)** Using Delaunay's triangulation method, triangles were formed among the 3-dimensional coordinates, and the areas of these triangles were computed. **(C)** Frequency distribution of these triangle areas were plotted (left), and the log-log plot of the frequency distribution (right) was examined. The log-log plot was later regressed to a line, and the slope and intercept were compared across different demographic cohorts.

4.2.4.5 Cross-correlation between different pairs magnetometer sensors

As a last set of analytics, cross-correlation was examined between different pairs of magnetometer sensors. Here, the time series of magnetometer data were normalized to values 0 to 1 following **Error! Reference source not found.**. (**Figure 4.10B**) Then, they were separated into 5 second segments. For each segment, cross-correlation was computed for each sensor pairs (**Figure 4.10D**). This is similar to the analytics described in **section 3.2.4**, but is different in that it was segmented by a fixed time unit rather than a variable inter-heart beat interval time. This is because the EKG data captured by the current study's instrument had too much noise to extract the exact timing of the R-peaks. For that reason, we resorted to a fixed time unit, and 5 second was the time frame that was best in characterizing different participant cohorts. Once cross-correlation was computed for each time segment, the median of these the cross-correlation values for all pairs were computed from each segment, and the median of all time segment's medians (of all paired sensors) were computed to obtain a single summarizing cross-correlation value per condition. These were then plotted for all participants, where the z-axis represented the median cross-correlation value during the control condition (W1 or P1), and x- and y-axis to represented the values during the metronome (W2 or P2) and paced (W3 or P3) condition respectively (**Figure 4.10E**).

We also computed cross-correlations of magnetometer data that were high-passed at 6Hz using Butterworth IIR filter at 2nd order, and compared this across the different participant cohorts. Tremor is one of the main symptoms of Parkinson's patients, and this tremor of the body motion is known to exist in the 4-6Hz range (Deuschl, Bain, Brin, & Committee, 1998; Jankovic, Schwartz, & Ondo, 1999; Lee et al., 2016). For that reason, we excluded the tremor by high-pass filtering the magnetometer data, to understand how the tremor impacts characterizations based on the cross-correlation analytics (**Figure 4.10C**).

Note, the same analysis had been done on the EEG component data as well, and similar results had been found as with those from using magnetometer data. However, we found the magnetometer data to be more informative in characterizing the Parkinson's patient cohort than the EEG data. Hence, in this study, we only share the magnetometer data results.

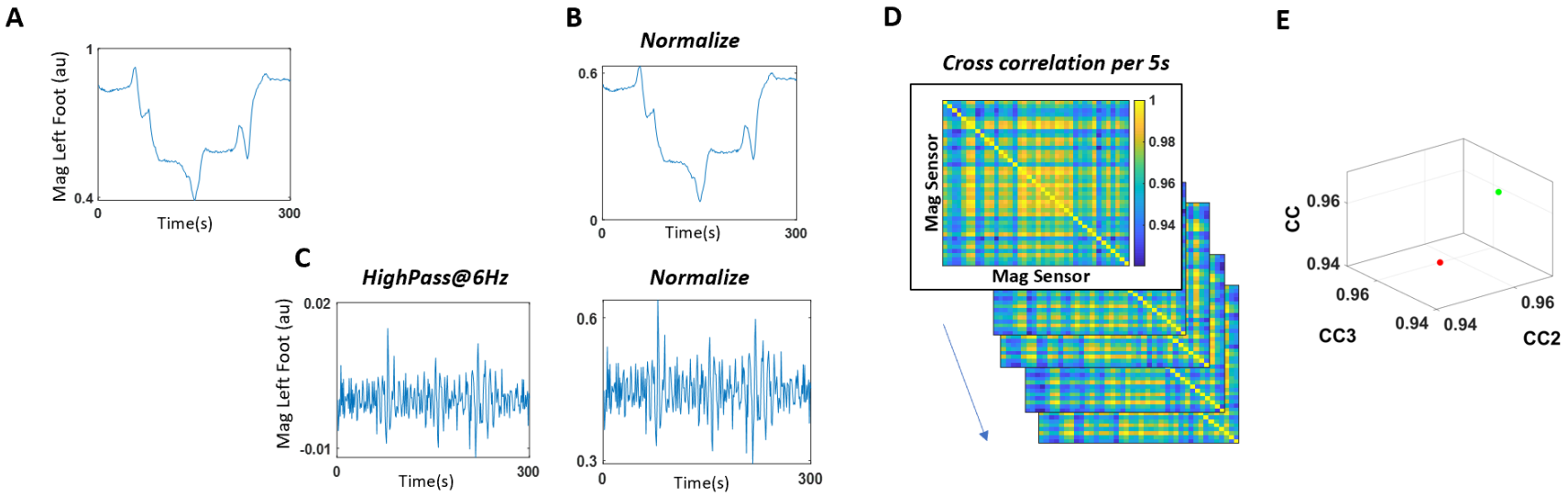

Figure 4.10. Analyzing cross-correlations between different magnetometer sensor data. (A) Magnetometer data of the left foot in arbitrary unit is plotted. **(B)** For all body sensors, the raw data was normalized as values to range between 0 and 1. **(C)** For all body sensors, the raw data was also high-passed at 6Hz (left), and then normalized as values to range between 0 and 1. **(D)** For each 5 second segment, cross-correlation between all sensor pairs for both normalized magnetometer data (from (B)), and high-passed and normalized data (from (C)). Maximal cross-correlation value was extracted for each pairs, and were plotted on a matrix. **(E)** The median maximal cross-correlation was computed for all sensor pairs and for all 5 second segments, and was plotted on a 3-dimensional plot, where the z-axis (CC) denoted the median value during control condition (P1, W1), x-axis (CC2) denoted the value from the metronome condition (P2,W2), and y-axis (CC3) denoted the value from the paced condition (P3,W3). The marker color denoted the different demographic cohort.

4.3 Results

4.3.1 Gamma PDF fit of pen movement during drawing tasks

Standardized spikes of the pen movement linear velocity were reduced by 0.5, and the histogram of such shifted standardized spikes were fitted with a Gamma PDF. The fitted Gamma parameters and their moments were plotted for all participants for each drawing task and is shown in **Figure 4.11**. For all drawing tasks, Parkinson's patients tend to have a lower scale and higher shape parameter than the NT cohorts. Here, the single participant with ASD and the patient with Essential Tremor did not show noticeable difference in its stochasticity compared to the NT cohorts. This separation is most pronounced during the clock and Benson2 (drawing the Benson figure from memory) task, which are the two tasks where the participant is given a blank sheet of paper and is instructed to draw with more freedom. These two tasks contrast with other drawing tasks, where participants are given a paper with some form of figures printed on it (e.g., circles with letters and/or numbers), and thus have relatively less freedom in their pen movement.

When we examine the general shape of the PDF in relation to the fitted parameters by plotting the Gamma moments (as shown in **Figure 4.11B,C**), skewness (3rd moment) is the most contrasting aspect that differentiates the Parkinson's patients to their NT cohorts. Overall, the Parkinson's patients tend to have a flatter distribution and is less skewed than the NT participants. Such separation is most pronounced in the clock and Benson2 tasks. Within these two tasks, we also observe the patient with ASD and patient with ET to be clustered within the Parkinson's patient cohort. In these representations, the two age-matched NT participants do not show much difference from their younger NT cohorts. These findings allude to the nature of contact control (control while body is in contact with an object) among individuals with low

cognitive-motor agency pertaining to Parkinson's disease, where they tend to exhibit less NSR in their hand motion stochasticity, especially in cases where there is less restrictions to their movement (as was shown in the clock and Benson figure tasks).

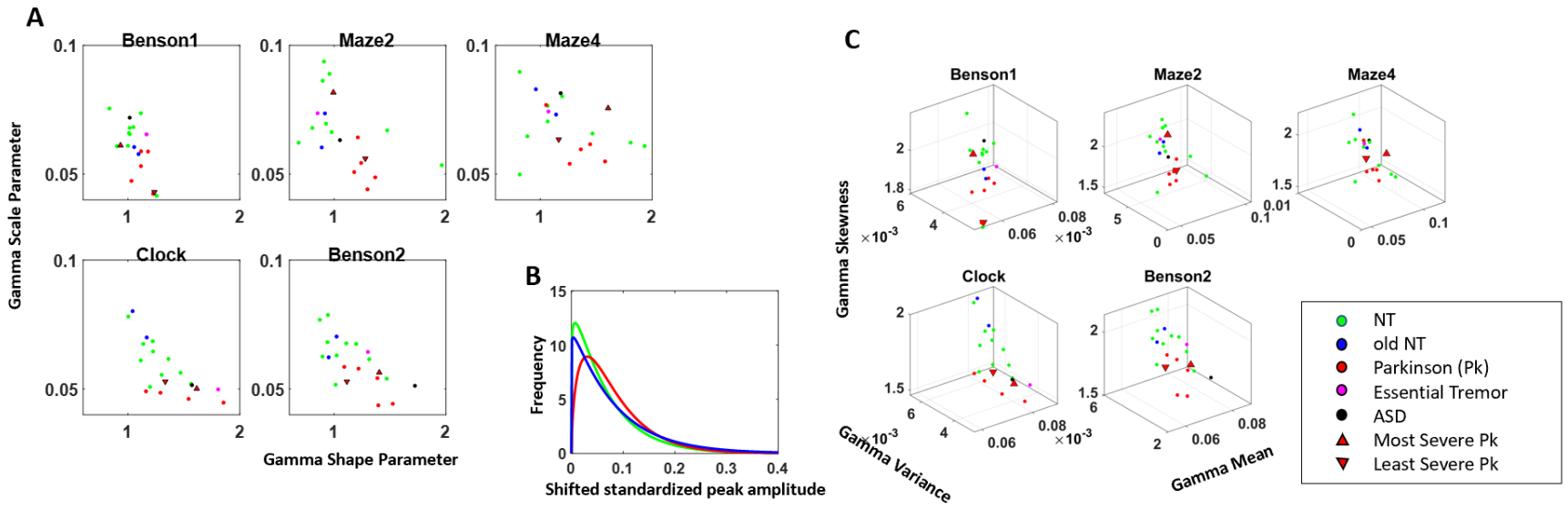

Figure 4.11. Stochasticity of pen movement. (A) Fitted Gamma parameters (of the frequency histogram of shifted standardized spike amplitudes from the pen motion linear velocity) are plotted on the Gamma parameter plane for each drawing task (subplot), with marker color denoting different demographic cohort. Overall, the healthy participant (green) tends to have a higher scale and lower shape parameter than the Parkinson's patient (red) **(B)** Fitted PDF of frequency histograms (of shifted standardized spike amplitudes from the pen motion linear velocity) of a typical healthy young participant (green), healthy age-matched participant (blue), and Parkinson's patient (red). The Parkinson's patient tended to have a flatter shape in its distribution. **(C)** Moments of the fitted PDF (x-axis denotes mean; y-axis denotes variance; and z-axis denotes skewness) for each drawing task (subplot). The Parkinson's patent tended to have a lower skewness value. The separation between the healthy and patient cohorts are most pronounced in the clock drawing (Clock) and Benson delayed task (Benson2).

4.3.2 Gamma PDF fit of center of mass (COM) during walking tasks

The trajectory of the COM was first examined for each participant during their walking tasks. In particular, when we compare the control condition (W1) across all participants, there is a noticeable difference in its regularity, where the NT participant would exhibit a pattern of regular cycles in their walking trajectories; while patients with Parkinson's disorder exhibit a pattern of a more variable and degraded cycle as shown in **Figure 4.12**.

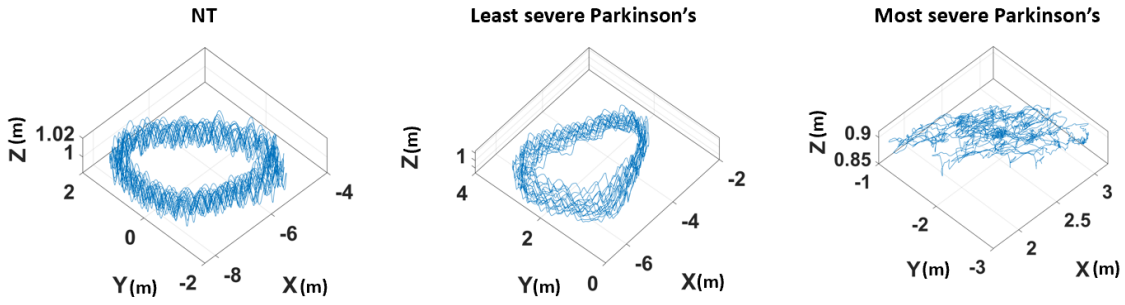

Figure 4.12. COM trajectory during a walking task (left) of a healthy young (NT) participant, **(middle)** of a Parkinson's patient with least severity, and **(right)** of a Parkinson's patient with most severity. We observe a degradational pattern in the COM trajectory as the symptoms of Parkinson's disease worsen.

To quantify such pattern, as with the pen movement data in **Figure 4.11**, standardized spike amplitudes of the COM linear velocity was reduced by 0.5, and aggregated across conditions to fit a Gamma PDF, allowing us to understand the stochastic nature of the COM kinematics.

When examining the fitted Gamma parameters, consistent with the patterns found in previous studies on Parkinson's patients (Torres et al., 2014), Parkinson's patients show a higher scale and lower shape parameters compared to their NT cohorts for all three walking tasks (Figure 4.13**A**). Noticeably, the most severe patient shows to be at the extreme end of the cluster within these Gamma parameter plots, while the least severe patient was shown to be at

the boundary of the cluster between the NT and Parkinson's cohort. When we examine the distributional shape of the Gamma PDF, by plotting the three Gamma moments, contrast to the pen movement data, skewness is noticeably high for the Parkinson's patients compared to their NT cohort, with the most severe Parkinson's patient showing a relatively high skewness level compared to the rest of the participants. Alongside, Parkinson's patient shows a higher mean and variance in its fitted PDF, compared to their NT cohort (Figure 4.13**B,C**).

In addition, one age-matched (old) NT participant shows a slight difference from their younger NT cohorts, as its fitted parameters and moments are positioned somewhere in the middle between the clusters of Parkinson's patient and the typical younger NT cohort; the other age-matched NT does not show much difference against their younger cohort. The patients with ASD and ET also do not show much difference from the NT cohort as well.

Lastly, the change in clustering pattern across the three conditions is not noticeable from the plots of Gamma parameters nor the moments. As such, the impact of actively pacing one's breathing rate does not seem to affect much to the stochasticity of COM. However, the clear separation of the COM stochasticity for all conditions between healthy individuals and Parkinson's patients illustrates how varying degrees of cognitive-motor agency can be characterized by the stochasticity of an individual's walking pattern.

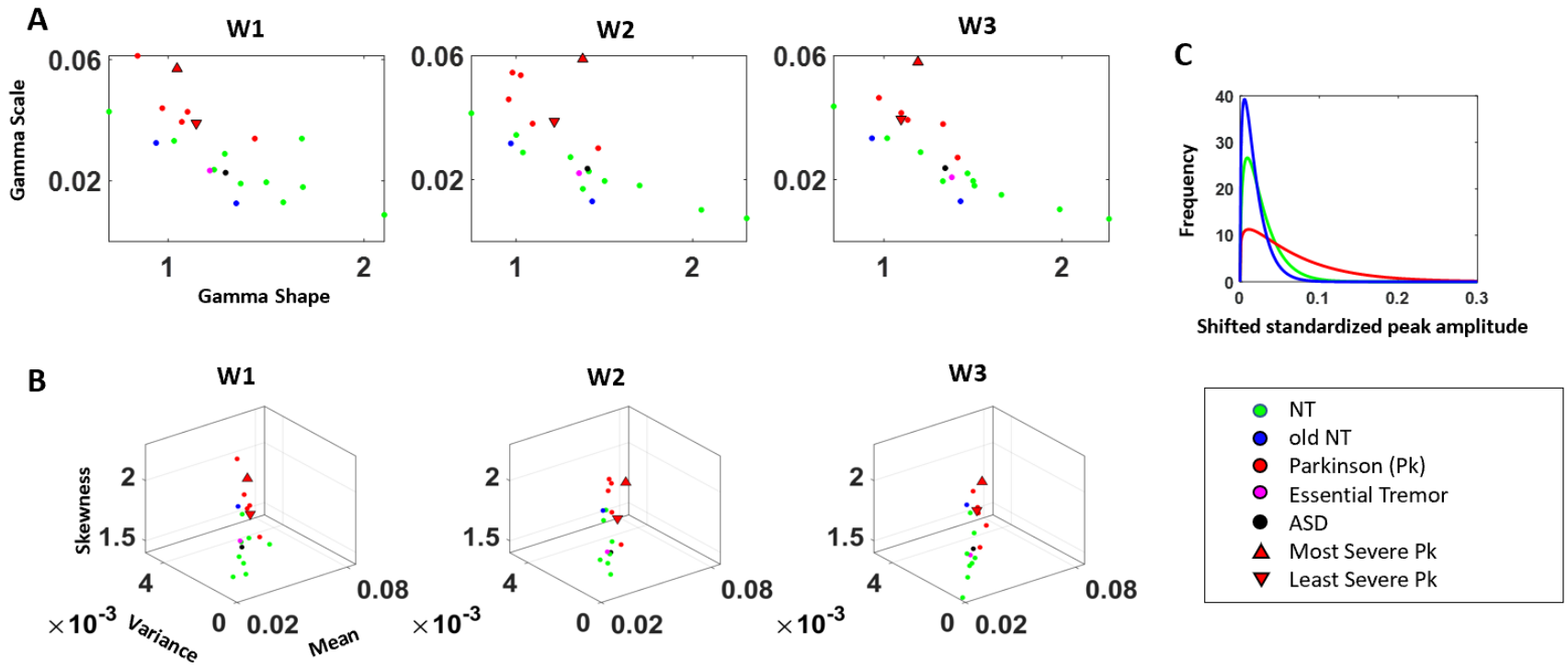

Figure 4.13. Stochasticity of COM during walking tasks (A) Fitted Gamma parameters (of the frequency histogram of shifted standardized spike amplitudes from COM linear velocity) are plotted on the Gamma parameter plane for each walking tasks (condition W1, W2, W3), with marker color denoting different demographic cohort. Overall, the Parkinson's patient (red) tends to have a higher scale and lower shape parameter than the NT participant (green) (**B)** Moments of the fitted PDF (x-axis denotes mean; y-axis denotes variance; and z-axis denotes skewness) for each walking tasks (subplot). The Parkinson's patient tends to have a higher skewness value. The separation between the NT and patient cohorts are noticeable for all walking conditions. **(C)** Fitted PDF of frequency histograms (of shifted standardized spike amplitudes from the COM linear velocity) of a NT participant (green), healthy age-matched participant (blue), and Parkinson's patient (red). The Parkinson's patient tends to have a flatter shape in its distribution.

4.3.3 Dynamical changes in body part distances from center of mass (COM)

The trajectory of the distance between right foot and COM were plotted on 3-dimensional graph with coordinates as the distance at time (t,t+1,t+2). These datapoints were then regressed onto a plane, and the projection of these datapoints onto the regressed plane was plotted in **Figure 4.14**. Here, we find contrasting shapes in the projection between the NT cohorts and the patient cohorts, such that the NT form a donut-like shape with a hole in the middle; while the patient cohort (Parkinson, ASD, ET) do not show such shape but shows a rather squashed version of those found among NT participants.

As interpretation, the hole in the middle is a reflection of the distance in datapoints diverging from the reference rector (1,1,1); that is, if the body part moves fast at each moment (i.e., instantaneous frame-by-frame change in position of the body part is large), which is most often the case for the most active body part (as shown in **Figure 4.5**), the datapoints would diverge from the reference vector, and if this fast action is regular and cyclical, the projection trajectory would exhibit a hole in the middle. The typical NT participant seems to show that pattern; whereas the patient participants have a relatively slow and irregular pattern in their trajectory cycle.

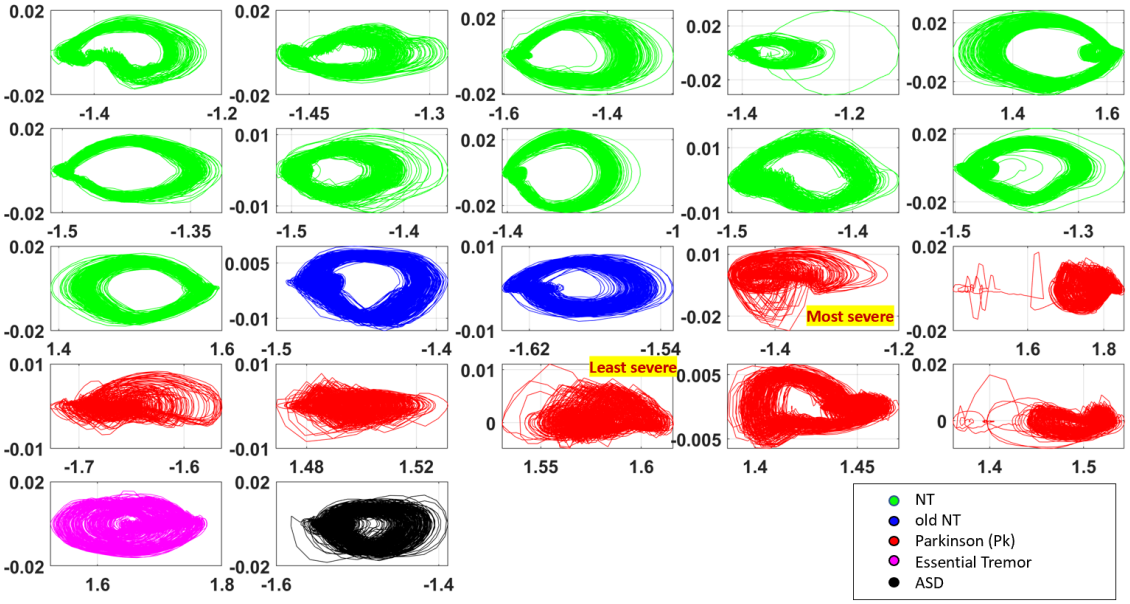

Figure 4.14. Projection of the 3-dimensional coordinates (of distance between right foot and COM) onto a regressed plane for each participant, with color denoting different demographic cohort. For most Parkinson's patients (red), we observe an absence of the donut-like shape in the projection trajectories, contrasted by the NT participants (green, blue).

In order to quantify the extent of how much these distance datapoints deviate from the reference vector, the angle between the reference vector and the normal vector of the regressed plane were computed. If the datapoints did not deviate at all (i.e., there were no motions), this angle would be exactly $\frac{\pi}{2}$; conversely if the datapoints deviated a lot (i.e., there were lots of cyclical fast motions) this angle would be different by a large degree from $\frac{\pi}{2}$. This angle deviation from $\frac{\pi}{2}$ was plotted for all participants and for each body parts in **Figure 4.15**, with each axis denoting different conditions of the walking task (W1, W2, W3). Overall, the clustering pattern is consistent across all body parts, such that NT cohorts tend to have a large angle deviation than the Parkinson's patients, and this is the case for all three conditions. However, the separation between the NT and Parkinson's patients do not seem as pronounced

in the extremities of the upper body (e.g., right upper arm, right forearm, left forearm) while the separation is better noticeable in the truck and lower body extremities.

Among the two age-matched NT participants, the datapoint of one participant generally lied within the cluster of the younger NT cohort, while the other participant's lied on the boundary between the NT and Parkinson cluster. The ASD patient's datapoint generally lied within the cluster of the younger NT cohort, while the ET patient's was found to lie within the Parkinson's cluster. This tendency is most visible in the torso and lower body parts (e.g., torso, right toe); while this is not necessarily the case in the upper body extremities (e.g., right hand, left forearm).

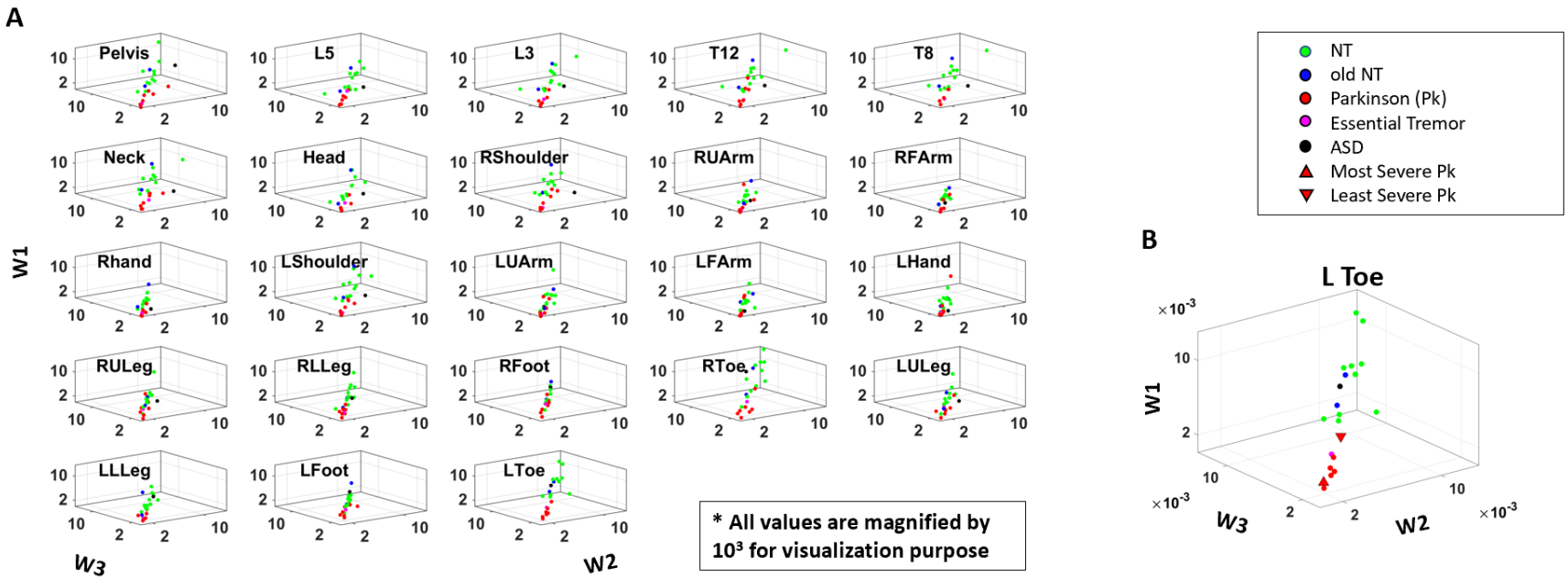

Figure 4.15. Deviation of the angle between the normal vector and reference vector from π/2 (i.e., abs(angle - π/2), where the normal vector is obtained from planar regression of the 3-dimensional coordinates of distance between body part and COM at time (t,t+1,t+2). **(A)** The angle deviations are plotted for each body part (subplot) and for each participant with color denoting different demographic cohort during condition W1 (z-axis), W2 (x-axis) and W3 (y-axis). In general, a small deviation value would imply small change in motions across 3 consecutive time frames; and this is found to be the case for Parkinson's patients (red) for all body parts, but most pronounced from the foot area (which is supposedly the most active body part during a walking task). **(B)** Magnified plot of (A) of Left Toe. We observe that the datapoint of a Parkinson's patient with the most severity (red triangle) lies on the lower end of the Parkinson's patient cluster; while the datapoint of a patient with least severity (inverted red triangle) to lie on the higher end of angle deviation values within the cluster.

For further analysis, we focused on the distance between left toe and COM as our parameter of interest for walking tasks, and the distance between the dominant hand and COM as the parameter for pointing task. These body parts were chosen, because the most active body part was shown to be the most informative in separating between different cohorts. We also examined the distance between left toe and COM during pointing tasks, to compare between walking versus pointing tasks.

During the three walking tasks, for the left toe, Parkinson's patients showed little angle deviation than their NT cohorts, with the most severe patient showing the least deviation, and the least severe patient showing the most deviation among the patients. For this particular body part, the two age-matched NT did not show much difference from their younger cohort. While the ASD participant showed similar tendencies as the NT, the ET participant exhibited similar pattern as the Parkinson's patient. Across the three conditions, there were little difference in this clustering pattern (**Figure 4.16-left)**.

On the other hand, during the three pointing tasks, for the same body segment data (left toe), there is some difference in clustering pattern across the different tasks. Specifically, there is little separation between the Parkinson's patient and NT participants for conditions P1 and P2; however, there is significant separation between the two cohorts for condition P3, such that the Parkinson's patient tend to have little angle deviation, while the NT participants tend to have larger angle deviation. Among the two age-matched NT participants, one's datapoint lied closer to the Parkinson's cluster, while the other participant's datapoint lied closer to the NT cluster. Also, the ET participant's datapoint lied closer to the NT cluster, while the ASD participant, in this case, lied closer to the Parkinson's cluster (**Figure 4.16-middle)**. This was also shown as a trend for the dominant hand during the pointing tasks (with no statistical significance), where we found similar clustering patterns, with more separation between the NT

and Parkinson's cohort for condition P3 (**Figure 4.16-right)**. See **Table A 12** for details of the statistics.

In general, patients with impeded motor control seemed to move slower, which is why they showed lower angle deviations in general. However, this was only noticeable during the walking tasks. This was not necessarily the case for pointing tasks, implying the lower cognitive-motor agency in PD is most characteristic when the entire body is balancing on its own (as in standing and walking) than when part of the body is not required to maintain balance (as in sitting). In addition, the smaller angle deviation in the toe during the paced pointing task for Parkinson's patient is an interesting pattern of an individual with limited agency, which we elaborate the finding in the Discussion. As NT controls have better cognitive-motor agency than PD patients, we can safely assume that the patterns found among PD patients are characteristics of lower cognitive-motor agency pertaining to the PD symptoms.

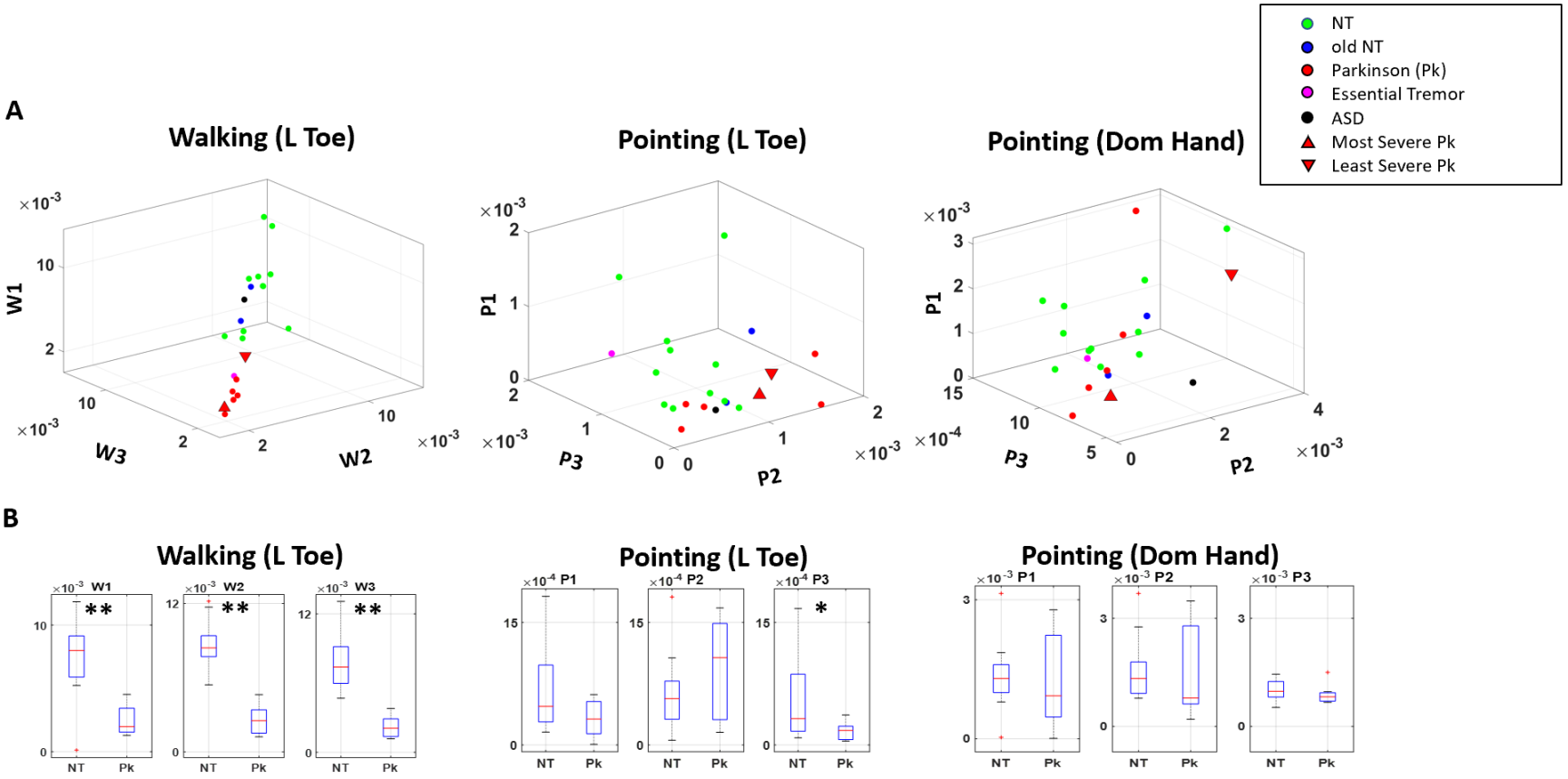

Figure 4.16 Angle deviations from π/2 of walking vs. pointing. (A) (Left) Angle deviation of the left toe during walking tasks (W1, W2, W3), (middle) left toe during pointing tasks (P1,P2,P3), (right) and dominant hand during pointing tasks (P1,P2,P3) are plotted for each participant with color denoting the demographic cohort. Separation between the NT and Parkinson's cohort are most visible during the walking tasks than the pointing tasks, and to a lesser degree during pointing tasks with similar level of separation for the most active body part (dominant hand) and the least active body part (left toe). **(B)** Box plot of the angle deviation values for NT and Parkinson's cohort for all 3 conditions of walking and pointing tasks, with statistical significance denoted by * ($p<0.05$) and ** ($p<0.01$).

4.3.4 Mutual information (MI) of inter-spike interval (ISI) between EEG independent components, EKG, and magnetometer data

The medians MI of ISI histograms between different modes of sensors were examined during the 3 walking tasks for all participants and plotted for all participants in **Figure 4.17**. Overall, Parkinson's patients exhibit less information dependency across all paired sensors, and show a narrower range of change in their dependences across conditions. We also observe that for some participants, the change in MI values are higher from condition W1 to W3, than from condition W1 to W2, as can be seen from the range of x- and y- values shown in **Figure 4.17-right**. That is, the change in connectivity is larger when the individual exerts control on the breathing rate, than when conscious control is not exerted.

The most severe Parkinson's patient shows a more similar pattern to the NTs, and the least severe patient showed a more similar pattern with a typical Parkinson patient. Also, among the two age-matched NT participants, one showed more similarity with the Parkinson's patients while the other was more similar to its younger NT cohort. Here, the ET participant showed a similar pattern with the NT participants; while the ASD participant showed more similarity with the Parkinson's patient.

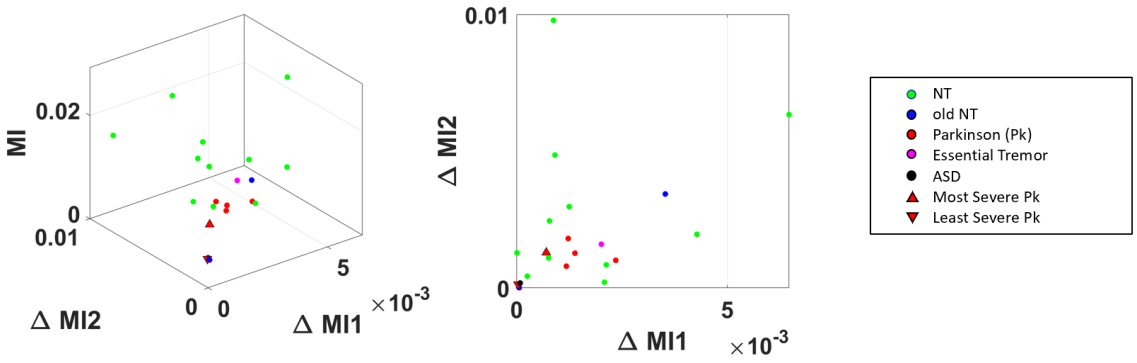

Figure 4.17. MI of inter-spike interval (ISI) between all sensor pairs (EEG, magnetometer, EKG). **(Left)** Median MI (informational dependency) during condition W1 is plotted on the z-axis (MI), and the change in median MI value from condition W1 to W2 is plotted on the x-axis (ΔMI1),

and from condition W1 to W3 on the y-axis (ΔMI2) for all participants, with colors denoting different demographic cohort. **(Right)** Same plot as the left, but from the viewpoint to observe the change in median MI values only. Overall, Parkinson's patients had lower MI values and narrower range in change across conditions, implying less informational dependency (connectivity) between the brain and body signals.

To further examine the interactions between different modes of sensors, these MI comparisons were subdivided by different categories of sensor pairs as shown in **Figure 4.18**. The range of MI is different by the category of sensor pairs that the computation is based on, with pairs of 1 magnetometer data and 1 EKG data having the most information dependency (shown from the large range of MI), and pairs of 2 EEG component data having the least information dependency (shown by the small range of MI). Consistent with the pattern shown in **Figure 4.17**, Parkinson's patients tend to have lower MI values than the NT cohorts for all sensor pairs, and the difference was found statistically significant for the pairs of: 1 magnetometer data and 1 EEG component data; 2 magnetometer data; and 2 EEG component data. Details of the statistical test can be found in **Table A 13**Table A 13.

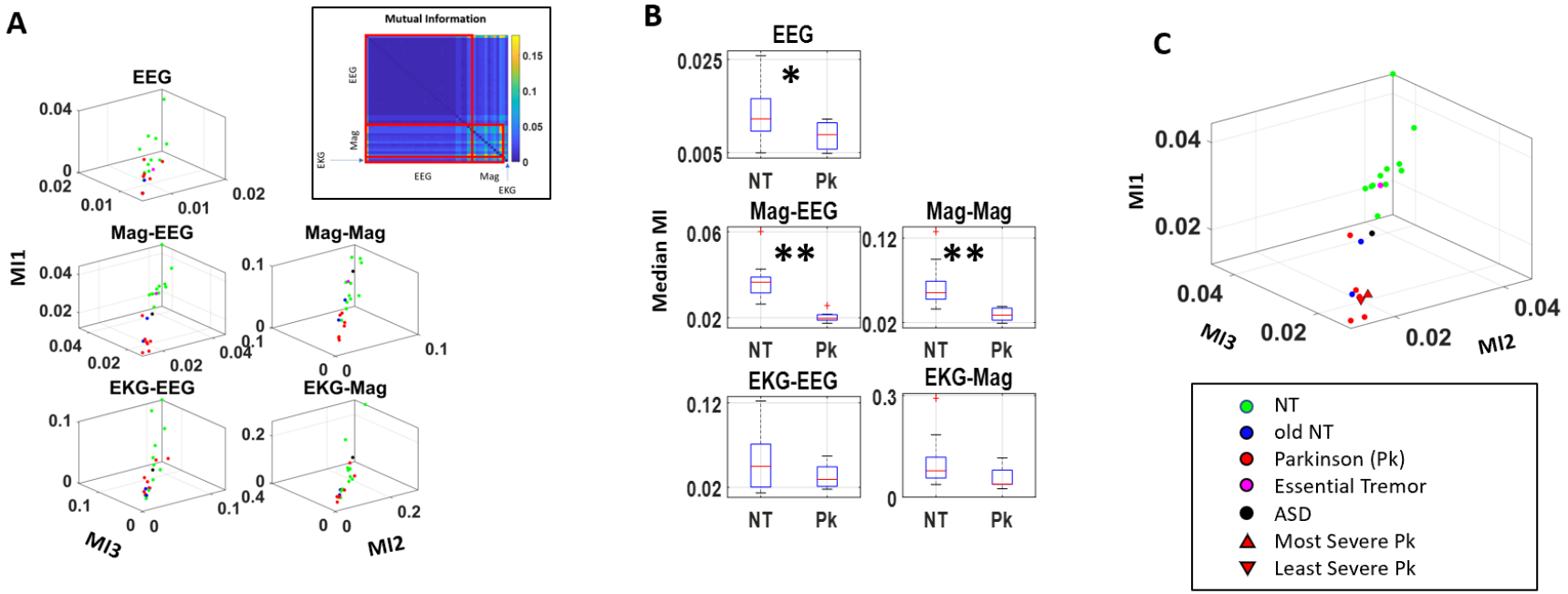

Figure 4.18 MI of inter-spike interval (ISI) for different sensor pair categories (A) Median MI (informational dependency) for condition W1 is plotted on the z-axis (MI1), for condition W2 on the x-axis (MI2), and for condition W3 on the y-axis (MI3); for different sensor pair categories (subplot) of each participant, with colors denoting different demographic cohort. **(B)** Box plot of median MI values were plotted and compared between NT participants (including young NT and age-matched NT) and Parkinson's patients. For all modes of signals, Parkinson's patients show a lower informational dependency; and this is most pronounced in the magnetometer data, and least pronounced in the EKG data. **(C)** Median MI from all sensor pairs are plotted for condition W1 on the z-axis (MI1), for condition W2 on the x-axis (MI2), and for condition W3 on the y-axis (MI3). We observe an observe an overall lower MI values for Parkinson's patients.

In order to see if such pattern persists when the EEG component data is analyzed separately for those that are generated by the brain activity, and those that are generated by non-brain activity (e.g., muscle motion), the same analysis was done as in shown in **Figure 4.19**, but separately for EEG components data from within the brain (IN EEG) and those outside the brain (OUT EEG).

Although the pattern remains the same, where the overall MI is lower for the Parkinson's patients than the NT cohort, the statistical significance is most pronounced in the pairs comprised of 1 OUT EEG and 1 magnetometer data. Given that much of the EEG component localized outside the brain are mostly due to motion artefacts (Delorme & Makeig, 2004), it can be assumed that the information dependency differs the most among the signals coming from the PNS, such that those with lower cognitive-motor agency exhibit less information connectivity in the bodily signals than those with higher cognitive-motor agency. However, we also caution that there were 4 less participant data within IN EEG data, compared to the OUT EEG data. This is because for those 4 participants, there were no ICs that were categorized as IN EEG from their EEG data. For that reason, we note that the statistical test performed on this comparison, in regards to the IN EEG data, has less statistical power to draw conclusions (**Table A 14**Table A 14).

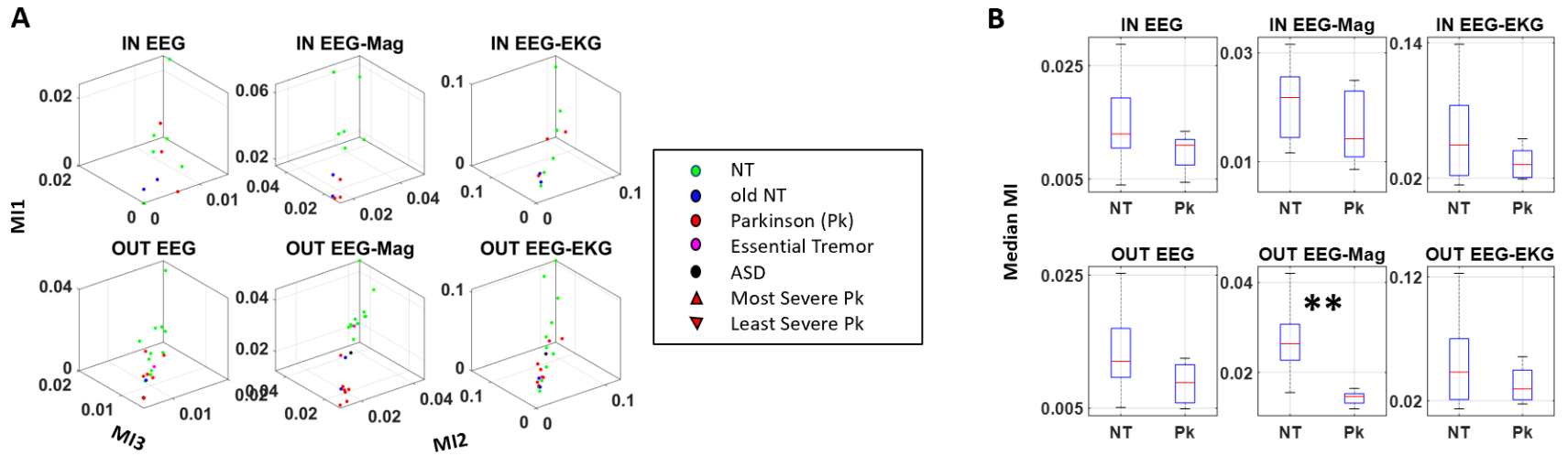

Figure 4.19. MI of inter-spike interval (ISI) for sensor pairs with EEG IC localized inside vs. outside. **(A)** Median MI (informational dependency) for condition W1 is plotted on the z-axis (MI1), for condition W2 on the x-axis (MI2), and for condition W3 on the y-axis (MI3); for different sensor pair categories (subplot) of each participant, with colors denoting different demographic cohort. Top row shows the sensor pairs that include EEG IC localized within the brain, and bottom row shows the sensor pairs that include EEG IC localized outside the brain. The separation between Parkinson's patients and NT cohorts are most pronounced among EEG IC data that are localized outside the brain. **(B)** Box plot of median MI values were plotted and compared between NT participants (including young NT and age-matched NT) and Parkinson's patients for sensor pairs that include the EEG IC data localized within the brain (top) and outside the brain (bottom). For all modes of signals, Parkinson's patients show a lower informational dependency; and this is most pronounced in the magnetometer data and EEG IC data localized outside the brain.

We further analyzed the overall variability of MI values across different modes and spatial location of sensor pairs within each condition, by plotting the histogram of the MI values of all sensor pairs, and fitting the logarithm of this histogram to a line. The slope of this regressed line was the parameters of interest. In particular, a steeper slope would imply less variability of MI values across sensor pairs than a flatter slope; conversely, a flatter slope would imply more variability of MI values.

Here, Parkinson's patients generally show a flatter slope than the NT cohort, implying more variability across their information dependency. As shown from this logarithm applied histogram, the Parkinson's patients generally have lower MI values across sensor pairs (**Figure 4.20-left**). However, when we examine the regressed line of such, we observe that the range of MI values are slightly wider for the Parkinson's patients. In fact, for the same intercept value of the regression line, the Parkinson's patient tends to have a flatter slope than the NT cohort. For interpretation, in this context, the typical Parkinson's patient's lower mean MI value imply less information flowing across the biophysical signals; and a wider variability of the MI values imply that this information flow is more variable across context (condition) and type of signals (sensor).

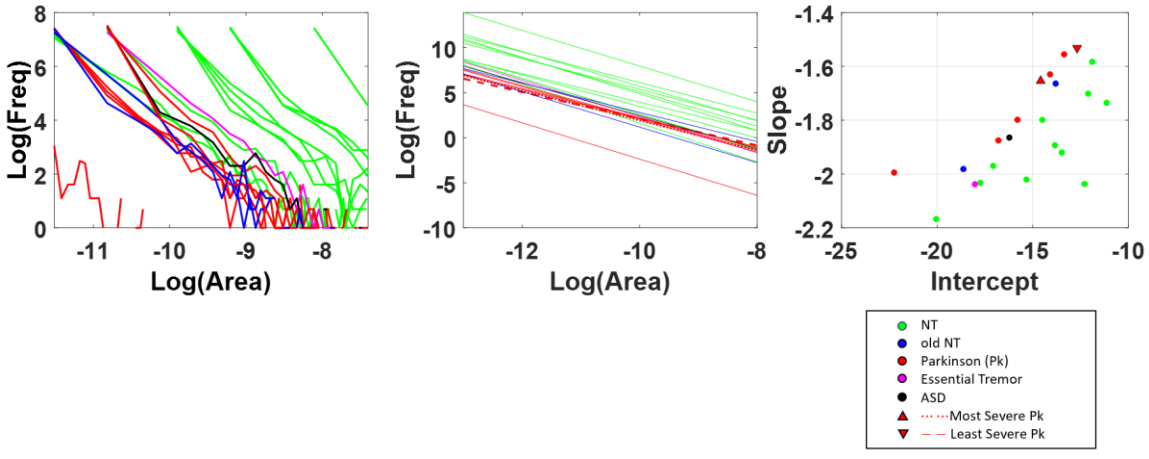

Figure 4.20. Dispersion of connectivity structure and dynamics characterized by MI. (Left) Areas of the triangles formed by Delaunay's triangulation method of MI datapoints of all sensor pairs were computed, and its frequency histogram is shown on a log-log plot, with colors denoting different demographic cohorts. The Parkinson's patients tend to have a smaller area values, implying lower level of connectivity. **(Middle)** The log-log plot of the frequency histogram is linearly regressed for each participant. We observe that the Parkinson's patient tend to have a lower intercept value and a flatter slope. **(Right)** The parameters of the linear regression are plotted on the x- (intercept) and y-axis (slope). For the same intercept, Parkinson's patient tends to have a flatter slope, and for the same slope value, Parkinson's patient tends to have a lower intercept value.

4.3.5 Cross-correlation between different pairs magnetometer sensors

As a last set of analytics, cross-correlation was performed on each 5 second segment magnetometer data for walking and pointing tasks, and on magnetometer data that were high-pass filtered at 6Hz. When comparing the two tasks – pointing and walking – Parkinson's patients tend to have more separation from their NT cohorts during the three walking tasks (**Figure 4.21**), such that their cross-correlation show statistically higher values ($\chi(1,17) = 7.78$, $p<0.01$) than the pointing tasks($\chi(1,17) = 3.78$, $p=0.05$) (**Table A 15**). Within these tasks, the most severe patient exhibits the highest value, while the least severe patient shows the lowest among the Parkinson's patient cohort. However, when we examine the clustering pattern of these cross-correlation based on the high-pass filtered data, the pattern no longer exists, and both Parkinson's patients and NT cohort show a similar range of cross-correlation. Moreover, we observe that datapoints of patients with ASD and ET to lie within the NT cluster for cross-correlation values of both filtered and un-filtered data.

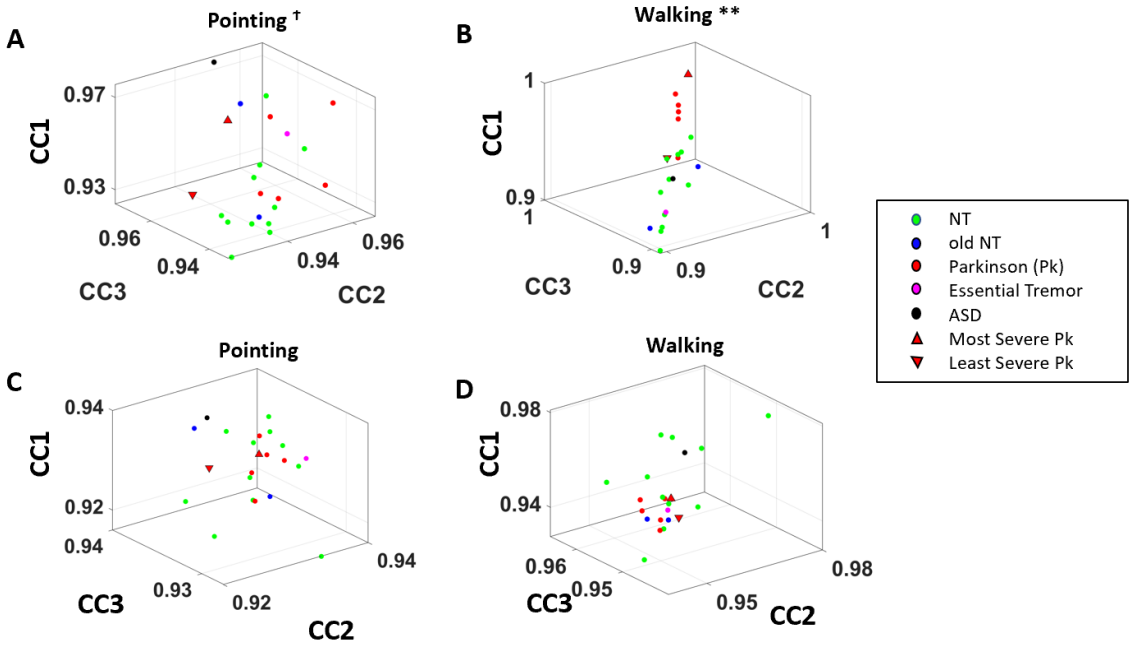

Figure 4.21. Median cross-correlation between all magnetometer sensor pairs of all 5 second segments for pointing vs. walking and for normalized data vs. high-passed and normalized data (A) Median cross-correlation between all magnetometer sensor pairs for the three pointing tasks (condition P1 in z-axis CC1; P2 in x-axis CC2; P3 in y-axis CC3) are denoted as a single data point for each participant, with colors representing different demographic cohorts. **(B)** Same as (A) but for the three walking tasks (condition W1 in z-axis CC1; W2 in x-axis CC2, and W3 in y-axis CC3). Parkinson's patients tend to show a higher cross-correlation across the different parts of the body, with the patient with highest severity to exhibit the higher end of the value. Also, separation between Parkinson's patients and NT participants are more pronounced during walking tasks than pointing tasks. **(C)** Same as (A) but for data that were high-passed at 6Hz. **(D)** Same as (A) but for data that were high-passed at 6Hz and obtained during the 3 walking tasks.

4.4 Discussion

In this study, we designed an experiment where the participant performs a variety of tasks that involve different cognitive and motor processes, while capturing the biophysical signals from the CNS, PNS, and ANS. We presented a set of analytics that reveal the connectivity of biophysical signals that varies with stochasticity. In particular, we found several methods that highlight the difference between Parkinson's patients and healthy participants, with the aim to understand the interactive nature of the biological system from individuals with differing levels of cognitive-motor agency.

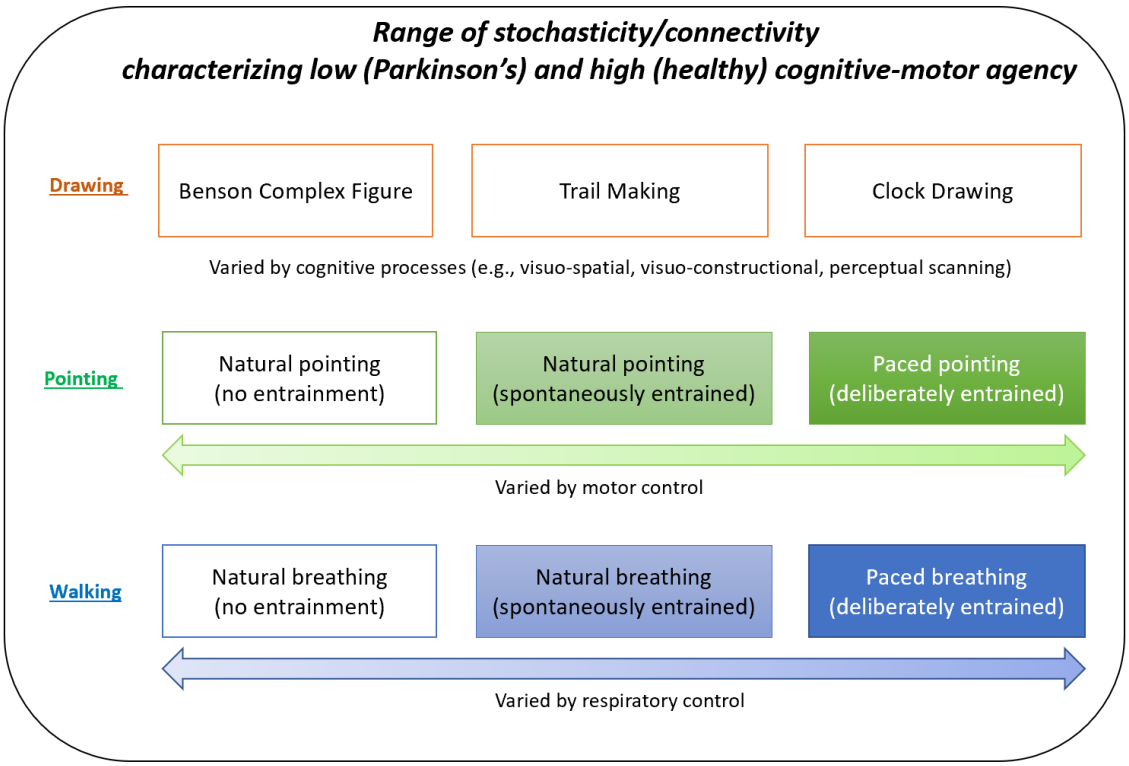

Figure 4.22 Schematic overview of the study

Based on the results of pen movement's stochasticity, we found that Parkinson's patients had lower NSR in their pen motions. However, when we examine the stochasticity of the rest of the body during the same drawing tasks, we did not see such separation between Parkinson's patients and their healthy counterparts (see **Figure A 4** for the Gamma fit of other body parts). This contrasts with the findings of the COM stochasticity during the 3 walking tasks, where the patients exhibited higher NSR in their kinematics signal, as was the case in previous studies (Torres et al., 2011b). It is important to note here that these are different types of motor control tasks. Walking and pointing do not engage the hands in contact with an object, as there is no direct haptic feedback. In contrast, drawing provides continuous haptic feedback to the brain. In the presence of tremor and involuntary micro-motions, the systems of the PD patient may compensate and reduce the NSR by closely monitoring the pressure of the pen against the tablet, as he/she may be interacting with an opposing force (force of the direction from the

tablet towards the pen) in a different manner than the healthy participant. Perhaps the patient pressed harder (or softer) onto the paper than the healthy individual, and thus relied more (or less) on the friction between the pen tip and tablet, leading to a different range of NSR from what would otherwise be observed if the patient freely moved the pen tip in the air. Indeed such 'contact control' have been found to possess different stochasticity than when control is exerted without contact (Yanovich, Isenhower, Sage, & Torres, 2013). We did not record the pen pressure/grip that the participant was exerting in this study, but in the future, this may be informative to understand the patterns that we observed.

We also introduced a new metric that borrows concepts from linear algebra, where we plotted a dynamical trajectory of distance between two body parts (e.g., left toe and COM) in a 3-dimensional coordinate (denoting the distance from 3 consecutive frames; thereby reflecting both linear velocity and acceleration), regressed these datapoints to a the plane, and observed the projections of such datapoints on the plane, and quantified how much those datapoints deviated from the reference vector (i.e., no motion). From the shape of the projections, we revealed the irregularity in body motions among the patient participants, which contrasted the regularity exhibited by the healthy participants' projected datapoints (described by the donut shaped projection in **Figure 4.14**). We also used a measure of angle deviation from the reference vector to quantify how much the body motion deviated from 'no motion', and found this to be small for Parkinson's patients. This was most pronounced during walking, which involved all body parts to actively move. Not surprisingly, the difference between the patients and healthy participants were insignificant during pointing tasks, as there are less motions across the body during this task. However, we noticed some difference in the paced pointing motions between the two cohorts. Although all participants moved the dominant hand at the same pace during this paced pointing condition (P3), the difference may be from the faster instantaneous motions

and jerks shown during the paced condition among the healthy participants (imagine a young person moving the hand fast to touch the target and retract, and waiting for a longer time to wait for the next metronome beat). However, it is interesting to see such separation to be more significant when this measure is based on the distance between left toe and COM (as opposed to the distance between the dominant hand and COM), as we would assume there to be minimal difference between the two cohort (since all participants are seated and merely moving the upper body). We conjecture that perhaps Parkinson's patients have limited motor control, and so during their paced pointing motions, as most control is exerted on the arm, there may be less energy left to exert all the way down to the toe. For that reason, it may be that these patients try to preserve that energy by minimizing the motions of non-acting body parts such as the foot. This finding alludes to the importance of the spontaneous motions (nonactive motions) as they inform us of the systems interactions, and of the cognitive/motor processes that underly it; particularly, among individuals with lower cognitive-motor agency. We also see this pattern from the ASD patient, but not from the Essential Tremor patient. As such, this may not necessarily be the characteristic of lower cognitive-motor agency in general, but of a lower cognitive-motor agency pertaining to Parkinson's disease.

In another analysis, as with the studies from previous chapters, we also looked at the MI across different modes of signals. Here, we further examined the informational dependency separately for EEG signals that were generated by sources within the brain, and those from the scalp and beyond (e.g., muscle artefacts). In general, as with the findings among ASD patients shown in **Figure 3.9**, Parkinson's patients had an overall smaller informational dependency across sensors, and a narrower range of change in dependency across time/condition. However, we found this to be most pronounced from the magnetometer signals, and with the EEG signals that are presumed to be due to muscle motions. These findings suggest that the low

informational dependency across different parts of the body for the Parkinson's patient may be a characterization and perhaps reason for the motor symptoms that they experience. This is because lower MI was found to be a description of less motor control among healthy individuals, as was to be found in their non-dominant side of the body and during their spontaneous actions (see **Figure 2.4**). For the Parkinson's patient with lower cognitive-motor agency, we conjecture that they are not able to exert as much motor control, since they have an overall reduced informational connectivity between the brain and body, hindering them to differentiate actions with varying levels of motor intent. In a later study, it would be informative to specifically quantify the MI range between different levels of motor intent (e.g., between deliberate and spontaneous motions) among PD patients, to see whether their differentiation is indeed muted compared to their NT counterparts.

As another measure of connectivity, we also examined the cross-correlations across different body parts while the participants performed pointing and walking tasks. In general, Parkinson's patients exhibited more similarity in their motions across the body, and these were more pronounced during the walking tasks. However, when we removed the tremor aspects in these motor signals, the correlation level was similar between the patients and healthy participants, implying that a main factor that contributes to such connectivity characteristics is tremor. To further understand the nature of this tremor, we can further examine the tremors within motor signals in a subsequent study.

Although this study introduces many analytics that are conducive to understanding the interactive processes of our nervous systems, these analytics nevertheless have some limitations. The main source of limitation is the imprecision of the EEG signals. The EEG data is fraught with signals that are not from the cortical processes, and ICA method was applied to relieve such concern. However, ICA does not allow extracting the same spatial components of

EEG signals for all participants (e.g., some participants' components are mainly from the frontal area, while another participants components are mainly from the parietal area), making it impossible to get a precise picture and comparison of the brain activities across individuals. Needless to say, the presence of artefacts (in the EEG data) that cannot be clearly identified further complicates the problem. However, the current technological state of brain measures, unfortunately, do not have a quick solution to this problem. Also, the small patient population data we obtained in this study is not large enough to make generalized characterization of the lower cognitive-motor agency pertaining to Parkinson's disease. To obtain a clearer picture of such disorder, we would need to collect more data from age-matched control, and other patient populations with compromised motor control.

Despite such limitation, the study nevertheless is informative in revealing methods and results of characterizing an individual's neurobiological system with varying levels of cognitive-motor agency. In particular, we found how lower cognitive-motor agency pertaining to Parkinson's disease symptoms is characterized by the lower NSR in their kinematics during contact control, and higher NSR during natural walking; narrower range of motions during pointing and walking; and narrower range of connectivity across the body kinematics. By comparing different demographic cohorts and finding clustering patterns among the cohorts, these methods provide clinical application value as a biomarker. I next discuss the research significance from a perspective of translational research.

5 Translational Research

In this thesis, I defined agency as the capacity to control one's behavior at will, and limited the study of agency to the cognitive-motor domain. I attempted to characterize the

different levels of cognitive-motor agency with respect to the processes within one's internal neurobiological system, in the face of various cognitive and memory demands. In this sense, the agency that I characterized is truly embodied, in that it is not a mere cognitive nor a motor capacity (as in physical volition), but is a concerted and integrated capacity of *both* cognitive and motor behaviors. This was done by examining multiple biophysical signals generated by the CNS, PNS, and ANS, and by viewing these signals taking the role of both cause and effect of each other in a recurrent manner (e.g., motor signals as efferent and afferent signals to the brain). By examining the variability of these signals in different cognitive states, and comparing these across patients with different neurological disorders (which are accompanied by symptoms of compromised motor and cognitive capacity), I presented analytics that are informative in characterizing different levels of cognitive-motor agency.

These analytics follow a series of work by E.B. Torres (2018), adhering to the theoretical and statistical framework, called 'Statistical Platform for Individualized Behavioral Analyses (SPIBA by E. B. Torres and Jose (2012))', that harnesses biophysical signals from the peripheral, autonomic, and central nervous systems to understand different levels of cognition, as it develops and as it decays in a variety of neural disorders. This framework was created to assess biophysical data on a personalized basis, according to the tenets of the Precision Medicine and mobile Health concepts (Hawgood et al., 2015). SPIBA makes use of the variability of biophysical waveforms (e.g., fluctuations of speed or acceleration during motor movement, heart's inter-beat-interval, brain signals obtained from electroencephalogram), as these are a rich source of information that is processed by the physical body. Specifically, the statistical properties of fluctuations in the ever-present biophysical waveforms are an output of the body, but are also an input to the entire system in the form of re-afferent signals, enabling coordination and forecasting of the subsequent moment's behavior. Examining the trajectory of various signals'

statistical properties at different time scales -from minutes to years – allows us to objectively and quantitatively track neural development, maintenance, and degeneration across different populations (e.g., neurotypical individuals, patients with ASD, patients with Parkinson's disease, female versus male).

As such, the analytics introduced in this thesis (embodied cognition analytics; ECA) can serve as dynamic digital biomarkers to both categorize the status of an individual's neurological health at a time point, and to track longitudinally as the disease progresses. Moreover, the ever-developing technology of wearable sensors (e.g., mobile phone, smartwatch) provide an affordable and convenient means to capture the biophysical signals to be used as biomarkers, as they have demonstrated to reliably capture the various statuses of the individual in previous studies (e.g., (Torres, Vero, & Rai, 2018)). Indeed, this is an improvement from the current diagnostic methods, because many of the clinical diagnostic tests (e.g., ADOS, MOCA, UPDRS) include components that primarily depend on the participant's self-reports and/or the experienced clinician's observation, which are inevitably subjective. As a result, the current diagnostic methods unfortunately leave out important information that transpires largely beneath their awareness. With the analytics offered by ECA (and of SPIBA), the biophysical data registered by wearable sensors can therefore complement the current diagnostic methods with more objectivity.

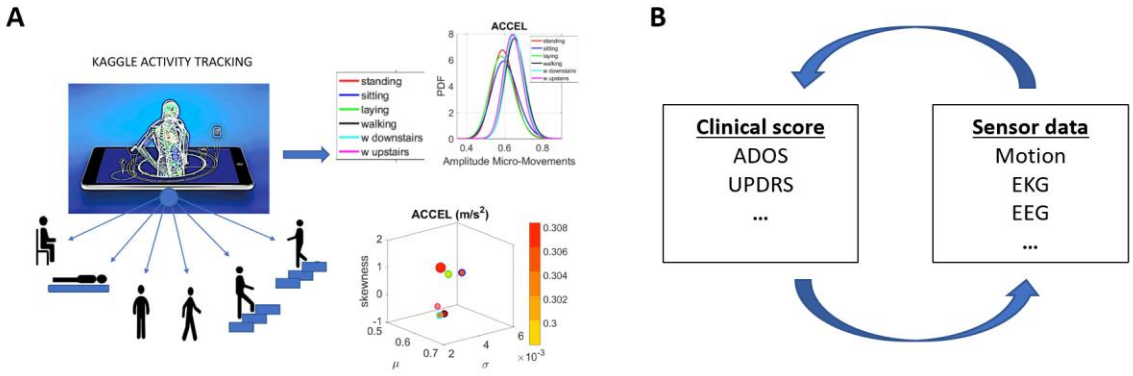

Figure 5.1. Translational research of ECA (A) Wearable sensors such as smartphones can be used with affordability and convenience to register the biophysical signals of an individual to characterize different statuses with the use of SPIBA (figure from Torres et al. (2018)). **(B)** The biophysical signals registered by wearable biosensors and analyzed through ECA (and of SPIBA) can be used as dynamic digital biomarkers to complement the current clinical diagnostic methods with more objectivity.

However, these are not the only merits of ECA (and of SPIBA) on improving the current clinical diagnostic methods. In fact, current diagnostic tests are most often criterion-reference tests rather than norm-referenced tests (Torres, Rai, Mistry, & Gupta, 2019). This means that they do not have a proper metric scale relative to normative data. Because they do not have normative data and lack a proper similarity metric, they are inefficient to track changes in an individual's nervous systems with respect to the neurotypical person's trajectory. This problem has only recently been recognized in the context of neurodevelopment, but applies to other disorders of neurodegeneration (e.g., PD) as well. Furthermore, these clinical tests are based on discrete scales with arbitrarily set ranges (with no correspondence to the biophysical data) and are built on a one-size-fits-all static model that assumes and imposes a given probability distribution function a priori; and this approach neglects the age-dependent shifts in stochastic signatures that needs to be assessed empirically (Torres, 2018).

The ECA (following the SPIBA platform) addresses these limitations of the current clinical diagnostic tests, as it characterizes the neurotypical data to provide norm-reference scales to these criterion-reference tests. Also, as ECA does not assume any distribution a priori, but rather empirically estimates the most adequate one for each person, it provides a range of stochastic regimes that allow an objective and accurate assessment of the patient in reference to the neurotypical person. The deviations of the stochastic regime from the neurotypical person are indicative of the compensatory strategies that the patient's nervous systems develop along the course of a disorder; by quantifying these deviations, we are able to objectively and empirically assess the individual's neural disorder in a personalized manner. The ECA presented in this thesis are, therefore, an improvement from the status quo, as they offer objective metric scales that reflect normative data, and empirically estimate the stochasticity of the biophysical signals on an individualized manner; thus allowing a more accurate dynamic assessment of the disorder of interest.

In assessing cognitive-motor agency among different populations, I have demonstrated the versatility of ECA and its use in clinical studies. Using this framework, I was able to characterize two disorders that are clinically defined by different criteria: ASD based on cognitive deficits and PD based on motor deficits. Through the lens of ECA, we were able to see that ASD also has somatic-sensory-motor deficits and that PD also has cognitive deficits, thus providing a motor criterion for the cognitive-based disorders (ASD) and a cognitive criterion for the motor-based disorder (PD). In this sense, defining agency in the cognitive-motor domain offers a new bridging solution to develop new lines of inquiry in the field of embodied cognition. By objectively measuring the physiological streams during cognitively controlled tasks (by systematically changing levels of cognitive control and types of cognitive processes), I posit that

the ECA framework would introduce a new avenue to inquire about mental spaces, and would thus be conducive to developing a more comprehensive digital biomarker.

6 Conclusion

In this thesis, I defined agency as the capacity to control behaviors at will, and attempted to characterize different levels of cognitive-motor agency through the lens of ECA , where the fluctuations of biophysical signals (MMS) were assessed and compared across different populations with varying levels of cognitive-motor agency. As part of the (coined) embodied cognition analytics framework (ECA), I introduced a set of experimental and analytical paradigms that allow characterizing these varying degrees of agency, through the dynamical patterns of connectivity across the brain and body, while an individual performs naturalistic tasks. By varying the levels of cognitive and memory demands within these experimental settings, alongisde capturing biophysical signals generated by the CNS, PNS, and ANS, I characterized agency through the cognitive-motor processes that unfold within a naturalistic setting. Furthermore, by finding patterns across different patient cohorts, I demonstrated that these characterizations have clinical value in serving as digital biomarkers of neurological disorders.

The novelty of the ECA framework is in capturing the interrelations between motor and cognitive processes that occur across the brain and body, by examining the internally generated activities of the nervous systems during simple drawing/pointing/walking tasks within a naturalistic setting. This framework allows representing both top-down (goal-directed) and bottom-up (spontaneous self-emerging) perspectives of agency (as described in section **1.3**), as an individual's behavior is quantified and tracked during their self-generative, self-monitoring

and self-correcting behaviors, while they perform a few externally imposed tasks (e.g., paced pointing, count backward). Moreover, by observing the range of stochasticity/connectivity across different levels of control, the framework provides a new way to see how systems of varying agency perceives and differentiates the diverse behaviors that oneself makes. For instance, by segmenting motions as deliberate and spontaneous (as done in section **2.2.4**), we were able to see how the system perceives its cause (deliberate motion) and effect (spontaneous motion); and by comparing this differentiation across different populations, we were able to see how different systems effectively (or ineffectively) perceives such differentiation. Indeed, the data analyzed within this framework are those that are not visible to the naked eye, as they are minute fluctuations of one's biophysical signal (MMS). Hence, it is revealing to see how such miniscule type of signal is informative of the cognitive processes that unfolds. Indeed, these re-entrant MMS signals (reafference) offers a new way to monitor the levels and quality of information feedback that the brain may be experiencing from moment to moment.

The data analyzed in this thesis provides a snapshot of an individual's performance under different contexts, as s/he exerts varying levels of control while performing a variety of tasks that require different cognitive-motor skills. As a next step, we can explore these analytics on a longitudinal basis, thereby track the trajectory of one's biophysical signal over longer periods of time. Also, in this thesis, we focused on characterizing the biophysical signals that varied across a range of motor and respiratory control, but as a next step, it would be useful to see them vary by other types of control (e.g., attention). Moreover, exploring different domains of agency (e.g., affect, social) would provide a more complete picture on characterizing agency. However, we should continue to look for ways to minimize instrumentation and extraneous noise in collecting these data as well.

In conclusion, the ECA is a framework that allows studying agency within a naturalistic setting, thereby reflecting the nature of the human body as a complex non-linear dynamical system, as it captures the interactive processes within the multiple layers of the nervous systems. It is an embodied approach to study cognition, and can potentially serve as a bridge to connect the various findings from different fields – from psychology to medical science.

Reference

Adams, R. A., Shipp, S., & Friston, K. J. (2013). Predictions not commands: active inference in the motor system. *Brain Structure and Function, 218*(3), 611-643.

Adolphs, R. (2003). Cognitive neuroscience: Cognitive neuroscience of human social behaviour. *Nature Reviews Neuroscience, 4*(3), 165.

Arzy, S., & Schacter, D. L. (2019). Self-Agency and Self-Ownership in Cognitive Mapping. *Trends in cognitive sciences*.

Asch, S. E. (1955). Opinions and social pressure. *Scientific American, 193*(5), 31-35.

Aston-Jones, G., & Cohen, J. D. (2005). An integrative theory of locus coeruleus-norepinephrine function: adaptive gain and optimal performance. *Annu. Rev. Neurosci., 28*, 403-450.

Bandura, A. (1969). Social-learning theory of identificatory processes. *Handbook of socialization theory and research, 213*, 262.

Barabasi, A.-L., & Oltvai, Z. N. (2004). Network biology: understanding the cell's functional organization. *Nature reviews genetics, 5*(2), 101.

Barlow, H. B. (1989). Unsupervised learning. *Neural computation, 1*(3), 295-311.

Battery, A. I. T. (1944). Army Individual Test Battery. *Manual of directions and scoring*.

Baumeister, R. F. (2008). Free will in scientific psychology. *Perspectives on Psychological Science, 3*(1), 14-19.

Beekly, D. L., Ramos, E. M., Lee, W. W., Deitrich, W. D., Jacka, M. E., Wu, J., . . . Kukull, W. A. (2007). The National Alzheimer's Coordinating Center (NACC) database: the uniform data set. *Alzheimer Disease & Associated Disorders, 21*(3), 249-258.

Bigdely-Shamlo, N., Mullen, T., Kothe, C., Su, K.-M., & Robbins, K. A. (2015). The PREP pipeline: standardized preprocessing for large-scale EEG analysis. *Frontiers in neuroinformatics, 9*, 16.

Box, G. E. P., Jenkins, G. M., Reinsel, G. C., & Ljung, G. M. (2016). *Time series analysis : forecasting and control*. In *Wiley series in probabilit and statistics* (pp. 1 online resource).

Bruineberg, J., & Rietveld, E. (2014). Self-organization, free energy minimization, and optimal grip on a field of affordances. *Frontiers in human neuroscience, 8*(599). doi:10.3389/fnhum.2014.00599

Buchanan, J., & Kelso, J. (1999). To switch or not to switch: Recruitment of degrees of freedom stabilizes biological coordination. *Journal of Motor Behavior, 31*(2), 126-144.

Bulea, T. C., Kilicarslan, A., Ozdemir, R., Paloski, W. H., & Contreras-Vidal, J. L. (2013). Simultaneous scalp electroencephalography (EEG), electromyography (EMG), and whole-body segmental inertial recording for multi-modal neural decoding. *JoVE (Journal of Visualized Experiments)*(77), e50602.

Bulea, T. C., Kim, J., Damiano, D. L., Stanley, C. J., & Park, H.-S. (2014). *User-driven control increases cortical activity during treadmill walking: An EEG study.* Paper presented at the Engineering in Medicine and Biology Society (EMBC), 2014 36th Annual International Conference of the IEEE.

Butkevičiūtė, E., Bikulčienė, L., Sidekerskienė, T., Blažauskas, T., Maskeliūnas, R., Damaševičius, R., & Wei, W. (2019). Removal of movement artefact for mobile EEG analysis in sports exercises. *IEEE Access, 7*, 7206-7217.

Cheron, G., Petit, G., Cheron, J., Leroy, A., Cebolla, A., Cevallos, C., . . . Clarinval, A.-M. (2016). Brain oscillations in sport: toward EEG biomarkers of performance. *Frontiers in Psychology, 7*, 246.

Clark, A. (2008). *Supersizing the mind: Embodiment, action, and cognitive extension*: OUP USA.

Delaunay, B. (1934). Sur la sphere vide. *Izv. Akad. Nauk SSSR, Otdelenie Matematicheskii i Estestvennyka Nauk, 7*(793-800), 1-2.

Delorme, A., & Makeig, S. (2004). EEGLAB: an open source toolbox for analysis of single-trial EEG dynamics including independent component analysis. *Journal of neuroscience methods, 134*(1), 9-21.

Deuschl, G., Bain, P., Brin, M., & Committee, A. H. S. (1998). Consensus statement of the movement disorder society on tremor. *Movement Disorders, 13*(S3), 2-23.

Fahn, S., & Elton, R. (1987). UPDRS program members. Unified Parkinsons disease rating scale. *Recent developments in Parkinson's disease, 2*, 153-163.

Flanders, M., Daghestani, L., & Berthoz, A. (1999). Reaching beyond reach. *Exp Brain Res, 126*(1), 19-30. doi:10.1007/s002210050713

Flanders, M., Pellegrini, J. J., & Geisler, S. D. (1996). Basic features of phasic activation for reaching in vertical planes. *Exp Brain Res, 110*(1), 67-79. doi:10.1007/bf00241376

Flash, T., & Hogan, N. (1985). The coordination of arm movements: an experimentally confirmed mathematical model. *J Neurosci, 5*(7), 1688-1703.

Freedman, D., & Diaconis, P. (1981). On the histogram as a density estimator: L theory. *Probability Theory, 57*(4), 453-476.

Freund, P., Friston, K., Thompson, A. J., Stephan, K. E., Ashburner, J., Bach, D. R., . . . Mohammadi, S. (2016). Embodied neurology: an integrative framework for neurological disorders. *Brain, 139*(6), 1855.

Fuschillo, V. L., Bagalà, F., Chiari, L., & Cappello, A. (2012). Accelerometry-based prediction of movement dynamics for balance monitoring. *Medical & biological engineering & computing, 50*(9), 925-936.

Galton, F. (1875). The history of twins, as a criterion of the relative powers of nature and nurture. *Fraser's Magazine, 12*(71), 566-576.

Gibson, J. J. (1978). The ecological approach to the visual perception of pictures. *Leonardo, 11*(3), 227-235.

Girvan, M., & Newman, M. E. (2002). Community structure in social and biological networks. *Proceedings of the national academy of sciences, 99*(12), 7821-7826.

Green, A. E., Munafò, M. R., DeYoung, C. G., Fossella, J. A., Fan, J., & Gray, J. R. (2008). Using genetic data in cognitive neuroscience: from growing pains to genuine insights. *Nature Reviews Neuroscience, 9*(9), 710.

Gwin, J. T., Gramann, K., Makeig, S., & Ferris, D. P. (2011). Electrocortical activity is coupled to gait cycle phase during treadmill walking. *Neuroimage, 54*(2), 1289-1296.

Haggard, P., & Chambon, V. (2012). Sense of agency. *Current Biology, 22*(10), R390-R392.

Haggard, P., & Clark, S. (2003). Intentional action: Conscious experience and neural prediction. *Consciousness and Cognition, 12*(4), 695-707.

Harris, C. M., & Wolpert, D. M. (1998). Signal-dependent noise determines motor planning. *Nature, 394*(6695), 780.

Hawgood, S., Hook-Barnard, I. G., O'Brien, T. C., & Yamamoto, K. R. (2015). Precision medicine: Beyond the inflection point. *Science translational medicine, 7*(300), 300ps317. doi:10.1126/scitranslmed.aaa9970

Herrero, J. L., Khuvis, S., Yeagle, E., Cerf, M., & Mehta, A. D. (2017). Breathing above the brain stem: volitional control and attentional modulation in humans. *Journal of neurophysiology, 119*(1), 145-159.

Hoehn, M. M., & Yahr, M. D. (1967). Parkinsonism: onset, progression, and mortality. *Neurology, 17*(5), 427-427.

Hoffmann, M., & Pfeifer, R. (2018). Robots as powerful allies for the study of embodied cognition from the bottom up. *arXiv preprint arXiv:1801.04819*.

Janis, I. L. (2008). Groupthink. *IEEE Engineering Management Review, 36*(1), 36.

Jankovic, J., Schwartz, K. S., & Ondo, W. (1999). Re-emergent tremor of Parkinson's disease. *Journal of Neurology, Neurosurgery & Psychiatry, 67*(5), 646-650.

Juarrero, A. (2015). What does the closure of context-sensitive constraints mean for determinism, autonomy, self-determination, and agency? *Progress in biophysics and molecular biology, 119*(3), 510-521.

Jung, T. P., Makeig, S., Humphries, C., Lee, T. W., Mckeown, M. J., Iragui, V., & Sejnowski, T. J. (2000). Removing electroencephalographic artifacts by blind source separation. *Psychophysiology, 37*(2), 163-178.

Kalampratsidou, V., & Torres, E. B. (2018). Peripheral Network Connectivity Analyses for the Real-Time Tracking of Coupled Bodies in Motion. *Sensors (Basel), 18*(9). doi:10.3390/s18093117

Kathirvel, P., Manikandan, M. S., Prasanna, S., & Soman, K. (2011). An efficient R-peak detection based on new nonlinear transformation and first-order Gaussian differentiator. *Cardiovascular Engineering and Technology, 2*(4), 408-425.

Klein, G. (2008). Naturalistic decision making. *Human factors, 50*(3), 456-460.

Lee, H. J., Lee, W. W., Kim, S. K., Park, H., Jeon, H. S., Kim, H. B., . . . Park, K. S. (2016). Tremor frequency characteristics in Parkinson's disease under resting-state and stress-state conditions. *Journal of the neurological sciences, 362*, 272-277.

Leicht, E. A., & Newman, M. E. (2008). Community structure in directed networks. *Physical review letters, 100*(11), 118703.

Libet, B. (1985). Unconscious cerebral initiative and the role of conscious will in voluntary action. *Behavioral and Brain Sciences, 8*(4), 529-539.

Luck, S. J. (2012). Event-related potentials. *APA handbook of research methods in psychology, 1*, 523-546.

Makeig, S., Bell, A. J., Jung, T.-P., & Sejnowski, T. J. (1996). *Independent component analysis of electroencephalographic data.* Paper presented at the Advances in neural information processing systems.

Malcolm, B. R., Foxe, J. J., Butler, J. S., Molholm, S., & De Sanctis, P. (2018). Cognitive load reduces the effects of optic flow on gait and electrocortical dynamics during treadmill walking. *Journal of neurophysiology, 120*(5), 2246-2259.

Miall, R. C., & Wolpert, D. M. (1996). Forward models for physiological motor control. *Neural Networks, 9*(8), 1265-1279.

Mosimann, J. E. (1970). Size Allometry: Size and Shape Variables with Characterizations of the Lognormal and Generalized Gamma Distributions. *Journal of the American Statistical Association, 65*(330), 930-945.

Nasreddine, Z. S., Phillips, N. A., Bédirian, V., Charbonneau, S., Whitehead, V., Collin, I., . . . Chertkow, H. (2005). The Montreal Cognitive Assessment, MoCA: a brief screening tool for mild cognitive impairment. *Journal of the American Geriatrics Society, 53*(4), 695-699.

Nguyen, J., Majmudar, U., Papathomas, T. V., Silverstein, S. M., & Torres, E. B. (2016). Schizophrenia: The micro-movements perspective. *Neuropsychologia, 85*, 310-326. doi:10.1016/j.neuropsychologia.2016.03.003

Nguyen, J., Papathomas, T., Ravaliya, J., & Torres, E. B. (2014). Methods to Explore the Influence of Top-Down Visual Processes on Motor Behavior. *J. of Vis. Exp.*(86). doi:e51422, doi:10.3791/51422

Niedermeyer, E. (2011). *Niedermeyer's electroencephalography: basic principles, clinical applications, and related fields*: Lippincott Williams & Wilkins.

Nordin, A. D., Hairston, W. D., & Ferris, D. P. (2019). Human electrocortical dynamics while stepping over obstacles. *Scientific Reports, 9*(1), 4693.

Onnela, J.-P., Saramäki, J., Kertész, J., & Kaski, K. (2005). Intensity and coherence of motifs in weighted complex networks. *Physical Review E, 71*(6), 065103.

Oostenveld, R., & Oostendorp, T. F. (2002). Validating the boundary element method for forward and inverse EEG computations in the presence of a hole in the skull. *Human Brain Mapping, 17*(3), 179-192.

Pavlov, I. P. (1957). Experimental psychology and other essays.

Possin, K. L., Laluz, V. R., Alcantar, O. Z., Miller, B. L., & Kramer, J. H. (2011). Distinct neuroanatomical substrates and cognitive mechanisms of figure copy performance in Alzheimer's disease and behavioral variant frontotemporal dementia. *Neuropsychologia, 49*(1), 43-48.

Roetenberg, D., Luinge, H., & Slycke, P. (2009). Xsens MVN: full 6DOF human motion tracking using miniature inertial sensors.

Ross, S. M. (1996). Stochastic processes. 1996. In: Wiley, New York.

Roy, M., Shohamy, D., & Wager, T. D. (2012). Ventromedial prefrontal-subcortical systems and the generation of affective meaning. *Trends in cognitive sciences, 16*(3), 147-156.

Rubinov, M., & Sporns, O. (2010). Complex network measures of brain connectivity: uses and interpretations. *Neuroimage, 52*(3), 1059-1069.

Ryu, J., & Torres, E. B. (2017). *Methods for Dynamically Coupled Brain Body Tracking.* Paper presented at the Fourth International Symposium on Movement and Computing, MOCO'17, London, UK.

Ryu, J., & Torres, E. B. (2018). Characterization of Sensory-Motor Behavior Under Cognitive Load Using a New Statistical Platform for Studies of Embodied Cognition. *Frontiers in human neuroscience, 12*, 116.

Ryu, J., Vero, J., Dobkin, R., & Torres, E. B. (2019). Dynamic Digital Biomarkers of Motor and Cognitive Function in Parkinson's Disease. *J. Vis. Exp, 149*, e59827.

Sasaki, K., & Maruyama, R. (2014). Consciously controlled breathing decreases the high-frequency component of heart rate variability by inhibiting cardiac parasympathetic nerve activity. *The Tohoku journal of experimental medicine, 233*(3), 155-163.

Shannon, C. (1948). A mathematical theory of communication *Bell System Technical Journal, 27*, 379-423, 623-656.

Skinner, B. (1947). Experimental psychology.

Snyder, K. L., Kline, J. E., Huang, H. J., & Ferris, D. P. (2015). Independent component analysis of gait-related movement artifact recorded using EEG electrodes during treadmill walking. *Frontiers in human neuroscience, 9*, 639.

Sporns, O. (2010). *Networks of the Brain*: MIT press.

Teitelbaum, O., Benton, T., Shah, P. K., Prince, A., Kelly, J. L., & Teitelbaum, P. (2004). Eshkol-Wachman movement notation in diagnosis: the early detection of Asperger's syndrome. *Proc Natl Acad Sci U S A, 101*(32), 11909-11914. doi:10.1073/pnas.0403919101

Tereshchenko, L. G., & Josephson, M. E. (2015). Frequency content and characteristics of ventricular conduction. *Journal of electrocardiology, 48*(6), 933-937.

Thelen, E., Kelso, J. S., & Fogel, A. (1987). Self-organizing systems and infant motor development. *Developmental Review, 7*(1), 39-65.

Thelen, E., & Smith, L. B. (1996). *A dynamic systems approach to the development of cognition and action*: MIT press.

Torres, E. B. (2011). Two classes of movements in motor control. *Experimental brain research, 215*(3-4), 269-283.

Torres, E. B. (2013). Atypical signatures of motor variability found in an individual with ASD. *Neurocase, 19*(2), 150-165.

Torres, E. B. (2016). Rethinking the Study of Volition for Clinical Use. In J. Laczko & M. L. Latash (Eds.), *Progress in Motor Control: Theories and Translations* (pp. 229-254). Cham: Springer International Publishing.

Torres, E. B. (2018). *Objective Biometric Methods for the Diagnosis and Treatment of Nervous System Disorder*: Elsevier.

Torres, E. B., Brincker, M., Isenhower, R. W., Yanovich, P., Stigler, K. A., Nurnberger, J. I., . . . Jose, J. V. (2013). Autism: the micro-movement perspective. *Frontiers in Integrative Neuroscience, 7*, 32. doi:10.3389/fnint.2013.00032

Torres, E. B., Cole, J., & Poizner, H. (2014). Motor output variability, deafferentation, and putative deficits in kinesthetic reafference in Parkinson's disease. *Frontiers in human neuroscience, 8*, 823. doi:10.3389/fnhum.2014.00823

Torres, E. B., & Denisova, K. (2016). Motor noise is rich signal in autism research and pharmacological treatments. *Sci Rep, 6*, 37422. doi:10.1038/srep37422

Torres, E. B., & Denisova, K. (2016). Motor noise is rich signal in autism research and pharmacological treatments. *Scientific Reports, 6*.

Torres, E. B., & Donnellan, A. M. (2015). *Autism: The movement perspective*: Frontiers Media SA.

Torres, E. B., Heilman, K. M., & Poizner, H. (2011a). Impaired endogenously evoked automated reaching in Parkinson's disease. *J Neurosci, 31*(49), 17848-17863. doi:10.1523/JNEUROSCI.1150-11.2011

Torres, E. B., Heilman, K. M., & Poizner, H. (2011b). Impaired endogenously evoked automated reaching in Parkinson's disease. *Journal of Neuroscience, 31*(49), 17848-17863. doi:31/49/17848 [pii]

10.1523/JNEUROSCI.1150-11.2011

Torres, E. B., Isenhower, R. W., Nguyen, J., Whyatt, C., Nurnberger, J. I., Jose, J. V., . . . Cole, J. (2016). Toward Precision Psychiatry: Statistical Platform for the Personalized Characterization of Natural Behaviors. *Frontiers in Neurology, 7*, 8. doi:10.3389/fneur.2016.00008

Torres, E. B., Mistry, S., Caballero, C., & Whyatt, C. P. (2017). Stochastic Signatures of Involuntary Head Micro-movements Can Be Used to Classify Females of ABIDE into Different Subtypes of Neurodevelopmental Disorders. *Front Integr Neurosci, 11*, 10. doi:10.3389/fnint.2017.00010

Torres, E. B., Nguyen, J., Mistry, S., Whyatt, C., Kalampratsidou, V., & Kolevzon, A. (2016a). Characterization of the statistical signatures of micro-movements underlying natural gait patterns in children with Phelan McDermid syndrome: towards precision-phenotyping of behavior in ASD. *Frontiers in Integrative Neuroscience, 10*.

Torres, E. B., Nguyen, J., Mistry, S., Whyatt, C., Kalampratsidou, V., & Kolevzon, A. (2016b). Characterization of the Statistical Signatures of Micro-Movements Underlying Natural Gait Patterns in Children with Phelan McDermid Syndrome: Towards Precision-Phenotyping of Behavior in ASD. *Front Integr Neurosci, 10*, 22. doi:10.3389/fnint.2016.00022

Torres, E. B., Rai, R., Mistry, S., & Gupta, B. (2019). Hidden Aspects of the Research-ADOS are Bound to Affect Autism Science. *bioRxiv*, 717827. doi:10.1101/717827

Torres, E. B., Raymer, A., Gonzalez Rothi, L. J., Heilman, K. M., & Poizner, H. (2010). Sensory-spatial transformations in the left posterior parietal cortex may contribute to reach timing. *J Neurophysiol, 104*(5), 2375-2388. doi:jn.00089.2010 [pii]

10.1152/jn.00089.2010

Torres, E. B., Smith, B., Mistry, S., Brincker, M., & Whyatt, C. (2016). neonatal Diagnostics: Toward Dynamic growth charts of neuromotor control. *Frontiers in Pediatrics, 4*.

Torres, E. B., Vero, J., & Rai, R. (2018). Statistical platform for individualized behavioral analyses using biophysical micro-movement spikes. *Sensors, 18*(4), 1025.

Torres, E. B., Yanovich, P., & Metaxas, D. N. (2013). Give spontaneity and self-discovery a chance in ASD: spontaneous peripheral limb variability as a proxy to evoke centrally driven intentional acts. *Front Integr Neurosci, 7*, 46. doi:10.3389/fnint.2013.00046

Uno, Y., Kawato, M., & Suzuki, R. (1989). Formation and control of optimal trajectory in human multijoint arm movement. Minimum torque-change model. *Biol Cybern, 61*(2), 89-101.

van Beers, R. J. (2009). Motor learning is optimally tuned to the properties of motor noise. *Neuron, 63*(3), 406-417.

van Beers, R. J., Wolpert, D. M., & Haggard, P. (2002). When feeling is more important than seeing in sensorimotor adaptation. *Current Biology, 12*(10), 834-837.

Vaschillo, E. G., Vaschillo, B., & Lehrer, P. M. (2006). Characteristics of resonance in heart rate variability stimulated by biofeedback. *Applied psychophysiology and biofeedback, 31*(2), 129-142.

Von Holst, E., & Mittelstaedt, H. (1950). The principle of reafference: Interactions between the central nervous system and the peripheral organs. In P. C. Dodwell (Ed.), *Perceptual Processing: Stimulus equivalence and pattern recognition* (pp. 41-72). New York: Appleton-Century-Crofts.

Watts, D. J., & Strogatz, S. H. (1998). Collective dynamics of 'small-world'networks. *Nature, 393*(6684), 440.

Whitmer, D., Worrell, G., Stead, M., Lee, I. K., & Makeig, S. (2010). Utility of independent component analysis for interpretation of intracranial EEG. *Frontiers in human neuroscience, 4*, 184.

Whyatt, C. P., & Torres, E. B. (2017). *The social-dance: decomposing naturalistic dyadic interaction dynamics to the'micro-level'.* Paper presented at the Proceedings of the 4th International Conference on Movement Computing.

Wu, D., Jose, J. V., Nurnberger, J. I., & Torres, E. B. (2018). A Biomarker Characterizing Neurodevelopment with applications in Autism. *Sci Rep, 8*(1), 614. doi:10.1038/s41598-017-18902-w

Yanovich, P., Isenhower, R. W., Sage, J., & Torres, E. B. (2013). Spatial-orientation priming impedes rather than facilitates the spontaneous control of hand-retraction speeds in patients with Parkinson's disease. *Plos One, 8*(7), 1-19.

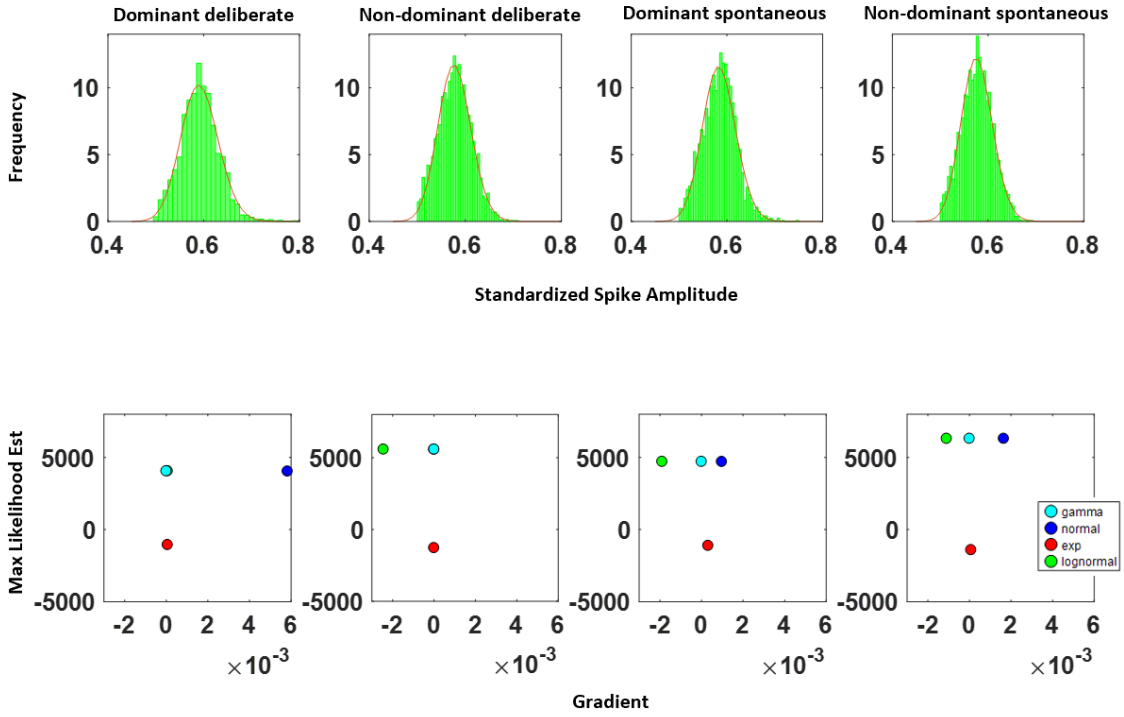

Figure A 1. MLE of angular acceleration standardized spike amplitudes

(Top) Histogram of normalized spike amplitude for different body parts (dominant body part extracted from right hand index finger motion; non-dominant body part extracted from left shoulder motion) and movement segment (deliberate forward; spontaneous backward) for a typical right-handed participant. These histograms were fitted to a Gamma probability distribution function, shown in red. (Bottom) Maximum likelihood estimated values for the corresponding histogram on top of each graph. The horizontal axis contains the value of the gradient at the end of the optimization process ($-3x10^{-3}$ ~ $6x10^{-3}$ range according to the set tolerance value of 10^{-30} for the optimization process). The vertical axis contains the maximum likelihood estimation (MLE) value for the Gamma, normal, exponential and lognormal distributions. The respective MLE values of each probability distributions are: for dominant deliberate amplitude data [4053.7, 4036.5, -1058.3, 4059.4], for non-dominant deliberate amplitude data [5578.0, 5574.2, -1285.2, 5577.6], for dominant spontaneous amplitude data [4706.8, 4701.6, -1116.4, 4707.2], for non-dominant spontaneous amplitude data [6305.7,6304.8,-1413.8,6303.9]. Overall, we found that the Gamma and lognormal distributions have a good fit to these kinematics data. However, because Gamma distributions have shown to be a better fit to the kinematics data from individuals with neurological disorders (Cite) than lognormal distributions, for consistency, we chose to use the Gamma probability distribution for fitting purpose.

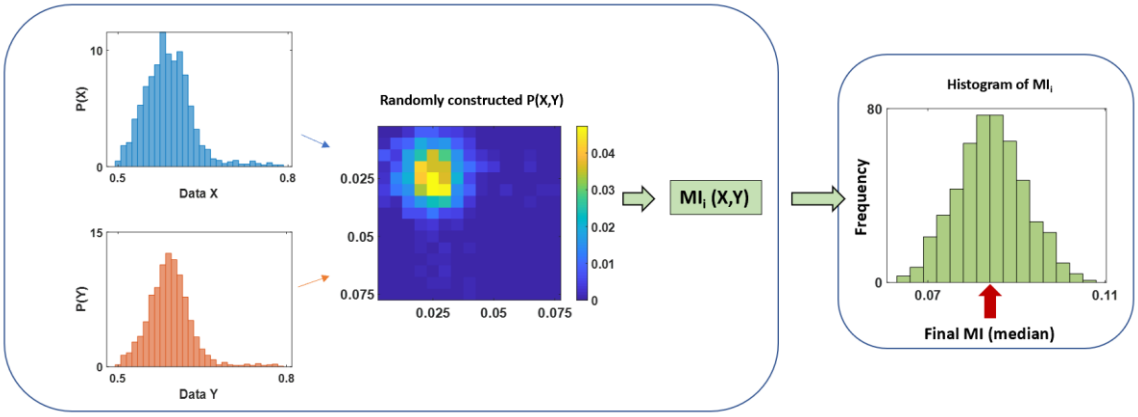

Figure A 2. Pipeline for computing mutual information. Because joint probability distributions P(X,Y) for a pair of different body parts P(X) and P(Y) could not be empirically determined, joint probability distributions were estimated by randomly sampling a pair from each body parts, X and Y, without replacement, and by constructing a joint histogram from these sampled pairs. Using the estimated joint probability distributions P(X,Y) along with the empirical single probability distribution P(X) and P(Y), we computed the mutual information (MI), and repeated this computation 100 times. The median of the 100 estimated mutual information values was determined as the final value.

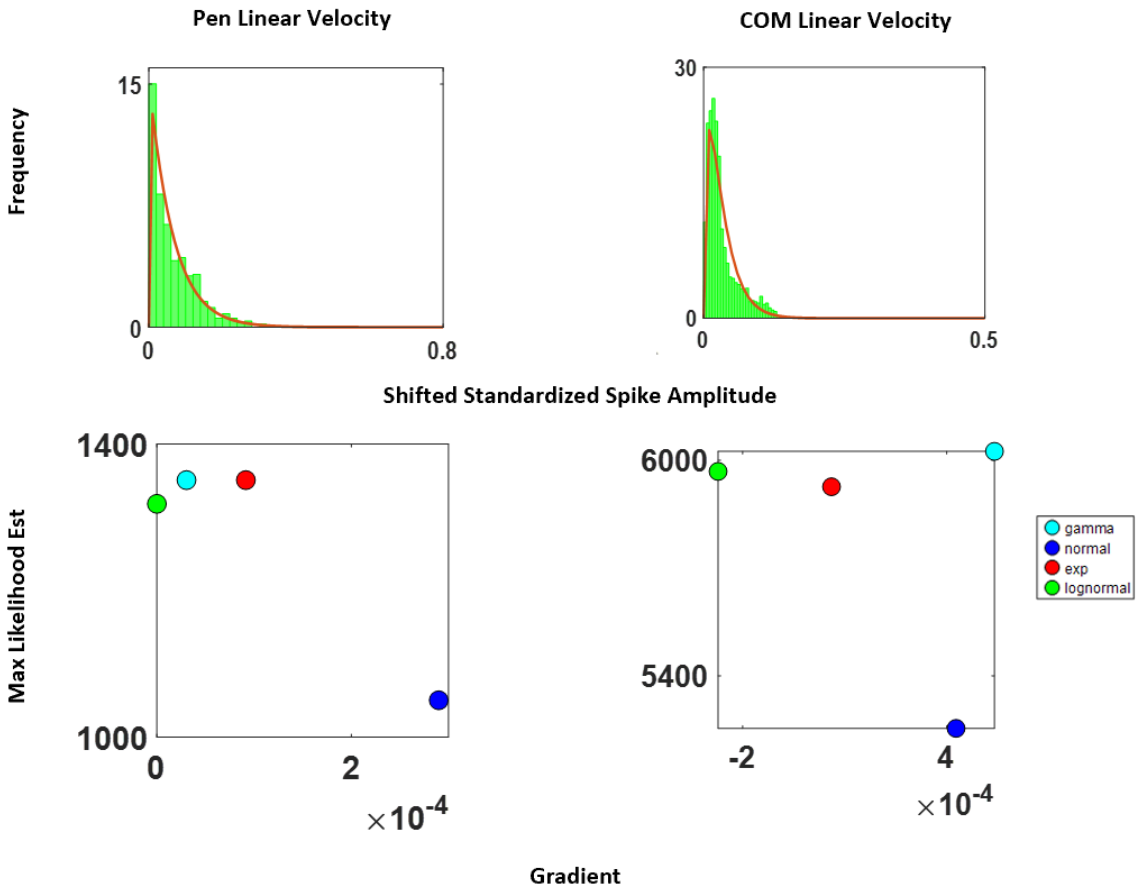

Figure A 3. MLE of Pen and COM linear velocity normalized spike amplitudes

(Top) Histogram of shifted normalized spike amplitude for pen linear velocity (left) and COM linear velocity (right) during a typical drawing task and a walking task, respectively. These histograms were fitted to a Gamma probability distribution function, shown in red. **(Bottom)** Maximum likelihood estimated values for the corresponding histogram on top of each graph. The horizontal axis contains the value of the gradient at the end of the optimization process (-$2x10^{-4}$ ~ $5x10^{-4}$ range according to the set tolerance value of 10^{-30} for the optimization process). The vertical axis contains the maximum likelihood estimation (MLE) value for the Gamma, normal, exponential and lognormal distributions. The respective MLE values of each probability distributions are: for pen data [1350, 1050, 1350, 1319], and for COM data [6024, 5253, 5926, 5968]. Overall, we found that the Gamma distributions have the best fit to these kinematics data.

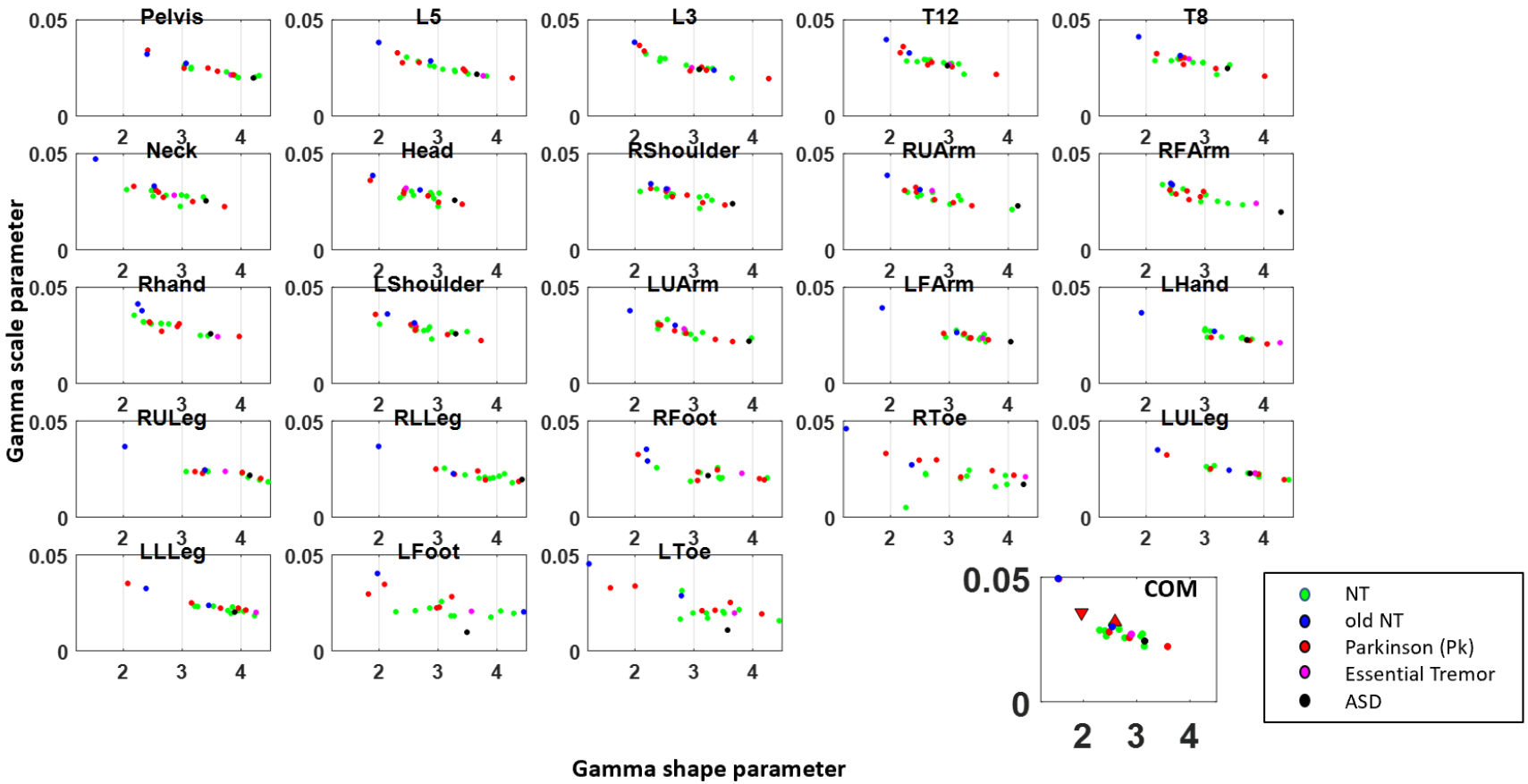

Figure A 4. Gamma fit for all body parts including COM during clock drawing Fitted Gamma parameters of each body part (R denotes Right; L denotes Left; U denotes Upper; F denotes Fore; LL denotes Left Lower; RL denotes Right Lower; U denotes Upper) for each individual during a clock drawing task. The fitted Gamma PDF is based on the shifted normalized spike amplitudes of the linear velocity of each body part. There is no observable cluster among different demographic cohorts.

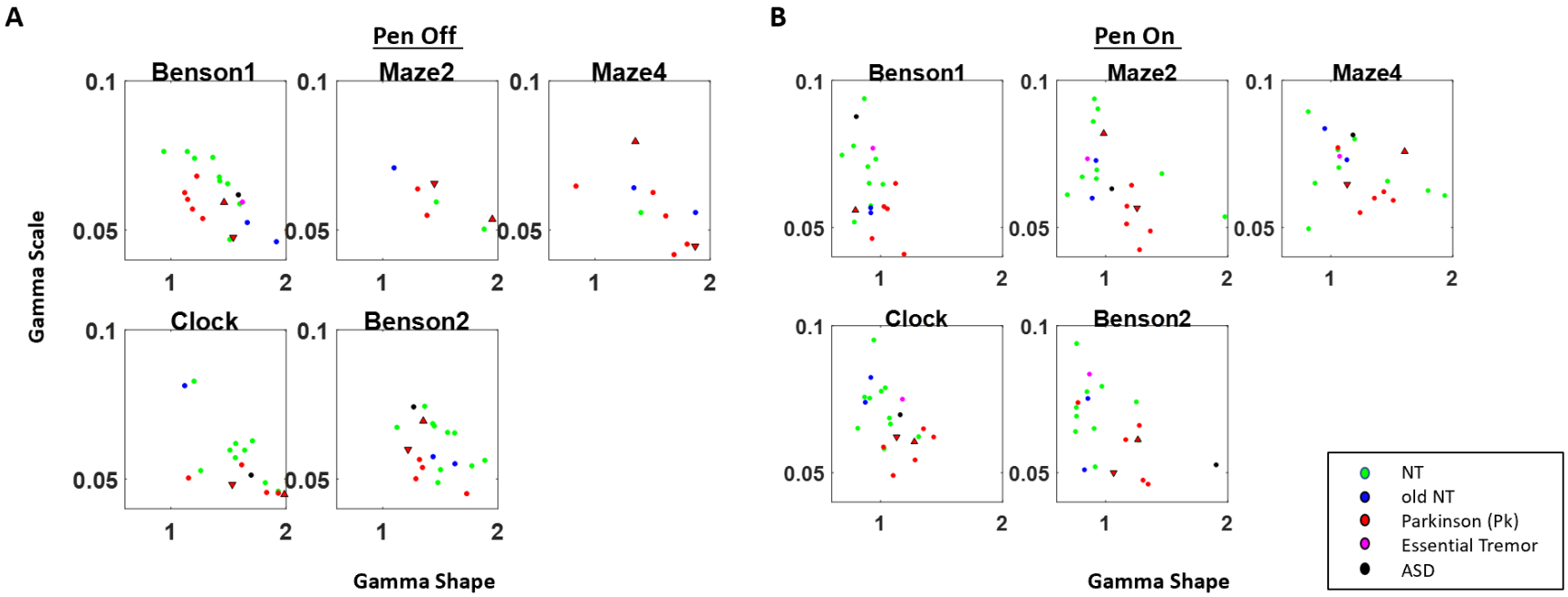

Figure A 5. Gamma fit of pen movement when pen was on the tablet (Pen On) and lifted from the tablet (Pen Off). Shifted and normalized spike amplitudes of pen movement linear velocity was fitted to a Gamma PDF, separately for motions when the pen was on the tablet, and when it was lifted from the tablet. We notice more separation between Parkinson's patients and NT participants when the pen was on the tablet, but we also caveat that there are fewer participant data for the "Pen Off" case, so the finding is not conclusive.

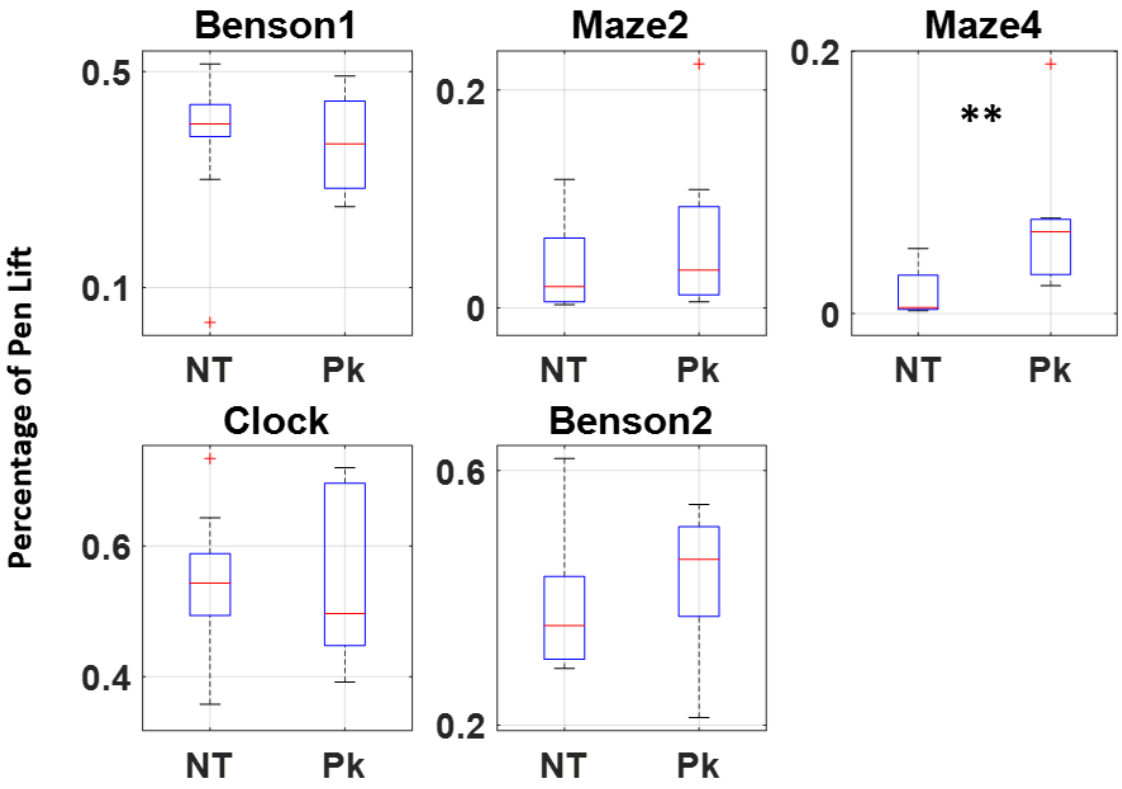

Figure A 6. Comparison of time percentage when pen tip was lifted from the tablet. There were little difference between Parkinson's patients and NT participants for all tasks, except the Maze4 task (to connect dots alternating between sequences of numbers and alphabet) which had statistical significance (χ (1,18) = 7.47, $p<0.01$).

Table A 1- Kruskal Wallis Test (p-values) on Mutual Information comparison: Dominant (D) vs. Non-Dominant (ND)

	D vs ND $X(1,22)$	**Deliberate: D vs ND** $X(1,10)$	**Spontaneous: D vs ND** $X(1,10)$
P1	4.08 (p=0.04) *	8.31 (p<0.01) **	7.41 (p<0.01) **
P2	6.75 (p<0.01) **	8.31 (p<0.01) **	6.56 (p=0.01) *
P3	3.00 (p=0.08)	8.31 (p<0.01) **	3.69 (p=0.05)
P4	4.32 (p=0.04) *	8.31 (p<0.01) **	8.31 (p<0.01) **
P5	15.87 (p<0.01) **	8.31 (p<0.01) **	5.77 (p=0.02) *
P6	17.28 (p<0.01) **	8.31 (p<0.01) **	8.31 (p<0.01) **
P7	11.21 (p<0.01) **	8.31 (p<0.01) **	5.03 (p=0.03) *
P8	11.60 (p<0.01) **	8.31 (p<0.01) **	3.69 (p=0.05)

Table A 2 - Kruskal Wallis Test (p-values) on Mutual Information comparison: Deliberate (Del) vs. Spontaneous (Sp)

	Del vs Sp $X(1,88)$	**Dominant: Del vs Sp** $X(1,10)$	**Non-Dominant: Del vs Sp** $X(1,10)$
P1	66.76 (p<0.01)**	8.31 (p<0.01) **	8.31 (p<0.01) **
P2	64.54 (p<0.01) **	8.31 (p<0.01) **	8.31 (p<0.01) **
P3	66.49 (p<0.01) **	8.31 (p<0.01) **	8.31 (p<0.01) **
P4	66.63 (p<0.01) **	8.31 (p<0.01) **	8.31 (p<0.01) **
P5	0.37 (p=0.54)	5.03 (p=0.03) *	4.33 (p=0.04) *
P6	12.07 (p<0.01) **	3.69 (p=0.05)	1.64 (p=0.20)
P7	40.90 (p<0.01) **	8.31 (p<0.01) **	1.26 (p=0.26)
P8	33.71 (p<0.01) **	0.23 (p=0.63)	8.31 (p<0.01) **

Table A 3. Kruskal Wallis Test (p-values) on NSR comparison: Dominant (D) vs. NonDominant (ND)

	D vs ND ***X*****(1,14)**	**Deliberate: D vs ND** ***X*****(1,6)**	**Spontaneous: D vs ND** ***X*****(1,6)**
P1	4.41 (p=0.04) *	5.33 (p=0.02) *	3.00 (p=0.08)
P2	4.86 (p=0.03) *	4.08 (p=0.04) *	1.33 (p=0.25)
P3	2.16 (p=0.14)	5.33 (p=0.02) *	0.33 (p=0.56)
P4	6.35 (p=0.01) *	5.33 (p=0.02) *	5.33 (p=0.02) *
P5	4.41 (p=0.04) *	4.08 (p=0.04) *	1.33 (p=0.25)
P6	9.93 (p<0.01) **	5.33 (p=0.02) *	5.33 (p=0.02) *
P7	8.04 (p<0.01) **	4.08 (p=0.02) *	5.33 (p=0.02) *
P8	9.27 (p<0.01) **	5.33 (p=0.02) *	5.33 (p=0.02) *

Table A 4. Kruskal Wallis Test (p-values) on NSR comparison: Deliberate (Del) vs Spontaneous (Sp)

	Del vs Sp $X(1,18)$	**Dominant: Del vs Sp** $X(1,6)$	**Non-Dominant: Del vs Sp** $X(1,6)$
P1	8.25 (p<0.01) **	3.00 (p=0.08)	5.33 (p=0.02) *
P2	5.49 (p=0.02) *	4.08 (p=0.04) *	4.08 (p=0.04) *
P3	8.69 (p<0.01) **	5.33 (p=0.02) *	3.00 (p=0.08)
P4	7.00 (p<0.01) **	5.33 (p=0.02) *	4.08 (p=0.04) *
P5	3.86 (p=0.05) *	3.00 (p=0.08)	0.08 (p=0.77)
P6	3.02 (p=0.08)	3.00 (p=0.08)	4.08 (p=0.04) *
P7	3.86 (p=0.05) *	5.33 (p=0.02) *	2.08 (p=0.15)
P8	5.14 (p=0.02) *	5.33 (p=0.02) *	5.33 (p=0.02) *

Table A 5. Pair-wise Kolmogorov-Smirnov Test on Modularity Togetherness comparison: Low vs. High Cognitive Load Condition

	Low vs High		Deliberate: Low vs. High		Spontaneous: Low vs High	
	KS	**p-value**	**KS**	**p-value**	**KS**	**p-value**
P1	0.28	<0.01**	0.24	0.12	0.33	0.01*
P2	0.21	0.03*	0.16	0.61	0.27	0.07
P3	0.26	<0.01**	0.18	0.44	0.42	<0.01**
P4	0.13	0.38	0.13	0.79	0.29	0.04*
P5	0.22	0.02*	0.20	0.30	0.44	<0.01**
P6	0.23	0.01*	0.16	0.61	0.40	<0.01**
P7	0.26	<0.01**	0.24	0.12	0.38	<0.01**
P8	0.38	<0.01**	0.31	0.02*	0.67	<0.01**

Table A 6. Pair-wise Kolmogorov-Smirnov Test on Cluster Coefficient comparison: Low vs. High Cognitive Load Condition

	Low vs High		Deliberate: Low vs. High		Spontaneous: Low vs High	
	KS	**p-value**	**KS**	**p-value**	**KS**	**p-value**
P1	0.30	<0.01**	0.23	<0.01**	0.37	<0.01**
P2	0.21	<0.01**	0.15	<0.01**	0.29	<0.01**
P3	0.23	<0.01**	0.33	<0.01**	0.32	<0.01**
P4	0.23	<0.01**	0.28	<0.01**	0.22	<0.01**
P5	0.28	<0.01**	0.27	<0.01**	0.31	<0.01**
P6	0.35	<0.01**	0.21	<0.01**	0.52	<0.01**
P7	0.27	<0.01**	0.38	<0.01**	0.32	<0.01**
P8	0.46	<0.01**	0.53	<0.01**	0.43	<0.01**

Table A 7. Pair-wise Kolmogorov-Smirnov Test on Modularity Togetherness comparison: Deliberate (Del) vs. Spontaneous (Sp)

	Del vs Sp		Low Cognitive Load: Del vs Sp		High Cognitive Load: Del vs Sp	
	KS	**p-value**	**KS**	**p-value**	**KS**	**p-value**
P1	0.12	0.28	0.16	0.61	0.18	0.44
P2	0.13	0.22	0.13	0.79	0.24	0.12
P3	0.15	0.09	0.11	0.93	0.38	<0.01**
P4	0.12	0.28	0.20	0.30	0.16	0.61
P5	0.21	0.01*	0.16	0.61	0.49	<0.01**
P6	0.13	0.17	0.22	0.19	0.36	<0.01**
P7	0.07	0.84	0.13	0.79	0.33	0.01*
P8	0.19	0.01*	0.22	0.19	0.58	<0.01**

Table A 8. Pair-wise Kolmogorov-Smirnov Test on Cluster Coefficient comparison: Deliberate (Del) vs. Spontaneous (Sp)

	Del vs Sp		Low Cognitive Load: Del vs Sp		High Cognitive Load: Del vs Sp	
	KS	**p-value**	**KS**	**p-value**	**KS**	**p-value**
P1	0.50	<0.01**	0.43	<0.01**	0.45	<0.01**
P2	0.61	<0.01**	0.61	<0.01**	0.58	<0.01**
P3	0.32	<0.01**	0.26	<0.01**	0.44	<0.01**
P4	0.22	<0.01**	0.21	<0.01**	0.26	<0.01**
P5	0.16	<0.01**	0.19	<0.01**	0.18	<0.01**
P6	0.17	<0.01**	0.29	<0.01**	0.07	0.10
P7	0.46	<0.01**	0.44	<0.01**	0.61	<0.01**
P8	0.12	<0.01**	0.34	<0.01**	0.15	<0.01**

Table A 9. Demographics of Patient Participant

ASD Patient	Sex	Age	ADOS	Class
1	F	13	Module 3 / Score 11	Autism
2	M	13	Module 1 / Score 7	Autism, moderate
3	M	18	Module 3 / Score 10	Autism

Table A 10. Pair-wise Kolmogorov-Smirnov Test for absolute delta CC per IBI

	C1 vs. C2		**C1 vs. C3**		**C2 vs. C3**	
	KS	p-value	KS	p-value	KS	p-value
NT1 (P08)	0.04	0.50	0.17	<0.01**	0.16	<0.01**
NT2 (P11)	0.13	<0.01**	0.42	<0.01**	0.48	<0.01**
NT3 (P12)	0.05	0.17	0.10	<0.01**	0.14	<0.01**
ASD1 (P09)	0.07	<0.01**	0.05	0.10	0.05	0.12
ASD2 (P10)	0.08	0.37	0.09	0.05	0.08	0.08

Table A 11. Pairwise Kolmogorov-Smirnov test for absolute delta CC per IBI during Condition C1

	KS statistic	p-value
NT1 vs. NT2	0.45	<0.01**
NT1 vs. NT3	0.35	<0.01**
NT2 vs. NT3	0.15	<0.01**
NT1 vs. ASD1	0.07	0.01*
NT1 vs. ASD2	0.06	0.37
NT2 vs. ASD1	0.50	<0.01**
NT2 vs. ASD2	0.46	<0.01**
NT3 vs. ASD1	0.40	<0.01**
NT3 vs. ASD2	0.36	<0.01**
ASD1 vs. ASD2	0.06	0.42

* Corresponding Participant ID number for the category names are found in **Table A 10**.

Table A 12. Kruskal Wallis test for angle deviations

Body Part	Condition	χ (1,18)	p-value
Left Toe	W1	9.31	p<0.01**
	W2	13.00	p<0.01**
	W3	13.00	p<0.01**
Left Toe	P1	3.18	0.07
	P2	0.83	0.36
	P3	4.41	0.04*
Dominant Hand	P1	0.69	0.41
	P2	0.69	0.41
	P3	1.71	0.19

Table A 13. Kruskal Wallis test for median MI values

	χ (1,18)	p-value
EEG	3.77	0.05*
Mag-EEG	13.00	<0.01**
Mag-Mag	11.88	<0.01**
EKG-EEG	0.45	0.50
EKG-Mag	3.47	0.06

Table A 14. Kruskal Wallis Test on MI (separated by EEG components generated within the brain and those outside the brain)

	χ	df	p-value
IN EEG	1.42	(1,14)	0.23
IN EEG - Mag	1.42	(1,14)	0.23
IN EEG - EKG	1.21	(1,17)	0.27
OUT EEG	3.47	(1,18)	0.06
OUT EEG-Mag	12.43	(1,18)	<0.01**
OUT EEG-EKG	0.69	(1,18)	0.41

Table A 15. Kruskal Wallis Test on Median Cross Correlation between Participant Cohort

	χ	df	p-value
Pointing	3.78	(1,17)	0.05
Walking	7.78	(1,17)	<0.01 **
Pointing HP	2.07	(1,17)	0.15
Walking HP	0.30	(1,17)	0.58